PROTECTION OF SYNCHRONOUS GENERATORS AND INDUCTION GENERATORS

A Dissertation
Presented to
The Academic Faculty

by

Liangyi Sun

In Partial Fulfillment
Of the Requirements for the Degree
Doctor of Philosophy in the
School of Electrical and Computer Engineering

Georgia Institute of Technology
August 2017

PROTECTION OF SYNCHRONOUS GENERATORS AND INDUCTION GENERATORS

Approved by:

Dr. A.P. Meliopoulos, Advisor
School of Electrical and Computer Engineering
Georgia Institute of Technology

Dr. Shijie Deng
H. Milton Stewart School of Industrial & Systems Engineering
Georgia Institute of Technology

Dr. Thomas G Habetler
School of Electrical and Computer Engineering
Georgia Institute of Technology

Dr. Santiago Carlos Grijalva
School of Electrical and Computer Engineering
Georgia Institute of Technology

Dr. Maryam Saeedifard
School of Electrical and Computer Engineering
Georgia Institute of Technology

Date Approved: May 3, 2017

ACKNOWLEDGEMENTS

The doctoral study at Georgia Tech is an exciting and rewarding journey. Though exciting, this journey was not without ups and downs. I am very grateful to have wonderful friends and family, who stood by my side, and held me up through this journey.

Firstly, I would like to express my deepest gratitude to my advisor, Dr. A. P. Sakis Meliopoulos, for giving me the life-reshaping opportunity to work under his supervision, as well as his trust, support and encouragement throughout my entire Ph.D. study. I am also thankful to him for his passion and enthusiasm, which guided me to steadily advance towards the successful completion of this thesis, and inspired me to embrace for my career. I also greatly appreciate Dr. Meliopoulos to be my mentor, whose precious life lessons to me will guide me and influence me throughout my whole life. A special thank you goes to Dr. George Cokkinides, who always made time out of his busy schedule to address questions and issues I had during my research.

I would also like to express my appreciation to all the academic members of the School of Electrical and Computer Engineering at the Georgia Institute of Technology for their helpful and critical reviews throughout the Ph.D. program. Special thanks go to Dr. Thomas G Habetler, Dr. Maryam Saeedifard, Dr. Shijie Deng and Dr. Santiago Carlos Grijalva, who provided me valuable and constructive suggestions on my work, and also kindly serve in my Ph.D. defense committee. All of their valuable comments have helped me complete my Ph.D. and achieve a solid research path towards this thesis.

I would also like to thank all current and former members of the Power Systems Control and Automation Laboratory, for their constant support and true friendship since

the very beginning. I would specially thank Dr. Renke Huang for his unwavering support, insightful suggestions, and kind advice. I would also like to thank Dr. Ye Tao, Dr. Dongbo Zhao, Dr. Rui Fan, Dr. Zhenyu Tan, Dr. Aniemi Umana, Yi Du, Bai Cui, Yu Liu, Boqi Xie, Chiyang Zhong, Yuan Kong, Orestis Vasios, Hussain F Albinali and Seyyedmohammadsadegh Vejdan for their friendship and support. I keep a vivid memory of all my days in the lab and all the fantastic people that I have met throughout these years. To all of you, thank you for the unique atmosphere we have had in the lab.

Most of all, I cannot find the words to express my gratitude to my family, and in particular my parents. This achievement would have not been possible without their love, support and encouragement.

TABLE OF CONTENTS

LIST OF TABLES

LIST OF FIGURES

SUMMARY

Synchronous generators and induction generators play a significant role in the power grid. Synchronous generators provide the majority of electric power and induction generators are widely used in wind power generation. Losing synchronous generators and induction generators can greatly impact the stability and the reliability of the power system. Thus, developing a secure and reliable method to protect synchronous generators and induction generators can bring huge benefits to the grid.

As one of the most expensive and important power apparatus in the power grid, synchronous generators should be protected securely and dependably. Generally, there are two protection aspects for synchronous generator protection: fault protection and abnormal operating condition protection. Fault protection refers to the protection when faults occur inside the synchronous generator, e.g. stator phase faults, stator ground faults, rotor winding faults, rotor ground faults, etc. [1],[2]. Abnormal operating condition protection means the protection of the synchronous generator when it is experiencing abnormal operating condition, e.g. abnormal frequency, overexcitation, underexcitation, out-of-step, etc. [3]. This dissertation focuses only on the fault protection of synchronous generator and induction generators. Legacy protective functions are being used to provide fault protection, such as differential protection, negative-sequence protection, instantaneous/time overcurrent protection, and distance protection. However, the above mentioned legacy protective functions can only cover stator ground fault up to 85-90% of the winding. Usually the rest of the 10-15% of the winding is protected by third-harmonic voltage protection. As a result, to provide 100% stator protection, legacy

protective functions are configured in complex schemes that use specialized methods. Complexity always has the potential of errors. New protection approaches are needed to provide simplified, secure and dependable protection for synchronous generators.

In earlier decades, most of the induction machines are used as motors. Induction motors consume up to 70% of the electric power across the United [4]. Nowadays, with the development of wind power, more and more doubly-fed induction generators (DFIG) are installed in wind farms. Compared with other generators for wind power production, like permanent magnet generators, DFIG has a much lower cost. Protection of DFIGs has become a challenging topic. Similar to the synchronous generators, induction generators can also experience stator/rotor phase and ground faults. Legacy protective functions, such as differential protection, negative-sequence protection, instantaneous/time overcurrent protection, are designed to detect internal faults of induction generators. Although legacy protective functions can do their job well most of the time, there are still some protection gaps such as phase turn-to-turn faults, DFIG faulted current limited by converters, etc.

Present protective technology has evolved from conventional electromechanical relays to numerical relays. Compared with electromechanical relays, numerical relays are microprocessor based digital devices, which analyze power system voltages, currents and other quantities for the purpose of detecting faults in the power system. The characteristics and behaviors of several protective functions can be programmed together into one numerical relay. This is definitely a big step for the development of protective relays. However, the protective functions that we are using in the numerical relays now still mimic the concepts of electromechanical relays. They are basically direct

comparisons between the pre-defined settings and real-time measurements after simple calculation. The advanced microprocessor based relays have the capability to perform high-speed complicated calculations. This is a huge potential that has not been fully explored yet so that a new revolution in protective relays could be started to seek the full potential of numerical relays.

Thus, the objective of this dissertation is to develop a novel protective function, which is called dynamic state Estimation Based Protection (EBP), that can protect the synchronous generators and induction generators securely and dependably when they experience internal faults. The objective has been achieved by the development of such an approach which is based on the following contributions: (1) development of an innovative protection function which is based on the dynamic state estimation of the protection zone, in this case, it is a synchronous generator or an induction generator; (2) development of an interoperable and unified syntax of a protection zone so that the EBP algorithm can be programmed in an object-oriented manner and no specific setting is needed for different types of machines; (3) development of physically based synchronous generator and induction generator models using the above syntax, which have the capability of representing both balanced and unbalanced machine conditions. The effectiveness of the EBP approach can be verified by utilizing these models; (4) development of a parameter estimation algorithm using dynamic state estimation, which can provide accurate parameters for the synchronous generator and induction generator so that an accurate device model could be obtained.

The dynamic state estimation based protection, as the name implies, uses dynamic state estimation to detect faults in a protection zone. Generally, the EBP method can be

utilized to protect any power system apparatus so a general methodology description will be introduced in this dissertation. The EBP monitors the consistency between the real-time measurements for the protection zone and protection zone dynamic model. If they line up with each other, it means the protection zone is healthy and under normal operating condition. Otherwise, any mismatch between the measurement and the model indicates abnormality inside the protection zone. In this case, protection actions should be taken to protect the device from further damage. Compared to the other protective functions, the EBP approach only needs very few simple settings, which reduces the complexity of relay settings greatly. In addition, the EBP method does not need any coordination with other protective functions, which also decreases the possibility of mis-operations.

In order to make the EBP algorithm applicable to any protection zone, the protection zone model should be written in a general format, which makes the entire protective function object oriented. This interoperable and unified syntax of a protection zone is called State Algebraic Quadratic Companion Form (SAQCF). It is derived directly from the protection zone physical circuit model and can represent the dynamics in the protection zone. In this dissertation, the SAQCF model derivation for synchronous generators and induction generators are shown step by step for the purpose of generator and machine protection.

Furthermore, modeling accuracy and fidelity are fundamental in this protection approach. For the synchronous generator and induction generator models, sometimes the generator and machine parameters may be hard to obtain or they may be changed during operation, thus the parameters may be inaccurate. To overcome this challenge, a

parameter estimation process is introduced by using the same dynamic state estimation algorithm. It treats the uncertain parameters as unknown states during the state estimation process. With the help of redundant measurements, the final state estimation results can provide the accurate parameters for those models.

CHAPTER 1 INTRODUCTION

1.1 Problem Statement

Synchronous generators and induction generators play a significant role in the power grid. Synchronous generators provide the majority of electric power and induction generators are widely used in wind power generation. Losing synchronous generators and induction generators can greatly impact the stability and the reliability of the power system. Thus, developing a secure and reliable method to protect synchronous generators and induction generators can bring huge benefits to the grid.

As one of the most expensive and important power apparatus in the power grid, synchronous generators should be protected securely and dependably. Generally, there are two protection aspects for synchronous generator protection: fault protection and abnormal operating condition protection. Fault protection refers to the protection when faults occur inside the synchronous generator, e.g. stator phase faults, stator ground faults, rotor winding faults, rotor ground faults, etc. [1],[2]. Abnormal operating condition protection means the protection of the synchronous generator when it is experiencing abnormal operating condition, e.g. abnormal frequency, overexcitation, underexcitation, out-of-step, etc. [3]. This dissertation focuses only on the fault protection of synchronous generator and induction generator. Legacy protective functions are being used to provide fault protection, such as differential protection, negative-sequence protection, instantaneous/time overcurrent protection, and distance protection However, the above mentioned legacy protective functions can only cover stator ground fault up to 85-90% of the winding. Usually the rest of the 10-15% of the winding is protected by

third-harmonic voltage protection. As a result, to provide 100% stator protection, legacy protective functions are configured in complex schemes that use specialized methods. Complexity always has the potential of errors. New protection approaches are needed to provide simplified, secure and dependable protection for synchronous generators.

In earlier decades, most of the induction machines were used as motors. Induction motors consume up to 70% of the electric power across the United States [4]. Nowadays, with the development of wind power, more and more doubly-fed induction generators (DFIG) are installed in wind farms. Compared with other generators for wind power production, like permanent magnet generators, DFIG has a much lower cost. Protection of DFIGs has become a challenging topic. Similar to the synchronous generators, induction generators can also experience stator/rotor phase and ground faults. Legacy protective functions, such as differential protection, negative-sequence protection, instantaneous/time overcurrent protection, are designed to detect internal faults of induction generators. Although legacy protective functions can do their job well most of the time, there are still some protection gaps such as phase turn-to-turn faults, DFIG faulted current limited by converters, etc..

Present protective technology has evolved from conventional electromechanical relays to numerical relays. Compared with electromechanical relays, numerical relays are microprocessor based digital devices, which analyze power system voltages, currents and other quantities for the purpose of detection of faults in the power system. The characteristics and behaviors of several protective functions can be programmed together into one numerical relay. This is definitely a big step for the development of protective relays. For the synchronous generator and induction generator protection, usually there

are more than ten protective functions used to protect the device and they need to coordinate with each other. This coordination is very complicated and it may bring human or setting errors when facing faults. Furthermore, the protective functions that are being used in the numerical relays now still mimic the concepts of electromechanical relays. They are basically direct comparisons between the pre-defined settings and real-time measurements after simple calculation. Since the advanced microprocessors are being utilized now, they have the capability to perform high-speed complicated calculation. This is a huge potential that has not been fully explored yet so that a new revolution in protective relays could be started to seek the full potential of numerical relays.

1.2 Research Objectives

The objective of this dissertation is to develop a novel protective function, which is called dynamic state Estimation Based Protective (EBP) relay, that can protect the synchronous generators and induction generators securely and reliably when they experience internal faults. The objective has been achieved by the development of such an approach which is based on the following contributions: (1) development of an innovative protection function which is based on the dynamic state estimation of the protection zone, in this case, it is a synchronous generator or an induction generator; (2) development of an interoperable and unified syntax of a protection zone so that the EBP algorithm can be programmed in an object-oriented manner and no specific setting is needed for different types of machines; (3) development of physical based synchronous generator and induction generator models using the above syntax, which have the

capability of representing both balanced and unbalanced machine conditions. The effectiveness of the EBP approach can be verified by utilizing these models.

The dynamic state estimation based protective function uses dynamic state estimation to detect the faults in the protection zone. Generally, the EBP algorithm can be utilized to protect any power system apparatus so a general methodology description will be introduced in this dissertation. The EBP monitors the consistency between the real-time measurements for the protection zone and protection zone dynamic model. If they line up with each other, it means the protection zone is healthy and under normal operating condition. Otherwise, any mismatch between the measurement and the model indicates abnormality inside the protection zone. In this case, protection actions should be taken to protect the device from further damage. Compared to the other protective functions, the EBP approach only needs very few simple settings, which reduces the relay settings complexity greatly. In addition, the EBP function does not need any coordination with other protective functions, which also decreases the possibility of mis-operations.

In order to make the EBP algorithm applicable to any protection zone, the protection zone model should be written in a general format, which makes the entire protective function object oriented. This interoperable and unified syntax of a protection zone is called State Algebraic Quadratic Companion Form (SAQCF). It is derived directly from the protection zone physical model and can represent the dynamics in the protection zone. In this dissertation, the SAQCF model derivation for synchronous generators and induction generators are shown step by step for the purpose of generator and machine protection.

Furthermore, modeling accuracy and fidelity are fundamental in this protection approach. For the synchronous generator and induction generator models, sometimes the generator and machine parameters may be different than the data base due to aging or temperature change, thus the parameters may be inaccurate. To overcome this challenge, a parameter estimation process is introduced by using the same dynamic state estimation algorithm. It treats the uncertain parameters as unknown states during the state estimation process. With the help of redundant measurements, the final state estimation results can provide the accurate parameters for those models.

1.3 Thesis Outline

The outline of the remaining parts of this dissertation is as follows.

In Chapter 2, background information is provided on the origin of the topic along with presently available technologies that are being used. In addition, a thorough literature survey is presented that summarizes related research work efforts. In particular, this literature survey starts with a summary of the protective relay evolution. Then legacy protective functions for generator and machine protection are introduced. A few newly developed protective approaches are studied as well. Finally, the parameter estimation technology for synchronous generators is summarized.

Chapter 3 presents the overall approach and the conceptual design of the dynamic state estimation based protection. The proposed protection algorithm is object-oriented, thus the same protection algorithm can be applied to all power system apparatus.

Chapter 4 shows the general and detailed methodology for the derivation of an object-oriented, interoperable, and unified model for the component in the power system.

The model is named as the State Algebraic Quadratic Companion Form (SAQCF). Examples of how to derive the SAQCF models for the synchronous generator and the induction generator are also given.

Chapter 5 introduces in detail the mathematical formulation and the solution methodology of the developed dynamic state Estimation Based Protection (EBP). More specifically, the EBP function can be divided into two parts: dynamic state estimation and protection logic.

Chapter 6 gives the hardware-in-the-loop test for the proposed EBP function. The laboratory is setup to mimic the field operating condition and test the effectiveness of the proposed EBP approach.

Chapter 7 presents several numerical cases in evaluating the performance of the proposed EBP algorithm. In addition, the comparison between the legacy protection functions and the proposed EBP method is given.

Chapter 8 shows that the dynamic state estimation can be utilized to fine tune the models and/or determine the parameters of the model with great accuracy. The basic approach is to expand the dynamic state estimation to include some key parameters as unknown states. The mathematical formulation of the synchronous generator physical parameters identification problem is described in this chapter.

Chapter 9 gives numerical examples for the synchronous generator parameter estimation. Data from simulation and from NERC are both utilized to verify the proposed algorithm.

Finally, Chapter 10 summarizes the research work and outlines the results and contributions of this dissertation.

CHAPTER 2 LITERATURE REVIEW

2.1 Overview

This chapter provides the background information of existing technologies related to the proposed research along with a literature review of the research efforts on these topics. Section 2.2 starts with a summary of the evolution of the protective relays for power system fault detection. Section 2.3 summarizes the present utilized technology in synchronous generator and induction generator protection and explores its biases and limitations. Section 2.4 provides a literature review on the parameters identification technology for a synchronous machine.

2.2 The Evolution of the Protective Relays

Prior to the transistor and computer era, relay technology was based on electromechanical elements to perform the relay logic. Electromechanical relays are invented as electrically operated switching devices to perform a specific task within an electrical circuit or system. The most common electromechanical components are the plunger relay, the induction disk/cup relay, and the balancing beam relay. Figure 2.1 shows a picture of a simple electromechanical relay. It consists of a coil of wire wrapped around a soft iron core, an iron yoke which provides a low reluctance path for magnetic flux, a movable iron armature, and one or more sets of contacts (there are two contacts in Figure 2.1). The armature is hinged to the yoke and mechanically linked to the moving contacts. The armature is held in place by a spring so that when the relay is de-energized there is an air gap in the magnetic circuit. In this condition, one of the two sets of contacts is closed, and the other set is open.

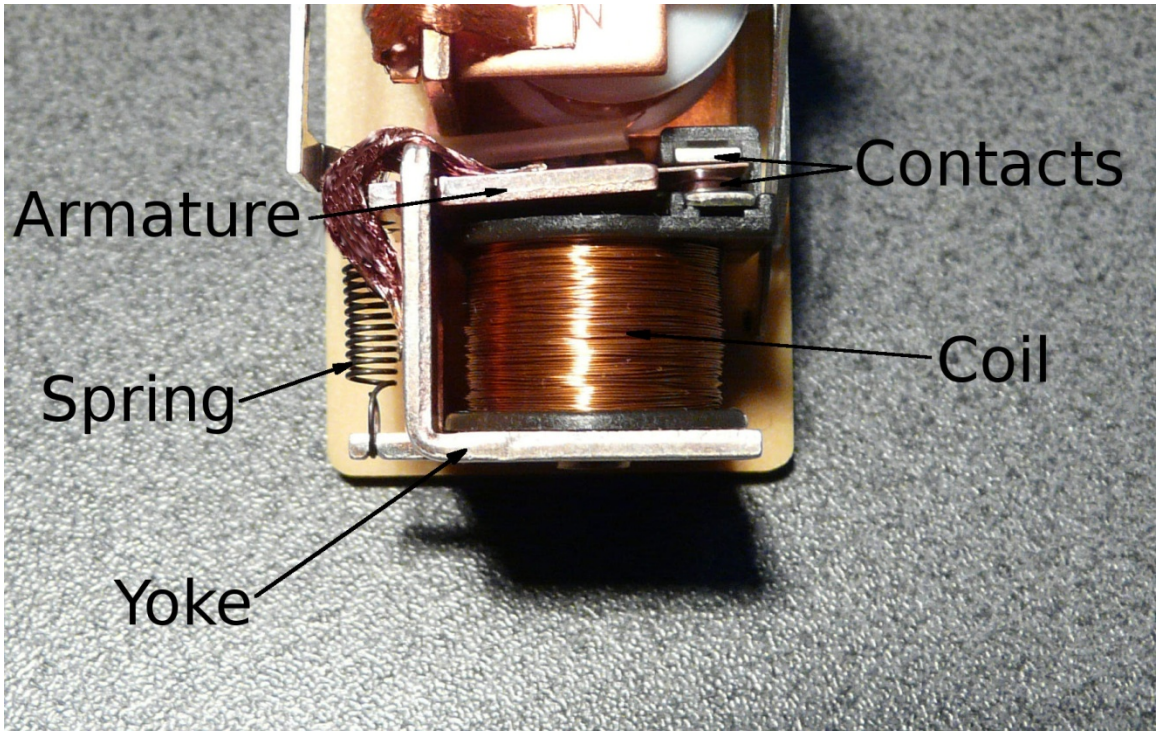

Figure 2.1. Simple Electromechanical Relay

When an electric current passes through the coil it generates a magnetic field that activates the armature, and the consequent movement of the movable contact(s) either makes or breaks (depending upon construction) a connection with a fixed contact. If the set of contacts was closed when the relay was de-energized, then the movement opens the contacts and breaks the connection, and vice versa if the contacts were open. When the current to the coil is switched off, the armature is returned by a force, approximately half as strong as the magnetic force, to its relaxed position. Usually this force is provided by a spring.

Basically, the relay takes inputs from instrument transformers. Typically, a signal conditioning circuit will be employed for filtering any unwanted transients and spikes in the signal. For the electromechanical relay, the filtered signals are fed to the logic circuit

of the electromechanical relay which may consists of an induction disk, plunger, etc.. The general structure of an electromechanical relay is shown in Figure 2.2.

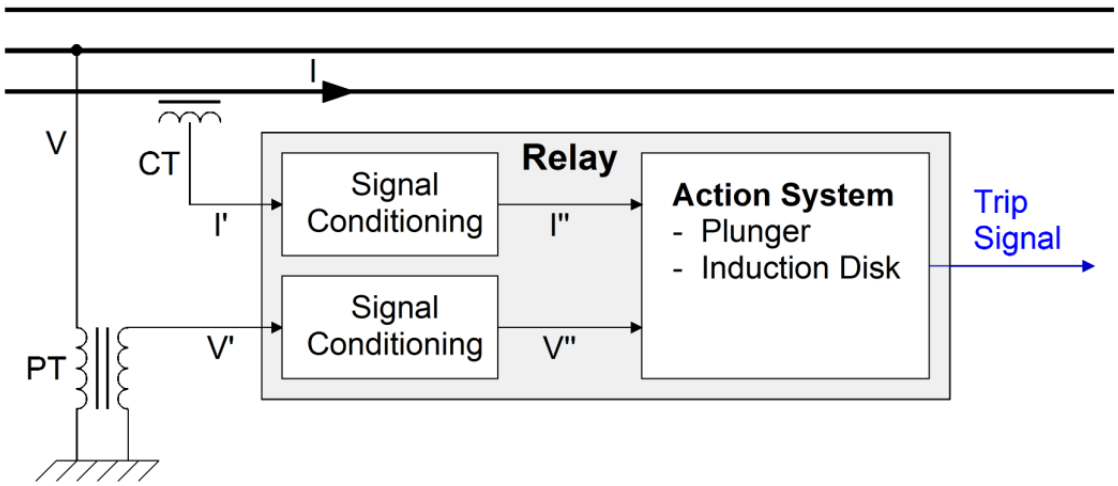

Figure 2.2. General Structure of an Electromechanical Relay

The invention of the transistor enabled the development of solid state relays. Solid state relays (static relays) are devices that include discrete component electronic circuits that mimic the logic of the electromechanical relays. The structure of the solid state relay is the same as the electromechanical relay except the action system is static. The advantages of the solid state relays are (a) smaller size and (b) ability to perform more complex logic than the electromechanical relays. The era of solid state relays was short lived because of the development of the microprocessor based relay (or numerical relay).

Numerical relays consist of an input section where the analog signals of voltages and currents are conditioned by appropriate analog filters (protection & isolation) and then digitized by means of analog to digital converters. The structure of the numerical relay is shown in Figure 2.3. The digitized signals are processed by microprocessors via algorithms that perform identification of the system conditions and the protective function. In addition, numerical relays can be directly interfaced with the control circuit

via input contacts and output contacts. Other major advantages of numerical relays are their ability to (a) display results, operational status, logic status, etc. on display screens via user interfaces, (b) store data when necessary (by appropriate triggering options) for later viewing and analysis (oscillography), and (c) communicate information with the rest of the world via different communication channels.

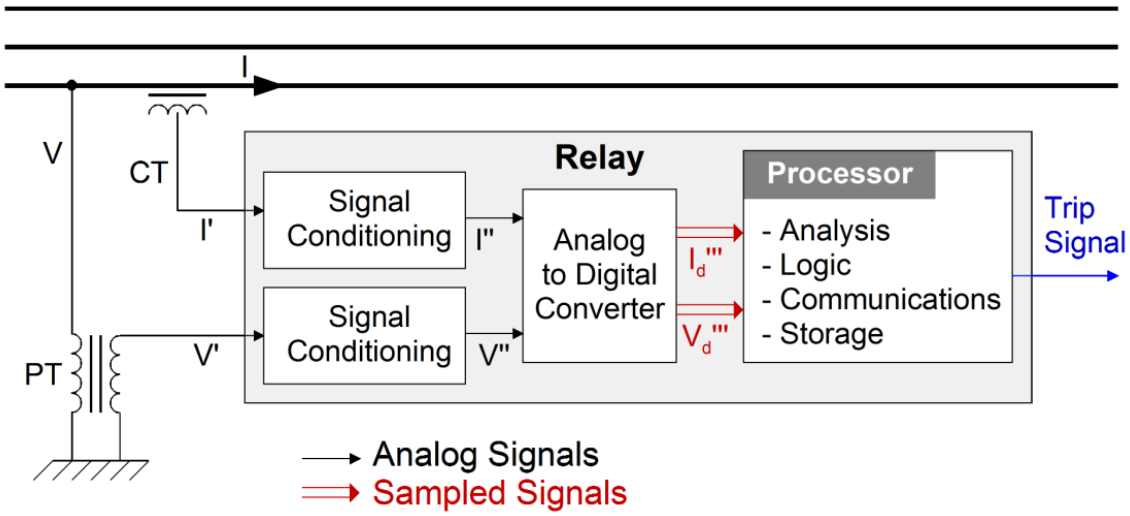

Figure 2.3. General Structure of a Numerical Relay

Tens of protective functions can be programmed together in one numerical relay, which reduces the cost of protective relays a lot. However, all the protective functions just mimic the concept of old-school electromagnetic protective functions. Although most of the fault conditions can be protected by the coordination of complex protective functions, protection gaps still exist. Since the microprocessor has the capability of high-speed computation, why do not we use the full potential of microprocessor and develop a brand new protective function? With this motivation, a dynamic state estimation based protection algorithm is proposed in this dissertation.

2.3 Survey of Legacy Machine Protection Functions

This section starts with a summary of machine stator/rotor phase faults and ground faults. The second, third and fourth subsections provide the concept of differential protection, instantaneous/time overcurrent protection and negative-sequence protection and their drawbacks respectively. The fifth subsection shows some other newly developed protection functions, like generator harmonic protection and signal injection protection.

2.3.1 General Fault Type of AC machines

Synchronous generators should be protected against fault conditions and abnormal operating conditions. As mentioned above, this dissertation mainly focuses on internal fault conditions. These internal fault conditions can occur both in synchronous generators and induction generators. Usually, internal faults can be categorized as ground faults and phase faults.

A ground fault is a fault that creates a path for current to flow from one of the phases directly to the neutral through the earth bypassing the load [5]. To limit the level of the ground fault current, an impedance is connected between the generator neutral and the system ground. This impedance can be in the form of a resistor, an inductor or grounding transformer sized to ensure maximum ground fault current is limited.

A phase fault is a fault that happens within the three phase windings. Phase faults are serious because they involve high levels of energy that can damage the machine [6]. The common phase faults are: 1) Phase to phase faults; 2) Three phase faults; 3) Double phase to ground faults; 4) Single phase to ground faults and 5) Turn to turn faults. Generating unit phase faults must be immediately cleared.

For induction generators, they can experience the same ground faults and phase faults as discussed above.

2.3.2 Differential Protection

Differential protection may be considered the first line of protection for phase-to-phase or phase-to-ground faults. Lots of research has been done on the differential protection to protect machines [7]-[13]. In the event of such faults, the quick response of differential protection may limit the damage that may have otherwise occurred to the machine. The differential protection is of the percentage type due to the potentially very high currents during external faults. The illustration of machine differential protection is shown in Figure 2.4. The difference between the currents at neutral and at the terminal is measured, and the ratio of this current difference and the restraining current exceeding a certain threshold makes the relay to respond.

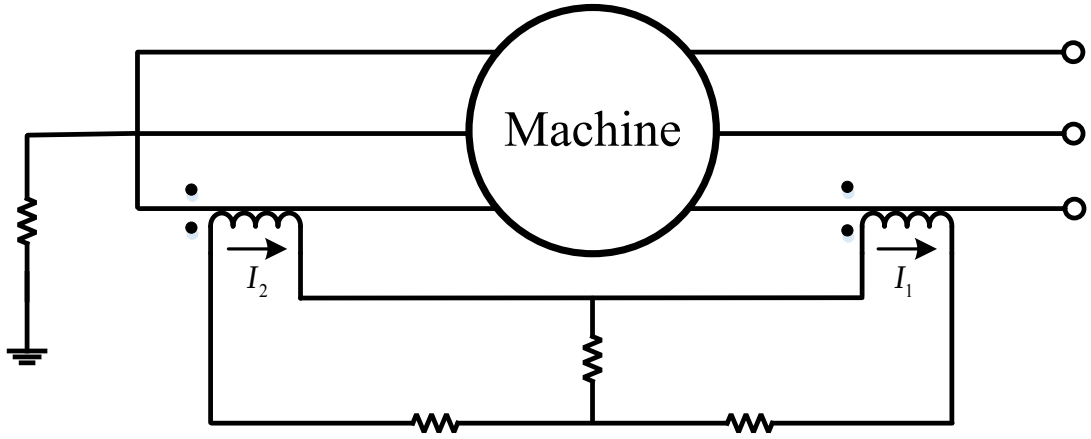

Figure 2.4. Machine Winding Differential Protection (One Phase)

Especially, the differential protection will trip the machine if two conditions are satisfied:

1) $(I_1 - I_2) > I_{\min}$ (2.1)

2) $\frac{(I_1 - I_2)}{I_{res}} > percetage\ threshold$ (2.2)

where $I_{\min}$ is the pickup current and I_{res} is the restraint current.

Some machines, due to physical construction, have windings that consist of multiple adjacent turns. It is therefore possible for faults to develop between turns on the same phase (inter-turn faults). These faults are not detected by the stator differential protection, as there is no difference between the currents at neutral side phase conductor and the phase conductor at the terminal side. In addition, if the fault is near the machine neutral, the fault may not be detected because it will produce current in the operating coil lower than the typical settings of the percentage differential relay settings. Typically, faults up to 10% of the coil from the generator neutral may not be detected.

2.3.3 Instantaneous/Time Overcurrent Protection

Overcurrent protection is applied for phase fault and ground fault protection [14]-[20]. It monitors the electric current in the secondary of the current transformer that connects to the device under protection and when this current exceeds a certain value the breaker trips this component. Instantaneous overcurrent protection is often used to limit the damage brought by high fault current to the machine. The setting for the pickup current should be greater than the locked-rotor starting current. To provide more sensitive overcurrent protection, time overcurrent protection could be used. The relay trigging criteria is the same as the instantaneous one with a delay. A lower pickup current is used for the time overcurrent relay to make the protection more sensitive. This sensitive time overcurrent protection is usually applied for backup protection of generators. However,

coordination among different protective functions can be difficult with multiple sources since the ground current magnitude will vary with addition or removal of sources [20]. In addition, faults like turn-to-turn faults and faults near neutral are still not 100% covered by the present protection technology.

2.3.4 Negative-Sequence Protection

Negative-sequence current or voltage protection is typically used to protect against machine unbalance conditions [21]-[30]. Asymmetrical faults generate negative-sequence currents that flow in the windings of the machine. These negative-sequence currents induce double line-frequency currents that flow in the damper or rotor parts. The magnitude of the double line-frequency depends on the location of the fault, number of turns shorted, mutual induction, and system and machine impedance. Usually machine is designed to tolerate negative-sequence currents for a short period of time. Specifically, machine can tolerate negative-sequence current for a time duration that meets the following rule:

$$I_2^2 t \le k \tag{2.3}$$

where k is a constant depending on machine design.

The operating region of negative-sequence current protection is illustrated in Figure 2.5.

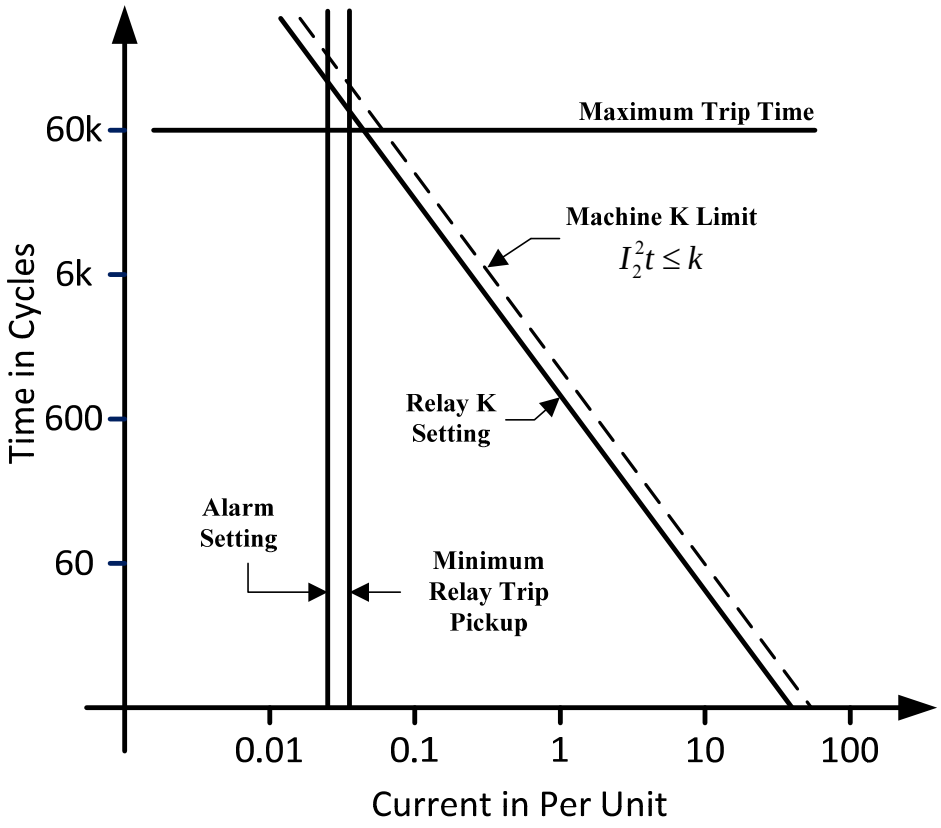

Figure 2.5. Negative-Sequence Current Protection Operating Region

2.3.5 Other Protection

Third-Harmonic Voltage-Based Machine Protection

Third-harmonic voltage components are present at the terminals of nearly every machine to varying degrees [1]. They arise due to the non-sinusoidal nature of rotor flux and vary based on the differences in design and manufacture. If a generator under normal operation has sufficient amount of third-harmonic voltage at the neutral and terminals, these third-harmonic voltages can be used to provide generator protection. The third-harmonic voltage at the neutral will drop when a fault near neutral occurs, and likewise the third-harmonic voltage at the terminal will drop when a fault near terminal occurs. Figure 2.6 shows the third-harmonic voltages present at the neutral and terminals of a

typical generator during different load conditions: (a) under normal operation, (b) for a fault at the neutral end, and (c) for a fault at the generator terminals.

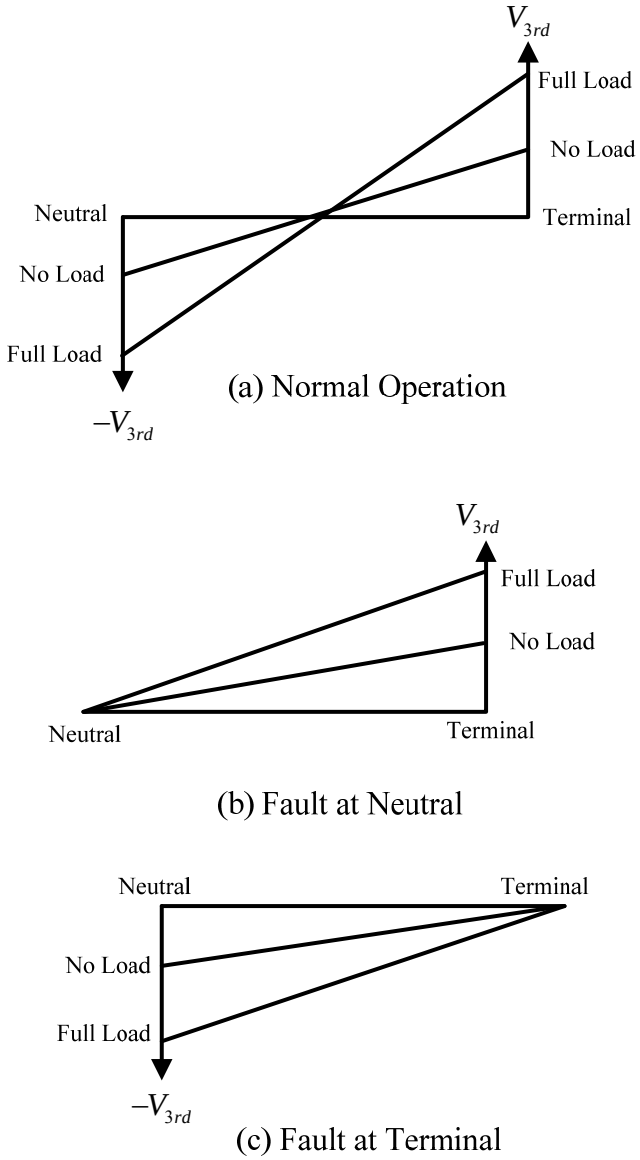

Figure 2.6. Third-Harmonic Voltage for Different Conditions in a Typical Generator [1]

Typical protection functions using third-harmonic voltage are: third-harmonic neutral undervoltage protection, third-harmonic terminal overvoltage protection and third-harmonic comparator (differential) protection [1], [31]-[37].

Third-harmonic neutral undervoltage technique uses the fact that for a fault near the neutral, the level of third-harmonic voltage at the neutral decreases. Therefore, an undervoltage relay operating from third-harmonic voltage measured at the neutral end could be used to detect the faults near the neutral.

Third-harmonic terminal overvoltage technique uses the fact that for a fault near the neutral, the level of third-harmonic voltage at the terminals increases. Therefore, an overvoltage relay using third-harmonic voltage measured at the terminals could be used to detect the faults near the neutral.

Third-harmonic comparator technique compares the magnitude of the third-harmonic voltage at the neutral to that at the terminals. The scheme is based on the premise that the ratio of the third-harmonic voltage at the terminals to that at the neutral remains constant during the normal operating conditions.

Usually the third-harmonic based protective function provides protection for stator ground winding up to 15% near neutral (which means the stator winding can be 100% covered with the coordination of other protective functions). However, it still cannot properly handle situations like machine shutdown or startup. Furthermore, sometimes when it is not fully loaded, the generator does not develop significant third-harmonic voltage which may result in protection failure.

Low Frequency Signal Injection Protection

Due to design variations, some machines may not produce sufficient third-harmonic voltages to apply the ground fault protection schemes based on third-harmonic signals. In addition, the ground fault protection cannot be applied when the machine is at standstill

because no third-harmonic signals exist at that time. Because the measurements are needed when machine is at standstill, they should be supplied by their own source and be immune to variable-frequency swept sine disturbances such as those present during generator ramp-up [1], [38]. As a result, low frequency signal injection protection was introduced [39]-[48].

Typically, a low frequency signal with fixed frequency (e.g. in range from 10Hz up to 25Hz) is used as an injection signal. Use 20Hz signal as an example, this signal is injected in the machine neutral. The resultant 20Hz current is measured. When a ground fault occurs, the 20Hz current increases and causes the function (64) to operate. Figure 2.7 is an illustration of low frequency signal injection protection using 20Hz signal.

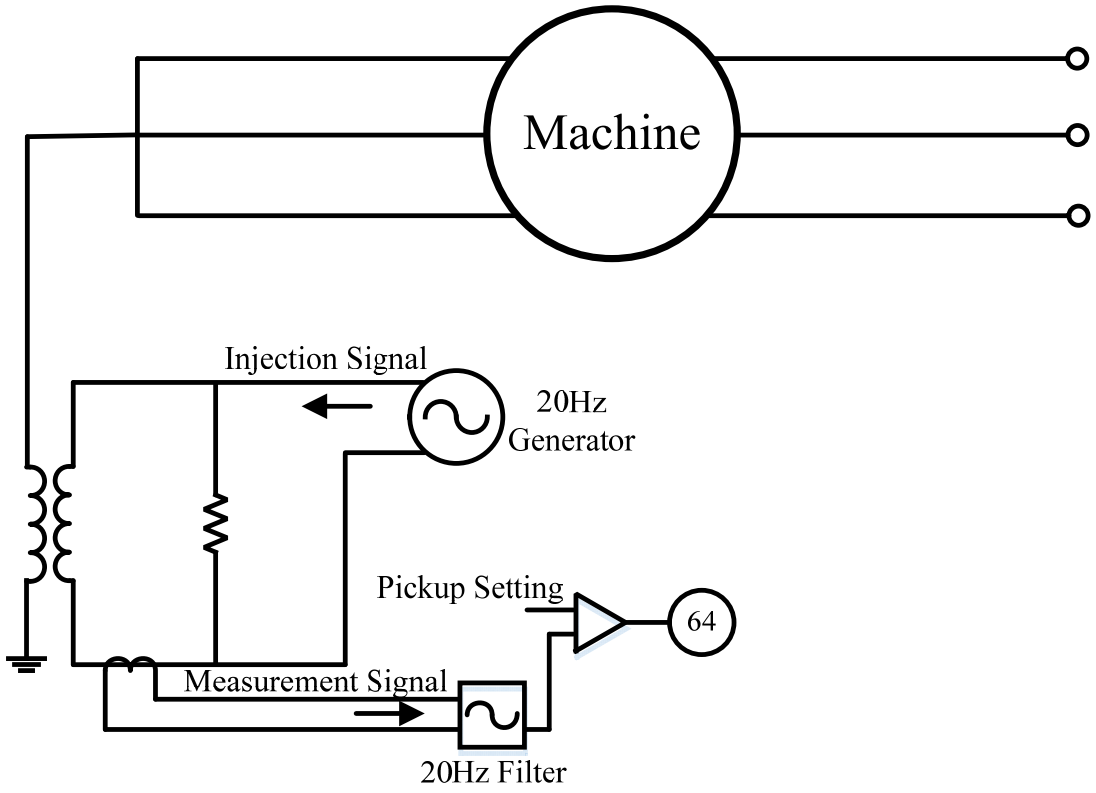

Figure 2.7. Low Frequency Signal Injection Protection

The use of low frequency signals offers improved sensitivity because of the higher impedance path of the machine capacitances at these frequencies. Also, the integration over a half cycle of the low frequency result in zero contributions from the signals of the system frequency and harmonics (i.e. 60Hz, 120Hz, 180Hz, etc.) and therefore do not influence the measurements. However, the high cost associated with providing and maintaining a reliable low frequency source is a big disadvantage.

2.4 Parameters Estimation of the Synchronous Machine

Accurate power system models of the dynamic elements are very important for optimal decision making, planning, efficient operation and protection of the power grid. Parameters of generators may differ from those in the utility's database due to aging processes, magnetic saturation, or changes of temperature during machine operation. As a matter of fact, many utilities around the world still use machine model parameters calculated during generator commissioning, leading to substantial differences between the actual and simulated dynamic behavior.

Many studies have been done to seek the best way to estimate the generator parameters. IEEE released Standard Procedures and Guide to obtain the synchronous generator parameters in [48], [49]. However, these methods can only be applied for the generator during offline status. When the generator is put into operation, the parameters may change again. Some other online approaches have been proposed by researchers in [50]-[53]. In [50], operational data from both steady state and disturbance operation are utilized to estimate the generator parameters. Reference [51] uses the least square algorithm to perform the parameter estimation from experimental data. In [52],

measurements from a hydro unit are used to extract the generator and exciter parameters. Reference [53] uses a simplified discrete auto-regression with an exogenous input model. Since it is a simplified model, it cannot represent the electromagnetic.

Among all the generator parameter estimation literatures (including [50]-[52]), most of them use the common synchronous generator dq0 model. The widely-used dq0 model is derived from the actual three phase model after applying Park's transformation. The application of Park's transformation reduces the three AC quantities to three DC quantities. In addition, it decouples the equations. Thus, the calculation can be simplified. However, the Park's transformation is carried out based on the assumption that the reference frame rotates at synchronous speed. So when frequency changes and there are imbalances, the dq0 model loses accuracy which is also amplified under asymmetrical or unbalanced generator conditions (which is quite normal when internal faults occur in the generator).

A more accurate approach to this problem is to model the synchronous generators with physical parameters, that is, the actual self and mutual inductances of the generator windings as a function of the rotor position. By this way, various loading conditions such as sudden application and removal of balanced and unbalanced loads, rectifier loads, and symmetrical and asymmetrical faults can be easily investigated.

2.5 Summary

This chapter presents an overall description and related work on the research topics of this dissertation. In particular, Section 2.2 gives a historical evolution of the protective relays. Section 2.3 provides a literature review of the legacy synchronous generator and

induction generator protection functions. Finally, in Section 2.4, the present state-of-the-art technology on generator parameters estimation is summarized.

CHAPTER 3 THE OVERALL APPROACH

3.1 Overview

In this chapter, a dynamic state estimation based protection (EBP) approach is proposed. It can be applied to any power components, and it needs very simple settings and no coordination with other protective functions.

The EBP protection method has been inspired from the fact that differential protection is one of the most secure protection schemes and it does not require coordination with other protection function. Differential protection simply monitors the validity of Kirchoff's current law in a device, i.e. the weighted sum of the currents going into a device must be equal to zero. This concept can be generalized into monitoring the validity of all other physical laws that the device must satisfy, such as Kirchoff's voltage law, Faraday's law, etc. Figure 3.1 depicts the general idea of the proposed EBP protective function. This monitoring can be done in a systematic way by the use of dynamic state estimation.

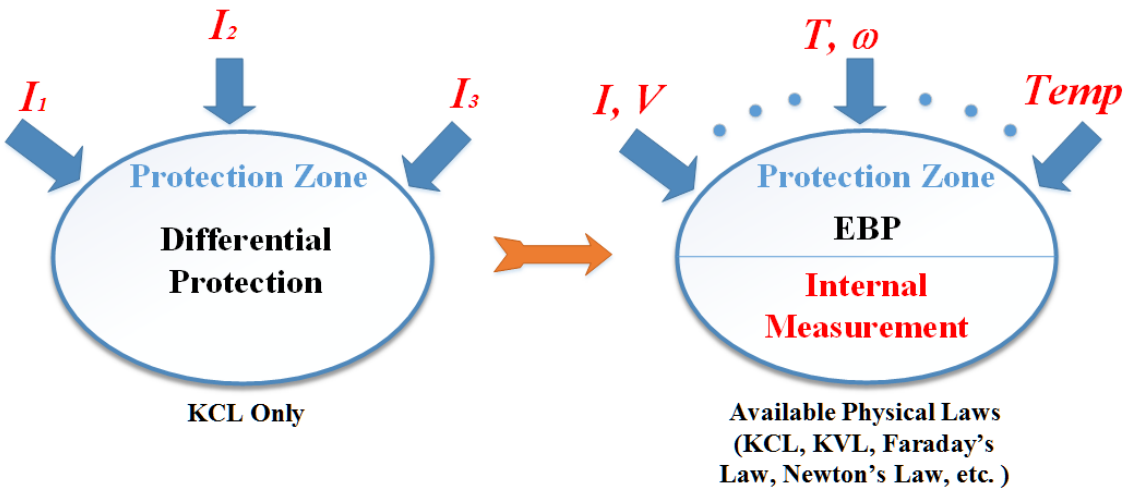

Figure 3.1. Concept of EBP Protective Function

Specifically, all the physical laws that a component must obey are expressed in the dynamic model of the component. Dynamic state estimation is used to continuously monitor the dynamic model of the component (zone) under protection. If any of the physical laws for the component under protection is violated, the dynamic state estimation will capture this condition. Thus, it is proposed to use dynamic state estimator to extract the dynamic model of the component under protection and to determine whether the physical laws for the component are satisfied. The dynamic model of the component accurately reflects the condition of the component and the decision to trip or not to trip the component is based on the condition of the component only irrespectively of the condition (faults, etc.) of other system components. Section 3.2 gives the detailed description of the proposed infrastructure.

3.2 The Proposed Infrastructure

The proposed EBP method requires a monitoring system of the component under protection that continuously measures terminal data (such as the terminal voltage, current), other variables such as temperature, speed, etc., as appropriate, and component status data (such as the tap setting, breaker status, etc.). For a three phase synchronous generator or an induction generator, the basic measurements are three terminal voltages, three terminal currents and mechanical speed of the shaft. If more measurements are available, the dynamic state estimation algorithm has more redundancy, which makes the algorithm more stable and accurate when facing the issues like bad data or missing measurements.

Details of the proposed infrastructure of the EBP machine protection are explained below. The inputs for the proposed EBP machine protection are machine SAQCF device model, machine measurement definition and real-time measurement (as shown in Figure 3.2). Machine SAQCF device model is the mathematical model of the machine after quadratization and quadratic integration [54]-[56]. The derivation of the SAQCF device model is addressed in the next section.

The measurement definition is the information about what the measurement is, i.e. it is Phase A to Phase N voltage, it is current flowing through Phase B, etc. Since location of meters is human selected, the measurement definition is quite easy to obtain.

The last input is the real-time measurements. It is utilized, within a dynamic state estimation algorithm, to track the machine dynamic model under protection. Measurement accuracy and measuring speed are two key points for the proposed protection scheme. With higher accuracy measurements, the dynamic state estimation provides more accurate estimation results. Meanwhile, faster measuring speed (higher sampling rate) could represent more accurate dynamic changing of machines.

By combining the first two inputs, the machine SAQCF measurement model is created. The purpose of creating this measurement model is to express each measurement as an algebraic combination of the machine states. Subsequently, the measurement model is used in the state estimation. The more measurements used in state estimation, the more redundancy the algorithm has. More details of the measurement model will be explained later in this chapter.

The machine measurement model is prepared before the on-line real-time protection starts and it will not change unless the machine condition or parameters are changed. The

proposed EBP function tries to fit the real-time measurements to this machine measurement model. Any mismatch indicates abnormalities inside the machine. The EBP algorithm and protection logic will be explained later.

The dynamic state estimation processes these measurements and extracts the real time dynamic model of the component and its operating conditions.

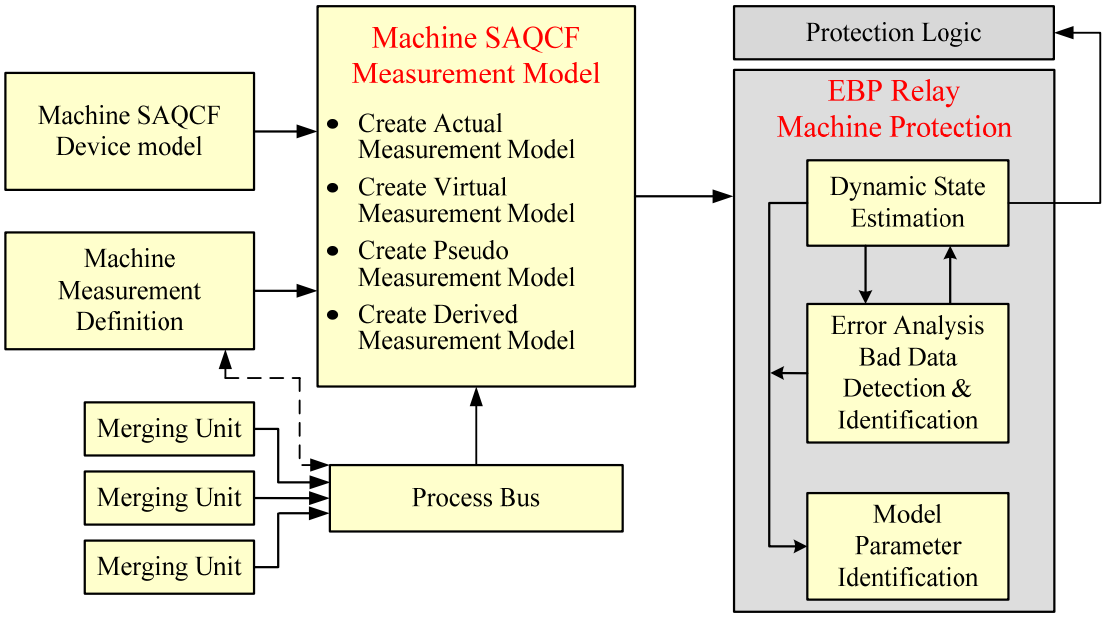

Figure 3.2. Illustration of EBP Machine Protection Scheme

In general, the proposed EBP approach can identify any internal abnormality of the protection zone within a cycle and trip the component immediately. It is important to note that the proposed scheme will perform best when: (a) the measurements are as accurate as possible - dependent on the type of instrument transformer used, i.e. VT, CT, etc. and the instrumentation channel, i.e. control cable, etc. and (b) the accuracy of the dynamic model of the component under protection. The measurement accuracy issue, while important, is beyond the scope of this dissertation. It will be addressed in the future work.

The model accuracy issue can be improved by performing the parameter estimation algorithm for the device under protection. It will be addressed later in this dissertation.

3.3 Summary

An overview of the proposed dynamic state estimation based protection scheme is provided in this chapter. The advantages of the proposed EBP method include: (1) it needs very few settings, which could greatly reduce the possibility of wrong or inappropriate settings for the legacy protective functions; (2) it has very fast fault detection speed (several samples after the fault occurs); (3) it needs no coordination with other protective functions (complex coordination always brings errors); (4) it is designed in an object-oriented way, which means it can easily be applied to any power components without any modification.

CHAPTER 4 OBJECT-ORIENTED MODELLING

4.1 Overview

To realize the object-oriented implementation of the dynamic state estimation based protection algorithm, the protection zone model for all the devices is required in a standard form. The standard form is defined as the State Algebraic Quadratic Companion Form (SAQCF), which is an object-oriented, interoperable, and unified syntax of any protection zone model. The SAQCF model is the result of applying the quadratic integration method to the quadratized model. The input required by the EBP algorithm is the protection zone measurement model in the SAQCF standard. The derivation of the SAQCF measurement model is shown step by step in this chapter.

Section 4.2 gives the general form of the protection zone model, which is basically derived from the protection zone physical circuit. Section 4.3 shows the derivation of the SAQCF device model from the model mentioned in Section 4.2. Section 4.4 introduces the measurement definition of the protection zone and Section 4.5 provides the SAQCF measurement model based on the SAQCF device model and measurement definition. Note that all the models are given in its general format, and the synchronous generator and induction generator device models are provide in Appendices.

4.2 The Quadratized Device Model

The quadratized device model (QDM) is used to represent the device physical model and it is a preliminary step to obtain the SAQCF model. The QDM is derived directly from the physical circuit of the power component. All the terms in the quadratized device

model are at most second order. The model can be developed in several forms. The specific model has been developed under the following requirements: (a) list all the linear equations for through variables (terminal currents) first; (b) list all the remaining linear equations; (c) all differential terms only appear in the linear equations; (d) list all the remaining quadratic equations; (e) the interface states must be listed at the beginning of the states and the interface states' order should be the same as terminal order; (f) the highest order of the model is second order. The requirements are always easily met by introduction of additional state variables.

The standard quadratized device model is shown below:

$$\mathbf{i}(t) = Y_{eqx1}\mathbf{x}(t) + D_{eqxd1}\frac{d\mathbf{x}(t)}{dt} + C_{eqc1}$$

$$0 = Y_{eqx2}\mathbf{x}(t) + D_{eqxd2}\frac{d\mathbf{x}(t)}{dt} + C_{eqc2}$$

$$0 = Y_{eqx3}\mathbf{x}(t) + \left\{ \begin{array}{c} \vdots \\ \mathbf{x}(t)^T \left\langle F^i_{eqxx3} \right\rangle \mathbf{x}(t) \\ \vdots \end{array} \right\} + C_{eqc3}$$

$$\mathbf{h}(\mathbf{x}) = Y_{feqx}\mathbf{x} + \left\{ \begin{array}{c} \vdots \\ \mathbf{x}^T \left\langle F^i_{feqxxx} \right\rangle \mathbf{x} \\ \vdots \end{array} \right\} + C_{feqc}$$

Connectivity: TerminalNodeName

Normalization Factors: StateNormFactor, ThroughNormFactor

$$subject\ to: \qquad \mathbf{h}_{\min} \le \mathbf{h}(\mathbf{x}) \le \mathbf{h}_{\max}$$

where:

$\mathbf{i}(t)$: the through variables of the device model

$\mathbf{x}(t)$: external and internal state variables of the device model

Y_{eqx1} : matrix defining the linear part for state variables in linear through variable equations,

D_{eqxd1} : matrices defining the differential part for state variables in linear through variable equations,

C_{eqc1} : constant vector of the device model in linear through variable equations,

Y_{eqx2} : matrix defining the linear part for state variables in linear virtual equations,

D_{eqxd2} : matrices defining the differential part for state variables in linear virtual equations,

C_{eqc2} : constant vector of the device model in linear virtual equations,

Y_{eqx3} : matrix defining the linear part for state variables in the remaining quadratic equations,

C_{eqc3} : constant vector of the device model in the remaining quadratic equations,

F_{eqxx}: matrices defining the quadratic part for state variables in the remaining quadratic equations,

TerminalNodeName: terminal names defining the connectivity of the device model,

StateNormFactor: Normalization Factors for the states

ThroughNormFactor: Normalization Factors for the through and zero variables

$\mathbf{h}_{\min} \le \mathbf{h}(\mathbf{x}) \le \mathbf{h}_{\max}$: functional constraints,

$\mathbf{x}_{\min}, \mathbf{x}_{\max}$: lower and upper bounds for the state variables.

Y_{feqx} : constraint matrix defining the linear part for state variables,

F_{feqx} : constraint matrices defining the quadratic part for state variables,

C_{feqc} : constraint history dependent vector of the device model.

4.3 The State Algebraic Quadratic Companion Form Device Model

Since the differential equations in the quadratized device model cannot be solved using symbolic computation (algebraic computation), numerical integration method is often used to find numerical approximations to the solution of the differential equations. Quadratic integration method [54] is used in this dissertation to convert the differential terms into algebraic form in the quadratized device model. After applying the quadratic integration, the state algebraic quadratic companion form device model can be obtained.

Quadratic integration assumes the variable varies quadratically over the integration period. Figure 4.1 illustrates the concept of the quadratic integration.

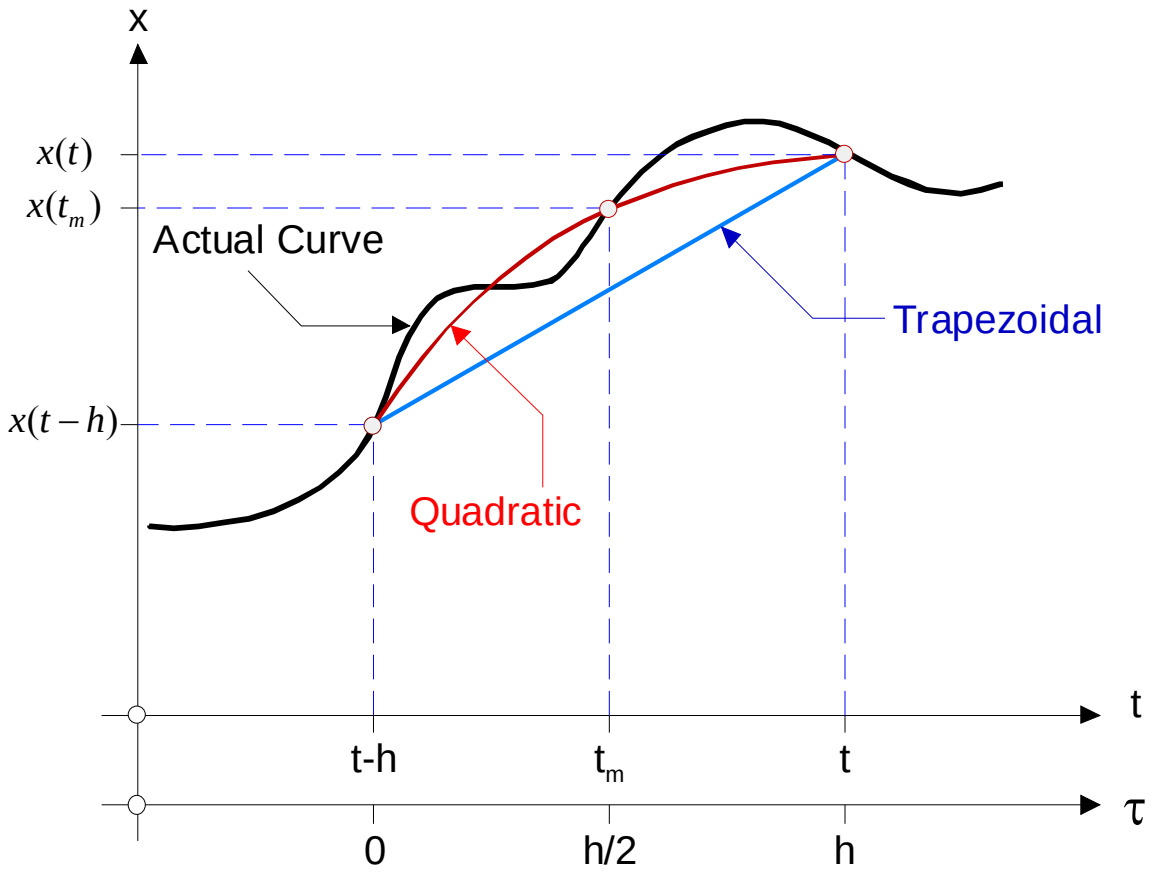

Figure 4.1. Illustration of EBP Quadratic Integration

Note that the three points $x(t-h)$, $x(t_m)$ and $x(t)$ on the curve fully define the quadratic function in the interval $[t-h, t]$. t_m is the midpoint of t and $t-h$, and h is the time step. The general integration results over time intervals $[t-h, t_m]$ and $[t-h, t]$ are listed as follows:

$$\int_{t-h}^{t} x(\tau)d\tau = \frac{h}{6}x(t-h) + \frac{2h}{3}x(t_m) + \frac{h}{6}x(t)$$

$$\int_{t-h}^{t_m} x(\tau)d\tau = \frac{5h}{24}x(t-h) + \frac{h}{3}x(t_m) - \frac{h}{24}x(t)$$

This quadratic integration method is applied to all equation sets of the quadratized device model to derive the SAQCF device model. Since there are three sets of equations, each one is analyzed below to show how they can be transferred to SCAQCF model.

1) Through variable equations:

$$\mathbf{i}(t) = Y_{eqx1}\mathbf{x}(t) + D_{eqxd1}\frac{d\mathbf{x}(t)}{dt} + C_{eqc1}$$

After applying quadratic integration, it becomes:

From time $t-h$ to t,

$$\mathbf{i}(t) = (\frac{4}{h}D_{eqxd1} + Y_{eqx1})\mathbf{x}(t) - \frac{8}{h}D_{eqxd1}\mathbf{x}(t_m) + (\frac{4}{h}D_{eqxd1} - Y_{eqx1})\mathbf{x}(t-h) + \mathbf{i}(t-h)$$

From time $t-h$ to t_m,

$$\mathbf{i}(t_m) = \frac{1}{2h}D_{eqxd1}\mathbf{x}(t) + (\frac{2}{h}D_{eqxd1} + Y_{eqx1})\mathbf{x}(t_m) + (\frac{1}{2}Y_{eqx1} - \frac{5}{2h}D_{eqxd1})\mathbf{x}(t-h) - \frac{1}{2}\mathbf{i}(t-h) + \frac{3}{2}C_{eqc1}$$

2) Linear virtual equations:

$$0 = Y_{eqx2}\mathbf{x}(t) + D_{eqxd2}\frac{d\mathbf{x}(t)}{dt} + C_{eqc2}$$

After applying quadratic integration, it becomes:

From time $t-h$ to t,

$$0=(\frac{4}{h}D_{eqxd1}+Y_{eqx1})\mathbf{x}(t)-\frac{8}{h}D_{eqxd1}\mathbf{x}(t_m)+(\frac{4}{h}D_{eqxd1}-Y_{eqx1})\mathbf{x}(t-h)$$

From time $t-h$ to t_m,

$$0=\frac{1}{2h}D_{eqxd1}\mathbf{x}(t)+(\frac{2}{h}D_{eqxd1}+Y_{eqx1})\mathbf{x}(t_m)+(\frac{1}{2}Y_{eqx1}-\frac{5}{2h}D_{eqxd1})\mathbf{x}(t-h)+\frac{3}{2}C_{eqc1}$$

3) Nonlinear equations

$$0=Y_{eqx3}\mathbf{x}(t)+\left\{\begin{array}{c}\vdots\\ \mathbf{x}(t)^T\left\langle F^i_{eqxx3}\right\rangle\mathbf{x}(t)\\ \vdots\end{array}\right\}+C_{eqc3}$$

Since this set does not have any differential terms, these equations are the same under time t and time t_m:

$$0=Y_{eqx3}\mathbf{x}(t)+\left\{\begin{array}{c}\vdots\\ \mathbf{x}(t)^T\left\langle F^i_{eqxx3}\right\rangle\mathbf{x}(t)\\ \vdots\end{array}\right\}+C_{eqc3}$$

$$0=Y_{eqx3}\mathbf{x}(t_m)+\left\{\begin{array}{c}\vdots\\ \mathbf{x}(t_m)^T\left\langle F^i_{eqxx3}\right\rangle\mathbf{x}(t_m)\\ \vdots\end{array}\right\}+C_{eqc3}$$

By restructuring and stacking the above three sets of equations into one matrix form, the standard SAQCF device model is derived as follows:

$$\begin{Bmatrix} \mathbf{i}(t) \\ 0 \\ 0 \\ \mathbf{i}(t_m) \\ 0 \\ 0 \end{Bmatrix} = Y_{eqx}\mathbf{x} + \begin{Bmatrix} \vdots \\ \mathbf{x}^T \left\langle F^i_{eqx} \right\rangle \mathbf{x} \\ \vdots \end{Bmatrix} + N_{eqx}\mathbf{x}(t-h) + M_{eq}\mathbf{i}(t-h) + K_{eq}$$

$$\mathbf{h}(\mathbf{x}) = Y_{feqx}\mathbf{x} + \begin{Bmatrix} \vdots \\ \mathbf{x}^T \left\langle F^i_{feqxxx} \right\rangle \mathbf{x} \\ \vdots \end{Bmatrix} + C_{feqc}$$

Connectivity: TerminalNodeName

Normalization Factors: StateNormFactor, ThroughNormFactor

$$\textit{subject to}: \qquad \mathbf{h}_{\min} \le \mathbf{h}(\mathbf{x}) \le \mathbf{h}_{\max}$$

The normalization factors, functional constraints and variable limits are the same as in the quadratized model.

where: $Y_{eqx} = \begin{bmatrix} \frac{4}{h}D_{eqxd1} + Y_{eqx1} & -\frac{8}{h}D_{eqxd1} \\ \frac{4}{h}D_{eqxd2} + Y_{eqx2} & -\frac{8}{h}D_{eqxd2} \\ Y_{eqx3} & 0 \\ \frac{1}{2h}D_{eqxd1} & \frac{2}{h}D_{eqxd1} + Y_{eqx1} \\ \frac{1}{2h}D_{eqxd2} & \frac{2}{h}D_{eqxd2} + Y_{eqx2} \\ 0 & Y_{eqx3} \end{bmatrix}$ $\qquad F_{eqx} = \begin{bmatrix} 0 & 0 \\ 0 & 0 \\ F_{eqxx3} & 0 \\ 0 & 0 \\ 0 & 0 \\ 0 & F_{eqxx3} \end{bmatrix}$

$$N_{eqx} = \begin{bmatrix} -Y_{eqx1} + \frac{4}{h} D_{eqxd1} \\ -Y_{eqx2} + \frac{4}{h} D_{eqxd2} \\ 0 \\ \frac{1}{2} Y_{eqx1} - \frac{5}{2h} D_{eqxd1} \\ \frac{1}{2} Y_{eqx2} - \frac{5}{2h} D_{eqxd2} \\ 0 \end{bmatrix} \qquad M_{eq} = \begin{bmatrix} I_{size(i(t))} \\ 0 \\ 0 \\ \frac{1}{2} I_{size(i(t))} \\ 0 \\ 0 \end{bmatrix} \qquad K_{eq} = \begin{bmatrix} 0 \\ 0 \\ C_{eqc3} \\ \frac{3}{2} C_{eqc1} \\ \frac{3}{2} C_{eqc2} \\ C_{eqc3} \end{bmatrix}$$

$\mathbf{i}(t)$ *and* $\mathbf{i}(t_m)$: the through variables of the device model

$\mathbf{x}$: external and internal state variables of the device model, $\mathbf{x} = [\mathbf{x}(t), \mathbf{x}(t_m)]$

Y_{eqx}: matrix defining the linear part for state variables,

F_{eqx}: matrices defining the quadratic part for state variables,

N_{eqx}: matrix defining the last integration step state variables part,

N_{equ}: matrix defining the last integration step control variables part,

M_{eq}: matrix defining the last integration step through variables part,

K_{eq}: constant vector of the device model,

TerminalNodeName: terminal names defining the connectivity of the device model,

StateNormFactor: Normalization Factors for the states

ThroughNormFactor: Normalization Factors for the through and zero variables

$\mathbf{h}_{\min} \le \mathbf{h}(\mathbf{x}) \le \mathbf{h}_{\max}$: functional constraints,

Y_{feqx}: constraint matrix defining the linear part for state variables,

F_{feqx}: constraint matrices defining the quadratic part for state variables,

C_{feqc} : constraint history dependent vector of the device model.

4.4 The Measurement Definition

Four types of measurements are introduced in this dissertation: (1) actual measurements; (2) pseudo measurements; (3) derived measurements and (4) virtual measurements [57].

Actual measurements are physical quantities which can be obtained directly from meters such as instrument transformers/relays, merging units and others; These measurements contain certain errors based on meter accuracy.

Pseudo measurements are hypothetical measurements that their expected values are known. An example is the neutral voltage for a grounded network. Since these measurements are not physically measured, they may contain larger errors.

Derived measurements are also physical quantities, which are derived from actual measurements. An example is shown in Figure 4.2. The derived measurements have the same uncertainty as the actual measurements.

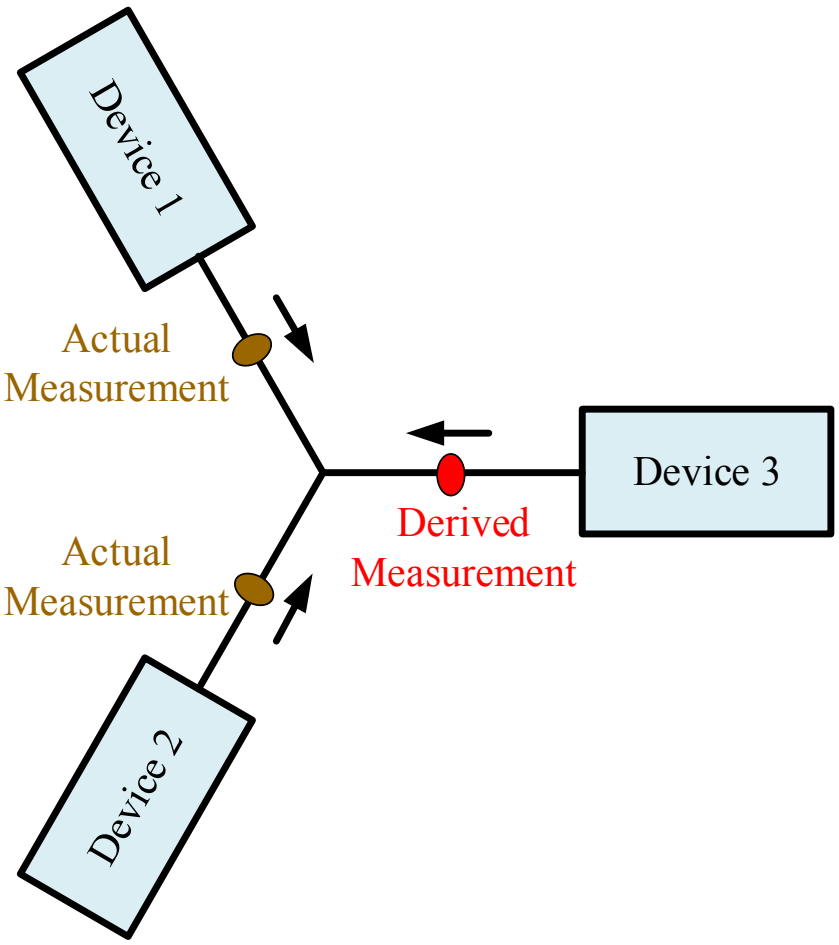

Figure 4.2. Illustration of Derived Measurements

Virtual measurements are not real measurements but rather quantities that are defined by the physical laws that the protection zone must obey, such as Kirchoff's current or voltage law. These measurements do not have any errors because the physical laws should be obeyed strictly.

4.5 The State Algebraic Quadratic Companion Form Measurement Model

Any type of measurement can obtain its mathematical expression from the measurement definition and SAQCF device model.

For any actual measurement (e.g. terminal voltage, terminal current, speed, torque, etc.), it can always be expressed as a combination of the protection zone states. Specifically, the actual across measurements (e.g. terminal voltage and speed), they can be expressed as:

$$z_{actual\_across} = h(x) + \eta = \sum_i a_{i,t,x} \cdot x_i(t) + \sum_i a_{i,t_m,x} \cdot x_i(t_m) + \eta$$

The actual through measurements (e.g. terminal current and torque), they can be expressed as a function of the states:

$$z_{actual\_through}(t) = h(x) + \eta = \sum_i a_{i,t,x} \cdot x_i(t) + \sum_i a_{i,t_m,x} \cdot x_i(t_m) + \sum_{i,j} b_{i,j,t,x} \cdot x_i(t) \cdot x_j(t) + \sum_{i,j} b_{i,j,t_m,x} \cdot x_i(t_m) \cdot x_j(t_m) + c(t) + \eta$$

For any pseudo measurement, it is always a combination of all the states:

$$z_{pseudo}(t) = h(x) + \eta = \sum_i a_{i,t,x} \cdot x_i(t) + \sum_i a_{i,t_m,x} \cdot x_i(t_m) + \sum_{i,j} b_{i,j,t,x} \cdot x_i(t) \cdot x_j(t) + \sum_{i,j} b_{i,j,t_m,x} \cdot x_i(t_m) \cdot x_j(t_m) + c(t) + \eta$$

For any derived measurement, it has the same expression as the actual measurements.

For any virtual measurement, it can be obtained from the SAQCF device model because the zero term equations of the SAQCF device model are all the physical laws that the protection zone should obey. They can be summarized as follows:

$$z_{virtual}(t) = 0 = h(x) + \eta = \sum_i a_{i,t,x} \cdot x_i(t) + \sum_i a_{i,t_m,x} \cdot x_i(t_m) + \sum_{i,j} b_{i,j,t,x} \cdot x_i(t) \cdot x_j(t) + \sum_{i,j} b_{i,j,t_m,x} \cdot x_i(t_m) \cdot x_j(t_m) + c(t) + \eta$$

In summary, any measurement in the above categories can be viewed as an object that consists of the measured value and a corresponding function that expresses the measurement as a function of state. In general, the mathematical functions for the all the measurements can be written into a matrix formation. For the purpose of introducing the

state estimation methods, the actual, pseudo and derived measurements are summarized into one matrix equation and the virtual measurements are summarized into another matrix equation. The two matrix equations are provided below:

SAQCF measurement model for the actual, pseudo and derived measurements:

$$\mathbf{h}_{w/o\_virtual}(\mathbf{x}) = Y_{mx}\mathbf{x} + \begin{Bmatrix} \vdots \\ \mathbf{x}^T \left\langle F_{mx} \right\rangle \mathbf{x} \\ \vdots \end{Bmatrix} + N_{m,x}\mathbf{x}(t-h) + M_m\mathbf{z}(t-h) + \mathbf{K}_m \tag{4.1}$$

SAQCF measurement model for the virtual measurements:

$$0 = \mathbf{g}(\mathbf{x}) = Y^v_{mx}\mathbf{x} + \begin{Bmatrix} \vdots \\ \mathbf{x}^T \left\langle F^v_{mx} \right\rangle \mathbf{x} \\ \vdots \end{Bmatrix} + N^v_{mx}\mathbf{x}(t-h) + \mathbf{K}^v_m \tag{4.2}$$

These are the models that will be used for the state estimation protection algorithm (see next chapter).

4.6 Summary

The general mathematical formulation and derivation of the SAQCF device and measurement models for power system components are presented in this chapter. The SAQCF measurement model is derived from the SAQCF device model and measurement definition. The dynamic state estimation protection algorithm (which will be introduced in the next chapter) uses the SAQCF measurement model directly for the protection purpose.

CHAPTER 5 DYNAMIC STATE ESTIMATION BASED PROTECTION

5.1 Overview

A dynamic state Estimation Based Protection (EBP) algorithm is proposed, which leverages dynamic state estimation to monitor the consistency between the protection zone SAQCF measurement model and the real-time measurements. Three state estimation methods (unconstrained weighted least square method, constrained weighted least square method and Extended Kalman Filter method) are introduced first, then the protection logic follows.

5.2 Dynamic State Estimation

Three dynamic state estimation algorithms are introduced in this section. They are: unconstrained weighted least square method, constrained weighted least square method and Extended Kalman Filter method.

5.2.1 Unconstrained Weighted Least Square Method

The first algorithm is a weighted least square that minimizes the objective function consisting of the squared normalized residuals of all measurements including virtual measurements:

$$Minimize \quad J_1(\mathbf{x}) = \left[\mathbf{z} - \mathbf{h}(\mathbf{x})\right]^T W \left[\mathbf{z} - \mathbf{h}(\mathbf{x})\right]$$

where:

$\mathbf{z}$: combination of the actual measurements, derived measurements, pseudo measurements and virtual measurements.

$\mathbf{h}(\mathbf{x})$: the mathematical expression for all the measurements which are obtained from equation (4.1) and equation (4.2):

$$\mathbf{h}(\mathbf{x}) = \begin{bmatrix} \mathbf{h}_{w/o\_virtual}(\mathbf{x}) \\ \mathbf{g}(\mathbf{x}) \end{bmatrix} = \begin{bmatrix} Y_{mx}\mathbf{x} + \begin{Bmatrix} \vdots \\ \mathbf{x}^T \left\langle F_{mx} \right\rangle \mathbf{x} \\ \vdots \end{Bmatrix} + N_{m,x}\mathbf{x}(t-h) + M_m\mathbf{z}(t-h) + \mathbf{K}_m \\ Y_{mx}^v\mathbf{x} + \begin{Bmatrix} \vdots \\ \mathbf{x}^T \left\langle F_{mx}^v \right\rangle \mathbf{x} \\ \vdots \end{Bmatrix} + N_{mx}^v\mathbf{x}(t-h) + \mathbf{K}_m^v \end{bmatrix} \tag{5.1}$$

W is the weighted matrix to normalize the residuals. The weighted matrix should reflect the noise statistics of the measurements. Typically it is assumed that noises are white and independent for each instrumentation channel, so that the standard deviation is used on the weights of each physical measurements, and the weight matrix should be diagonal. For example, if the standard deviation is 0.01 per unit, then the weight on W is $(1/(0.01)^2)$. However, the weights for pseudo and virtual measurements need to be tailored. For example, pseudo measurements may be the neutral voltage of one protection zone which is usually not measured. Its typical value is 0 given a nearby solid or low-impedance grounded transformer, thus the weight $(1/(0.1)^2)$ is assigned. In this algorithm virtual measurements are treated as data with higher accuracy, so that the weight $(1/(0.001)^2)$ is assigned for virtual measurements.

The solution is obtained by Newton's iterative method until it meets convergence criteria:

$$\hat{\mathbf{x}}^{j+1} = \hat{\mathbf{x}}^j + \left(H^T W H\right)^{-1} H^T W \left(\mathbf{z} - \mathbf{h}\left(\hat{\mathbf{x}}^j\right)\right) \tag{5.2}$$

where H is the Jacobean matrix: $H = \dfrac{\partial \mathbf{h}}{\partial \mathbf{x}}$

$$H = \frac{\partial \mathbf{h}(\mathbf{x})}{\partial \mathbf{x}} = \begin{bmatrix} \vdots \\ Y_{m,x} + \left\{ \mathbf{x}^T F_{m,x} + F_{m,x}\mathbf{x} \right\} \\ \vdots \\ \vdots \\ Y^{v}_{m,x} + \left\{ \mathbf{x}^T F^{v}_{m,x} + F^{v}_{m,x}\mathbf{x} \right\} \\ \vdots \end{bmatrix}$$

5.2.2 Constrained Weighted Least Square Method

The second algorithm is also a weighted least square that minimizes the following objective function consisting of the squared normalized residuals of all measurements excluding virtual measurements:

$$\textit{Minimize} \quad J_2(\mathbf{x}) = \left[\mathbf{z}_{w/o\_virtual} - \mathbf{h}_{w/o\_virtual}(\mathbf{x}) \right]^T W \left[\mathbf{z}_{w/o\_virtual} - \mathbf{h}_{w/o\_virtual}(\mathbf{x}) \right]$$

by subjecting to the virtual measurements:

$$0 = \mathbf{g}(\mathbf{x}) = Y^{v}_{mx}\mathbf{x} + \begin{Bmatrix} \vdots \\ \mathbf{x}^T \left\langle F^{v}_{mx} \right\rangle \mathbf{x} \\ \vdots \end{Bmatrix} + N^{v}_{mx}\mathbf{x}(t-h) + \mathbf{K}^{v}_{m}$$

where $\mathbf{z}_{w/o\_virtual}$ is the measurement vector without virtual measurements and $\mathbf{g}(\mathbf{x})$ is the mathematical expressions for virtual measurements extracted from SAQCF device model.

The solution is obtained by forming Lagrangian function:

$$L(\mathbf{x}, \boldsymbol{\lambda}) = J(\mathbf{x}) + 2\boldsymbol{\lambda}^T g(\mathbf{x})$$

with the necessary condition as:

$$\frac{\partial L(\mathbf{x}, \boldsymbol{\lambda})}{\partial \mathbf{x}} = -2\mathbf{z}^T W \frac{\partial h(\mathbf{x})}{\partial \mathbf{x}} + 2h(\mathbf{x})^T W \frac{\partial h(\mathbf{x})}{\partial \mathbf{x}} + 2\boldsymbol{\lambda}^T \frac{\partial g(\mathbf{x})}{\partial \mathbf{x}} = 0$$

$$\frac{\partial L(\mathbf{x},\boldsymbol{\lambda})}{\partial \boldsymbol{\lambda}} = 2g^T(\mathbf{x}) = 0$$

such that the updated equation for each iteration by neglecting second and higher order terms is:

$$\begin{bmatrix} \mathbf{x}^{v+1} \\ \boldsymbol{\lambda}^{v+1} \end{bmatrix} = \begin{bmatrix} \mathbf{x}^{v} \\ \boldsymbol{\lambda}^{v} \end{bmatrix} - \begin{bmatrix} H^T W H & G^T \\ G & 0 \end{bmatrix}^{-1} \begin{bmatrix} H^T W(\mathbf{h}_{w/o\_virtual}(\mathbf{x}^v) - \mathbf{z}_{w/o\_virtual}) \\ \mathbf{g}(\mathbf{x}^v) \end{bmatrix}$$

where H is the Jacobean matrix: $H = \dfrac{\partial \mathbf{h}_{w/o\_virtual}}{\partial \mathbf{x}}$

$$H = \frac{\partial \mathbf{h}_{w/o\_virtual}(\mathbf{x})}{\partial \mathbf{x}} = Y_{m,x} + \begin{Bmatrix} \vdots \\ \mathbf{x}^T F_{m,x} + F_{m,x}\mathbf{x} \\ \vdots \end{Bmatrix}$$

G is the Jacobean matrix: $G = \dfrac{\partial \mathbf{g}}{\partial \mathbf{x}}$

$$G = \frac{\partial \mathbf{g}(\mathbf{x}^v)}{\partial \mathbf{x}} = Y^v_{m,x} + \begin{Bmatrix} \vdots \\ \mathbf{x}^T F^v_{m,x} + F^v_{m,x}\mathbf{x} \\ \vdots \end{Bmatrix}$$

5.2.3 Extended Kalman Filter Method

The Kalman filter has been identified as the minimum variance filter for linear state space models with Gaussian white noise or the minimum linear variance filter with non-Gaussian white noises. To apply the extended Kalman filter method, the quadratized device model introduce in Section 4.2 is first reorganized as:

$$\begin{cases} \dfrac{d\mathbf{x}_1(t)}{dt} = Y_{EKFx1}\begin{bmatrix}\mathbf{x}_1(t)\\ \mathbf{x}_2(t)\end{bmatrix} + Y_{EKFi1}\begin{bmatrix}\mathbf{i}_1(t)\\ 0\end{bmatrix} + C_{EKF1} \\ 0 = -\begin{bmatrix}\mathbf{i}_2(t)\\ 0\end{bmatrix} + Y_{EKF2}\begin{bmatrix}\mathbf{x}_1(t)\\ \mathbf{x}_2(t)\end{bmatrix} + \left\{\begin{matrix}\vdots \\ \begin{bmatrix}\mathbf{x}_1(t)\\ \mathbf{x}_2(t)\end{bmatrix}^T \left\langle F_{EKF2}^i \right\rangle \begin{bmatrix}\mathbf{x}_1(t)\\ \mathbf{x}_2(t)\end{bmatrix} \\ \vdots \end{matrix}\right\} + C_{EKF2} \end{cases}$$

where $\mathbf{x}_1(t)$ is the dynamic states, $\mathbf{x}_2(t)$ is the static states. Then the protection zone model and measurements are discretized:

$$\begin{cases} \mathbf{x}_{1,k} = Y_{EKFx1}\mathbf{x}_{1,k-1} + Y_{EKFx2}\begin{bmatrix}\mathbf{x}_{2,k}\\ \mathbf{x}_{2,k-1}\end{bmatrix} + D_{EKFi1,k}\begin{bmatrix}\mathbf{i}_{1,k}\\ \mathbf{i}_{1,k-1}\end{bmatrix} + C_{EKF1} \\ 0 = -\begin{bmatrix}\mathbf{i}_{2,k}\\ 0\end{bmatrix} + Y_{EKF2}\begin{bmatrix}\mathbf{x}_{1,k}\\ \mathbf{x}_{2,k}\end{bmatrix} + \left\{\begin{matrix}\vdots \\ \begin{bmatrix}\mathbf{x}_{1,k}\\ \mathbf{x}_{2,k}\end{bmatrix}^T \left\langle F_{EKF2}^i \right\rangle \begin{bmatrix}\mathbf{x}_{1,k}\\ \mathbf{x}_{2,k}\end{bmatrix} \\ \vdots \end{matrix}\right\} + C_{EKF2} \end{cases}$$

$$\mathbf{z}_k = h(\mathbf{x}_{1,k}, \mathbf{x}_{2,k}) = Y_{m,x}\begin{bmatrix}\mathbf{x}_{1,k}\\ \mathbf{x}_{2,k}\end{bmatrix} + \left\{\begin{matrix}\vdots \\ \begin{bmatrix}\mathbf{x}_{1,k}\\ \mathbf{x}_{2,k}\end{bmatrix}^T F_{m,x}^i \begin{bmatrix}\mathbf{x}_{1,k}\\ \mathbf{x}_{2,k}\end{bmatrix} \\ \vdots \end{matrix}\right\} + D_{m,x}\begin{bmatrix}\mathbf{x}_{1,k}\\ \mathbf{x}_{1,k-1}\end{bmatrix} + C_m$$

where Y_{EKFx1} , Y_{EKFx2} and other matrices are the coefficient matrices of discretized protection zone model. The current measurement vector **i** and virtual measurement vector 0 are used as control inputs since it involves previous states. Finally, the extended Kalman filter method is applied with a two-step prediction-correction procedure to solve the state estimation problem:

Prediction:

$$\begin{cases} \mathbf{x}_{1,k}^{-} = Y_{d,EKFx1}\mathbf{x}_{1,k-1} + Y_{d,EKFx2}\begin{bmatrix} \mathbf{x}_{2,k}^{-} \\ \mathbf{x}_{2,k-1} \end{bmatrix} + D_{EKFi1,k}\begin{bmatrix} \mathbf{i}_{1,k} \\ \mathbf{i}_{1,k-1} \end{bmatrix} + C_{EKF1} \\ 0 = -\begin{bmatrix} \mathbf{i}_{2,k} \\ 0 \end{bmatrix} + Y_{EKF2}\begin{bmatrix} \mathbf{x}_{1,k}^{-} \\ \mathbf{x}_{2,k}^{-} \end{bmatrix} + \begin{Bmatrix} \vdots \\ \begin{bmatrix} \mathbf{x}_{1,k}^{-} \\ \mathbf{x}_{2,k}^{-} \end{bmatrix}^T \left\langle F_{EKF2}^{i} \right\rangle \begin{bmatrix} \mathbf{x}_{1,k}^{-} \\ \mathbf{x}_{2,k}^{-} \end{bmatrix} \\ \vdots \end{Bmatrix} + C_{EKF2} \\ P_k^{-} = Y_{d,EKFx1}P_{k-1}Y_{d,EKFx1}^{T} + Q_k \end{cases}$$

Correction:

$$\begin{cases} K_k = P_k^{-}H_k^{T}(H_k P_k^{-} H_k^{T} + R_k)^{-1} \\ \mathbf{x}_{1,k} = \mathbf{x}_{1,k}^{-} + K_k\left(\mathbf{z}_k - h\left(\mathbf{x}_{1,k}^{-}, \mathbf{x}_{2,k}^{-}\right)\right) \\ P_k = \left(I - K_k H_k\right)P_k^{-} \end{cases}$$

where

H_k : Jacobian matrix $H_k = \dfrac{\partial h(\mathbf{x}_{1,k}, \mathbf{x}_{2,k})}{\partial \mathbf{x}}$

P_k^{-} : Prior state covariance

P_k : Post state covariance

K_k : Kalman gain

Q_k : Process noise

R_k : Measurement noise

5.3 Protection Logic

The solution of the dynamic state estimation provides the best estimate of the protection zone states. The well-known Chi-square test provides the probability that the

measurements are consistent with the dynamic measurement model of the protection zone. Thus the Chi-square test quantifies the goodness of fit between the model and measurements (i.e., confidence level). The goodness of fit is expressed as the probability that the measurement errors are distributed within their expected range (Chi-square distribution). The Chi-square test requires two parameters: the degree of freedom (v) and the Chi-square critical value (ξ).The Chi-square value is calculated as follows:

$$\xi = \sum_i \left(\frac{h_i(x) - z_i}{\sigma_i}\right)^2$$

where

$h(x)$: calculated measurements with the best estimate from dynamic state estimation

z : value of real-time measurement

σ : standard deviation of the measurement error corresponds to the meter error specification.

Using the Chi-square value, the confidence level (or probability) that the measurements and the measurement model fit together within the accuracy of the meters is computed with:

$$Pr[\chi^2 \geq \xi] = 1 - Pr[\chi^2 \leq \xi] = 1 - Pr(\xi, v)$$

where v is the degree of freedom, which is the difference between the number of measurements and states.

The proposed method uses the confidence level as the health index of the protection zone. A high confidence level indicates good fit between the measurement and the measurement model, and thus it can be concluded that the physical laws of the protection zone are satisfied and the component has no internal fault. A low confidence level, however, implies inconsistency between the measurement and the measurement model;

therefore, it can be concluded that an abnormality (internal fault) has occurred in the component and has altered the model. The discrepancy is an indication of how different the faulty model of the protection zone is as compared to the model of the component in its healthy status.

The protection logic consists of two test: 1) if the operating limits are exceeded (for example, temperature above allowable limit) the component is tripped. and 2) if the average value of the confidence level over a sliding window exceeds a threshold. The window size and threshold can be set by users. Such tripping model effectively filters any transients caused by external faults, while also sensitive and faster enough to detect high resistance fault. The mathematical description of this tripping equation is:

$$trip(t) = \begin{cases} 1 & \frac{1}{Nf_s / f} \sum_{1 \le i \le Nf_s / f} confidence\_level(t - \frac{N}{f} + \frac{i}{f_s}) < confidence\_level\_threshold \\ 0 & Otherwise \end{cases}$$

Where N is the number of cycles in the integration window, f_s is the sampling rate and f is the frequency of the system. The average of the confidence level is given by summation of the confidence level over an integration window and divided by the number of samples in that window.

It is important to point out that the component protection relay must not trip circuit breakers except when the component itself is faulty (internal fault). For example, in case of a motor, start-up currents should be considered normal and the protection system should not trip the motor. The proposed protection scheme can adaptively differentiate these phenomena from internal faults.

5.4 Summary

Three dynamic state estimation methods have been presented in this chapter. The unconstrained weighted least squares method treats the virtual measurements as high accuracy measurements with very small errors, while constraint weighted least squares method treats the virtual measurements as constraints with no error. Extended Kalman Filter method is a two-step state estimation method. All of the three algorithms are implemented as object-oriented programs. In addition, the protection logic is presented in this chapter. The proposed EBP approach can detect the protection zone internal faults and ignore the external faults.

CHAPTER 6 HARDWARE-IN-THE-LOOP TEST

6.1 Overview

This chapter describes the laboratory implementation and testing procedure. For the laboratory implementation, it consists of the signal simulator, data acquisition system and the EBP relay. The details of the laboratory implementation and test procedure are presented in Section 6.2 and 6.3 separately.

6.2 Laboratory Implementation

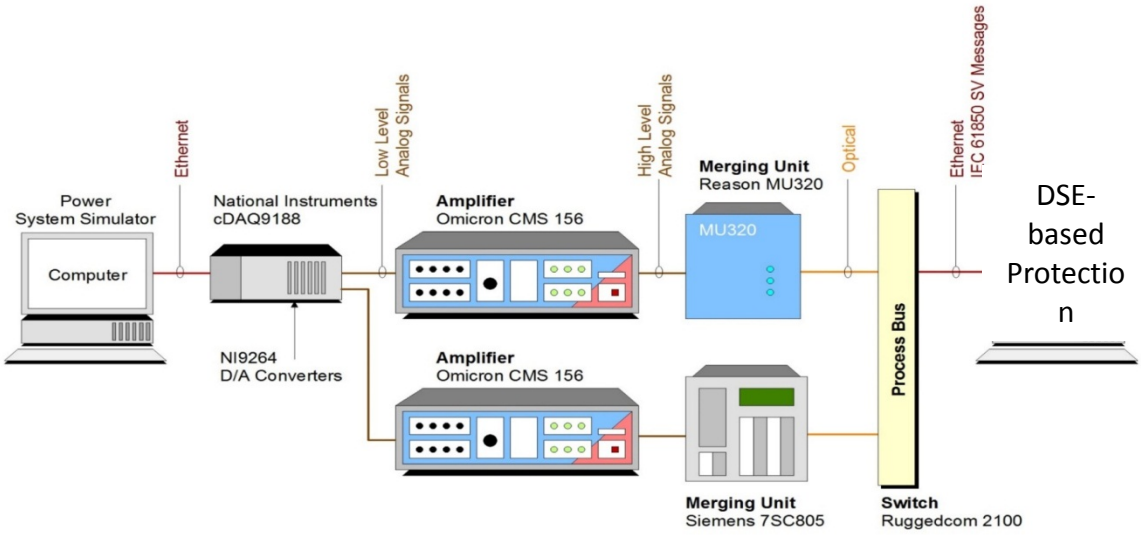

Figure 6.1. Laboratory Implementation Illustration

The laboratory implementation is illustrated in Figure 6.1. Since it is impractical to achieve real measurements from CTs/PTs in the lab, computer simulation based signals are utilized alternatively. Each part in the implementation is introduced next.

Power System Simulator: the WinXFM program generates digital streaming waveforms representing the terminal voltages and currents of the protection zone (power

system component) to the NI 32 channel DC/AC converter. It is emphasized here that the source for the digital streaming waveforms can be simulated voltages and currents of the power system component, or field collected measurements from the CTs/PTs in the COMTRADE format.

Digital to Analog converter: the digital streaming waveform from the simulator passes through the Ethernet and enters the D/A converter. The National Instrument D/A converter (NI9264) contains 32 channels with a maximum sampling rate of 25 kbps. The outputs of the D/A converter drive the inputs of several Omicron voltage and current amplifiers.

Omicron Amplifier: Omicron amplifiers receive the analog signals from the NI D/A converter and amplify these signals to a range which is very similar to real output of electronic CTs/PTs (for voltages around 50V and for currents around 5A). In this manner, the electrical output (voltages and currents) of the Omicron amplifiers are treated as the secondary electrical quantities from the CTs/PTs in this lab implementation.

Merging Unit: several merging units from Reason and Siemens are connected to the output terminals of the Omicron amplifiers. The merging units are utilized to collect the analog signals from the amplifiers and convert them to digital signals. These digital signals are transmitted to a personal computer, which is used as a dynamic state estimation based protection relay, via process bus.

Process Bus: process bus is generically defined as the digital transmission of process measurements between the substation switchyard and digital protective relays in the control house. It replaces hard wired connections with communication lines. In this laboratory setup, the Merging Units continuously transmit data over the process bus and

the upstream device, the EBP relay, uses the data for protection by monitoring the communications.

DSE-based Protection: The dynamic state estimation based protection algorithm is installed in the computer. The computer communicates with the merging units in accordance to IEC 61850-8-1 and IEC 61850-9-2 and captures the measurements, performs the dynamic state estimation and issues protection logic.

The sampling rate of the waveform generated by WinXFM is 4800 samples/sec (similar to the present top merging unit data transmission speed), and the merging units sample the analog data at the same rate of 4800 samples/sec (defined in IEC 61850), which means the proposed EBP protection approach should determine the protection decision in 400 μs to avoid coming data overlap.

6.3 Testing Procedure - User Interface

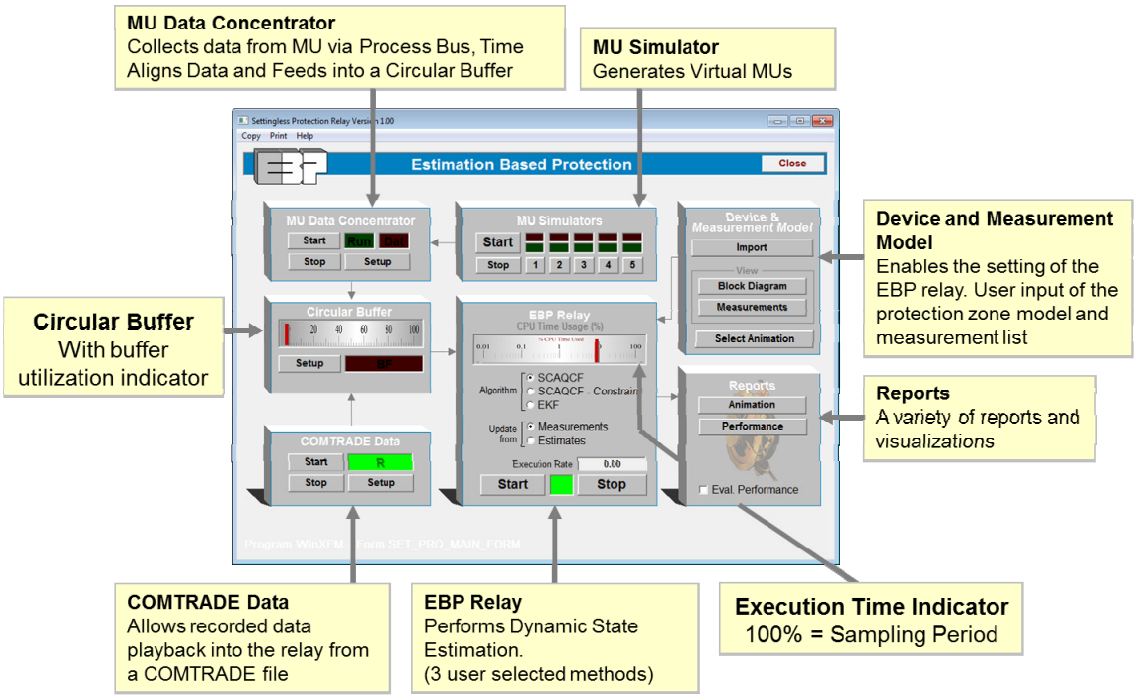

Figure 6.2. EBP Relay User Interface

The main user interface of EBP relay is shown in Figure 6.2. The working sequence is to first input the device and measurement model, and then setup the measurement channels from the merging units where the data would be coming from, or the COMTRADE file where the data would be generated from. If the data are coming from multiple merging units, the merging unit data concentrator would concentrate/time align the data based on the sample count in merging units. The circular buffer receives data from either the MU module or COMTRADE module. The next step is to choose the desired dynamic state estimation algorithm (protection logic involved) to start processing the data, and finally read the visualization results from the report. Each module is introduced below.

Device & Measurement Model: in this module, the SAQCF device model and the measurement definition is selected. The user interface of this module is shown in Figure 6.3.

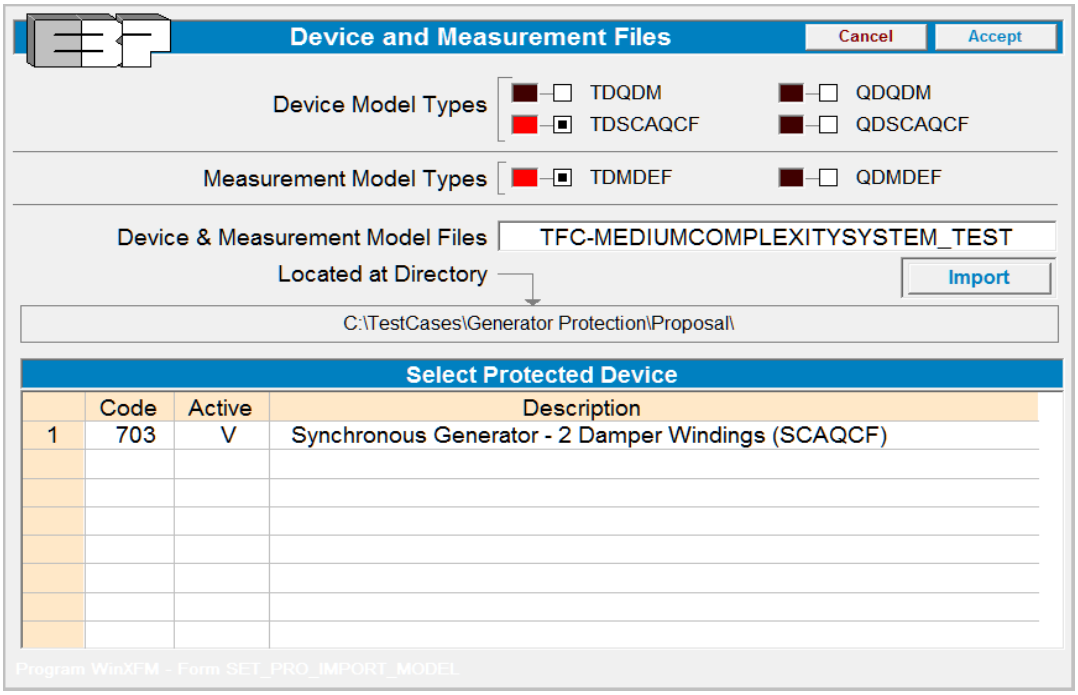

Figure 6.3. Device & Measurement Model User Interface

EBP Relay: EBP relay module has two inputs and one output. It creates the SAQCF measurement model from the SAQCF device model measurement definition at the initialization step and reads real-time measurements from circular buffer continuously. The proposed algorithm in Chapter 5 is integrated in this module. It tries to fit the real-time measurements to the SAQCF measurement model of the device under protection. Any mismatch between the real-time measurements and estimated measurements indicates the measurements not coming from the healthy device model thus the device under protection is in the unhealthy status (internal faults). EBP relay outputs the results of dynamic state estimation and the confidence level of the device under protection. Also the CPU usage is shown in this module.

Circular Buffer: circular buffer is the module which provides a buffer for the real-time measurements coming into the EBP relay module. For test and lab implementation purpose, the real-time data can either come from a simulated COMTRADE file or directly from the Merging Units.

COMTRADE Data: this module reads the real-time measurements from existing COMTRADE data files from local computer and transfers these data to circular buffer.

Reports: in the reports module, two functions are established, animation and performance. Animation shows the device terminal voltage and current phasors while performance shows how the dynamic estimation performs.

MU Data Concentrator: this module indicates the merging units' operation status and concentrates the data from multiple merging units and transfers these data to the circular buffer. The user interface of the MU data concentrator is shown in Figure 6.4.

Since this module provides the capability of align the measurements from different merging units with the same time stamp (data concentration), the user interface provides the functionality of setting the maximum latency for each sample at a specific time point, which means if the data concentrator receives a measurement at time T1, it will wait a maximum latency, which is set by the user, for other measurements with the same time T1, and after waits for the maximum latency time, the data concentrator will transfer the measurements with the time stamp T1 to the circular buffer and treat the missing packets as error packets. The user interface also provides other useful information of the data concentrator, such as the average latency of the coming measurements and the percentage of the usage of the circular buffer.

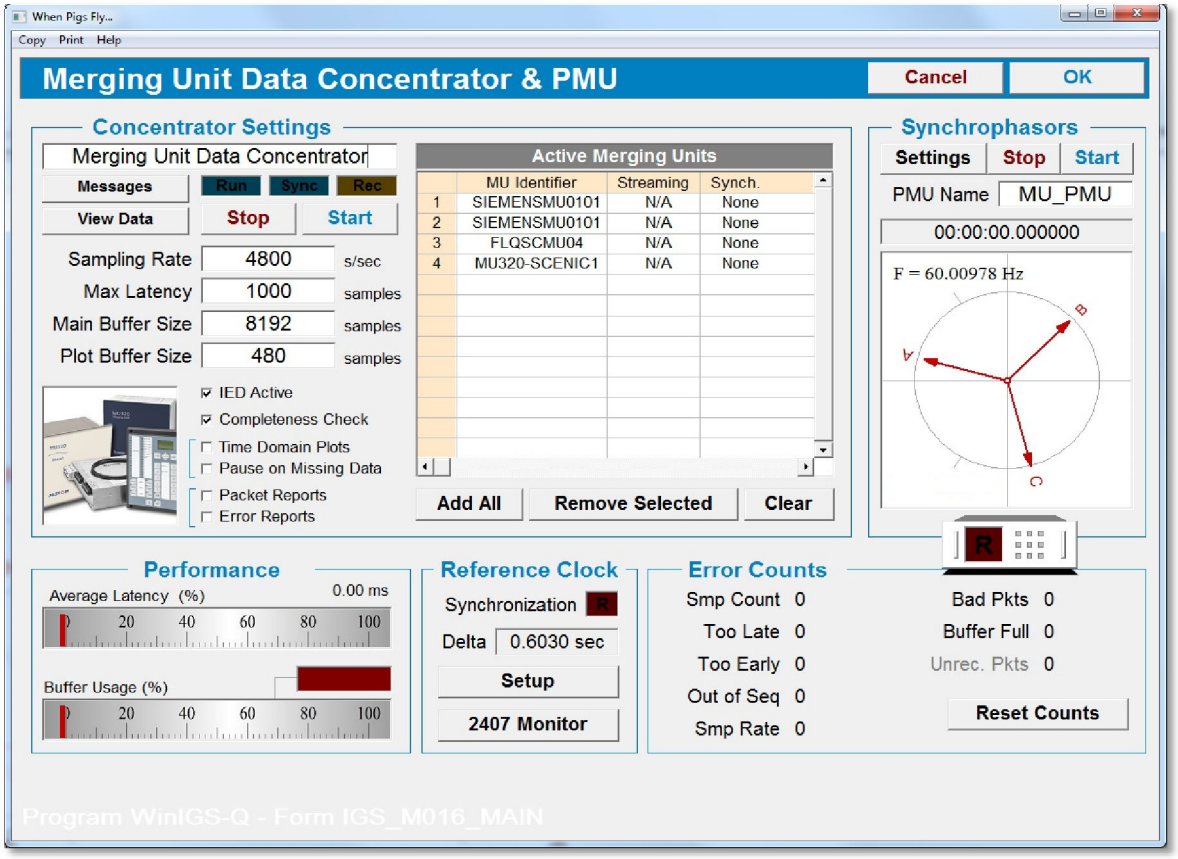

Figure 6.4. Merging Unit Data Concentrator User Interface

For each Merging Unit, the user has to define which merging unit in the network should this program target to. The user has to choose the network adaptor, then the program can see all the origin MAC addresses that is uploading IEC 81850-9-2 compliant sampled value data and choose one that the program needs. The user interface of Merging Unit Property is shown in Figure 6.5.

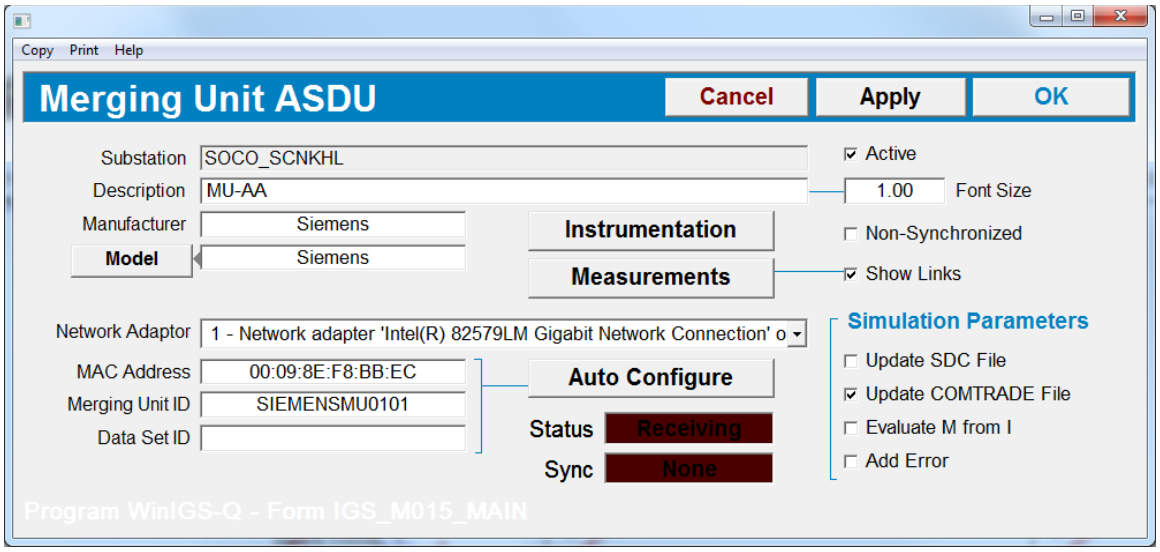

Figure 6.5. Merging Unit Property User Interface

The instrumentation channel can be selected via Instrumentation button and the user can modify the settings for each measurement channel, such as the measurement type, the scaling factor, and the instrument transformer ratio, in Measurements button. The user interfaces for instrumentation and measurements are shown in Figure 6.6 and Figure 6.7.

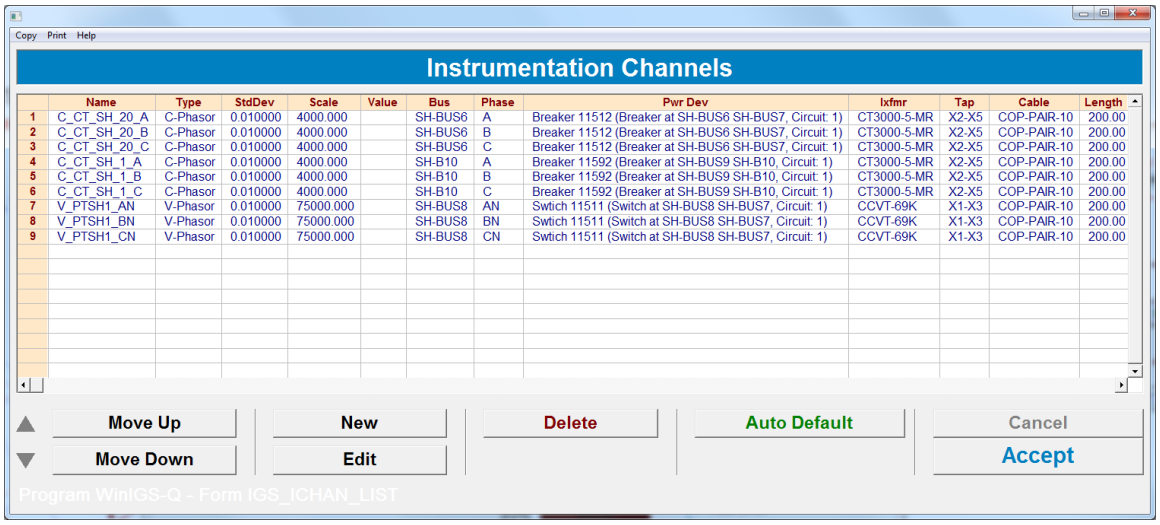

Figure 6.6. Instrumentation Channels User Interface

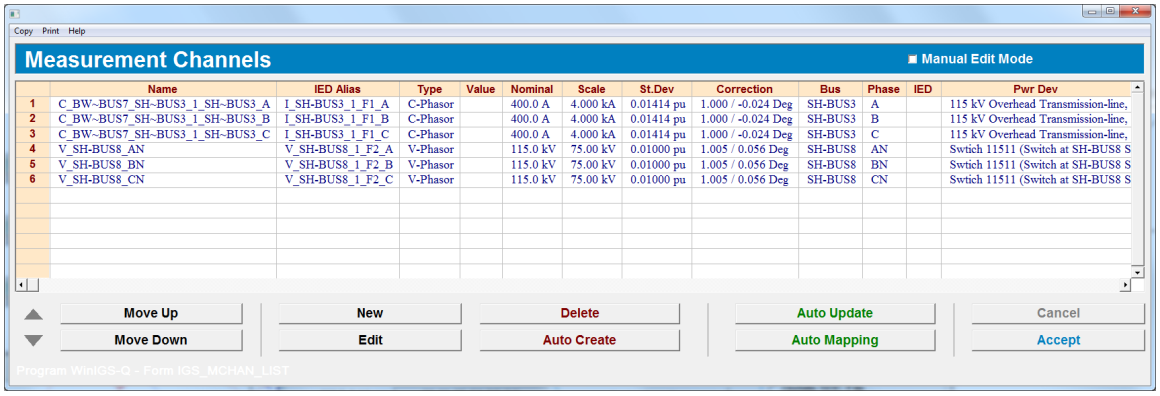

Figure 6.7. Measurement Channels User Interface

6.4 Summary

This chapter presents the laboratory implementation and the software design of the EBP relay. The hardware-in-the-loop test mimics the field conditions and is used to test the performances of the proposed EBP relay. Each module of the laboratory implementation is described in this chapter and how to setup the software is also introduced.

CHAPTER 7 ESTIMATION BASED PROTECTION NUMERICAL CASES

7.1 Overview

This chapter demonstrates the proposed EBP algorithm on a test system. In addition, the EBP method is compared with the legacy protection functions for the same events. Note that for a dependable and secure protective algorithm, it should detect the device internal fault, trip the faulty component, and ignore the external fault that is outside the protection zone. The external and internal fault cases are all described in this chapter.

7.2 Synchronous Generator Test System

The test system is shown in Figure 7.1 where the synchronous generator under protection is in the blue block. The ratings of generator are 825 MVA, 18 kV and 60 Hz. To save space the parameters of the generator are not provided. The step-up transformer is 725 MVA, 18kV/230kV for the interconnection to the system, which is rated 230 kV.

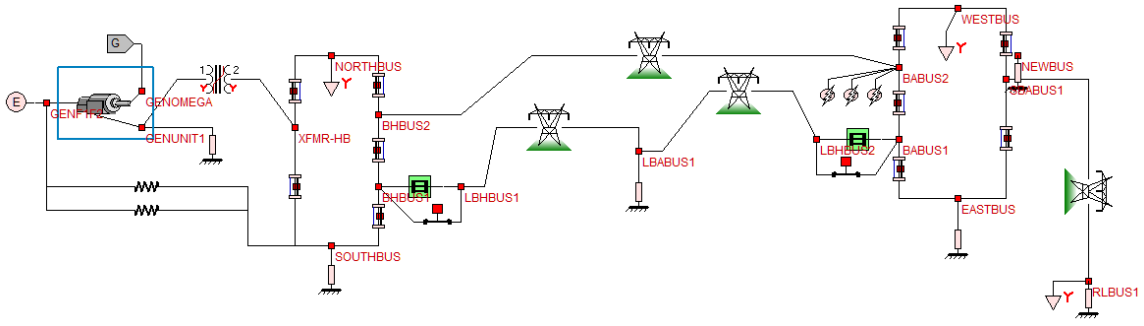

Figure 7.1. Synchronous Generator Protection Test System

Three events were simulated for a total 20 seconds period. The system operates normally until time 8.0 second when a three phase to ground fault occurs in the transmission line connecting BHBUS2 and BABUS2. This is an external fault for the generator. The fault is cleared within 8 cycles. Subsequently at time 15.1 second, a fault on the phase A stator winding of the generator occurs. The fault is close to the neutral point and the shorted portion is 8% of the stator winding. Then at time 18.5 second, a turn-to-turn fault on the phase A stator winding of the generator occurs. 5% of the winding is shorted. For the synchronous generator protection, nine measurements are utilized in this case, which are the following: three phase terminal voltages, three phase terminal currents, mechanical speed of the shaft, excitation voltage and current.

7.3 Legacy Relay Settings

Four legacy protection functions - differential protection, instantaneous overcurrent protection, negative-sequence current protection and third-harmonic neutral undervoltage protection are provided for comparison with the proposed EBP method. The settings of the above four legacy protective functions are as follows (for simplicity the settings are provided on primary values):

For differential protection, the minimum operating current is 8% of the generator rated current (26kA), so $I_{\min} = 2.08\ kA$. The slope setting (percentage) is 15% in this case. So the differential protection will trip the machine when (1) operating current $I_0 = I_{in} - I_{out}$ is greater than $I_{\min}$ and (2) the ratio of operating current I_0 over the restraining current I_{res} is greater than 15%.

For instantaneous overcurrent protection, the pickup current is set to be about 300% of the generator rated current, so $I_{pickup} = 75\ kA$.

The negative-sequence current protection will trip the generator when the time t satisfies the equation: $I_2^2 t \le k$, where k=7, I_2 is the per unit negative-sequence current.

For the third-harmonic neutral undervoltage protection, the pickup voltage is set to be 40% of the normal third harmonic voltage at the neutral point. In this case, $V_{3rd\_neutral\_normal} = 560\ V$ and $V_{pickup} = 40\% * V_{3rd\_neutral\_normal} = 224\ V$.

7.4 Results for Event 1: External Fault

For the external fault, the measurements from 7.9 second to 8.1 second are depicted in Figure 7.2. Three phase terminal voltages, three phase terminal currents, mechanical speed of the shaft, excitation voltage and current are shown in the figure.

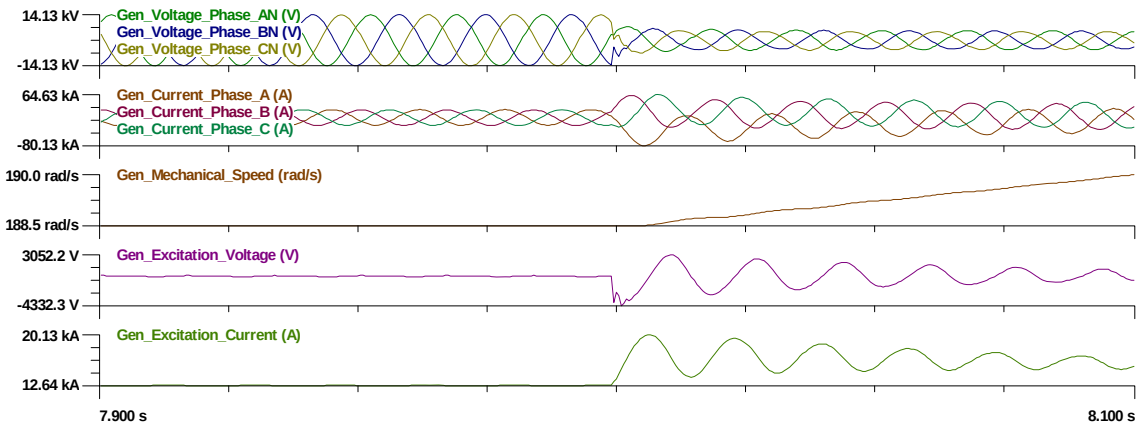

Figure 7.2. Measurements from 7.9 second to 8.1 second

7.4.1 Estimation Based Protection

Recall that as mentioned in Section 5.3, the settings for the EBP function are the length of integral time window and the confidence level threshold. The length of the integral time window is set to be 2 cycles and confidence level threshold is set to be 50%. These settings mean that when the confidence level drops to 0, the EBP will issue the trip signal in one cycle.

The EBP result from 7.9 second to 8.1 second is shown in Figure 7.3.

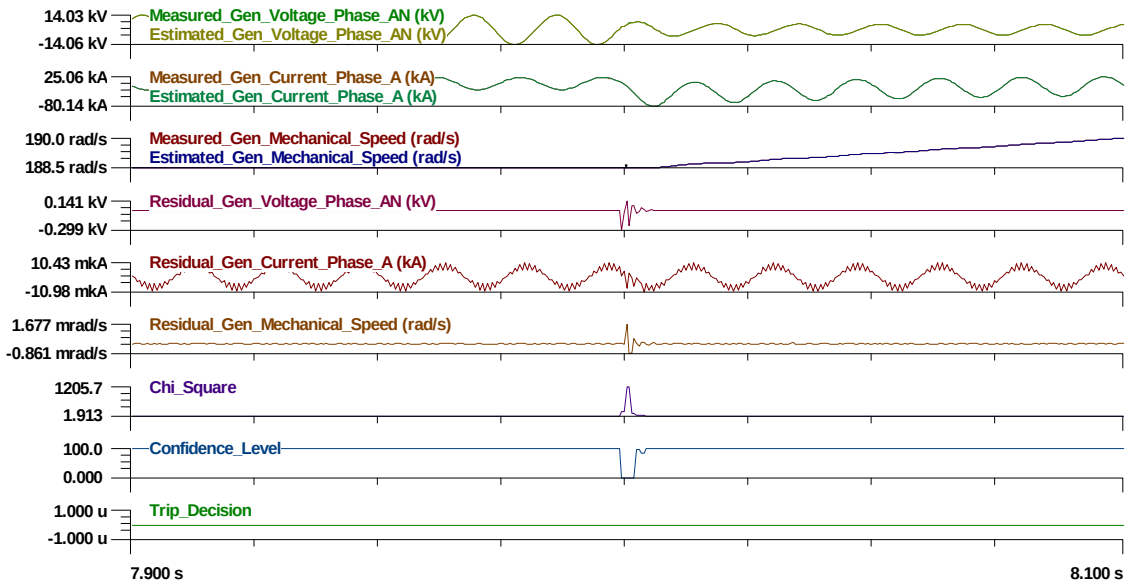

Figure 7.3. Estimation Based Protection Result for Event 1

There are 9 sets of traces in the above figure. The first three sets are the measured and estimated voltages of Phase AN, currents of Phase A and mechanical speed, respectively. Their residuals are shown in the fourth, fifth and sixth traces. The seventh trace is the chi-square value and the eighth trace is the confidence level. The last trace is the EBP relay trip decision. Notice that when the external fault happens the confidence level drops for several samples due to the system transient, and it goes back to the 100

immediately. The estimation based protection makes the correct protection decision and does not trip the generator.

7.4.2 Differential Protection

As mentioned in Section 7.3, the minimum operating current is 8% of the generator rated current (26kA), so $I_{\min} = 2.08\ kA$. The slope setting (percentage) is 15% in this case.

The differential protection result is shown in Figure 7.4.

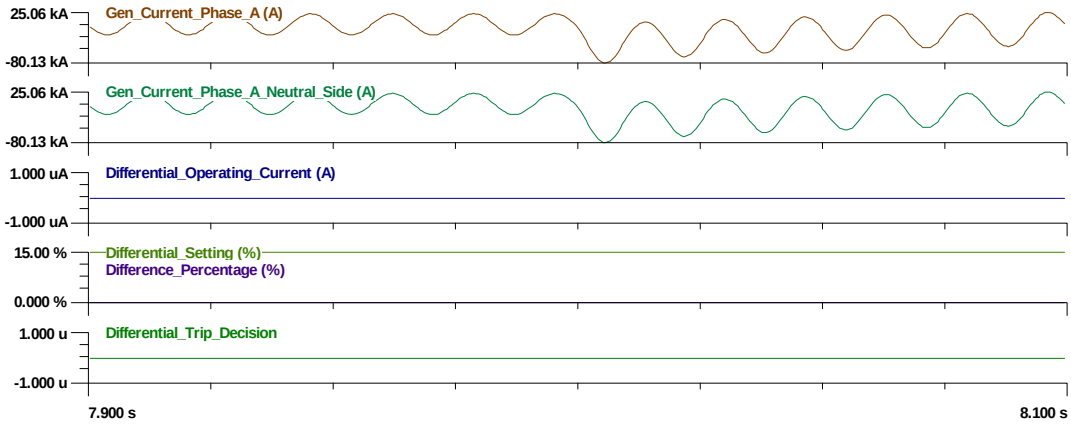

Figure 7.4. Differential Protection Result for Event 1

The differential protection operating current is zero and it does not trip the generator. This is because the fault is not inside the generator and the currents measured at the stator winding terminal side and neutral side are the same during the fault.

7.4.3 Instantaneous Overcurrent Protection

As mentioned in Section 7.3, the pickup current is set to be about 300% of the generator rated current, so $I_{pickup} = 75\ kA$.

The instantaneous overcurrent protection result is shown in Figure 7.5.

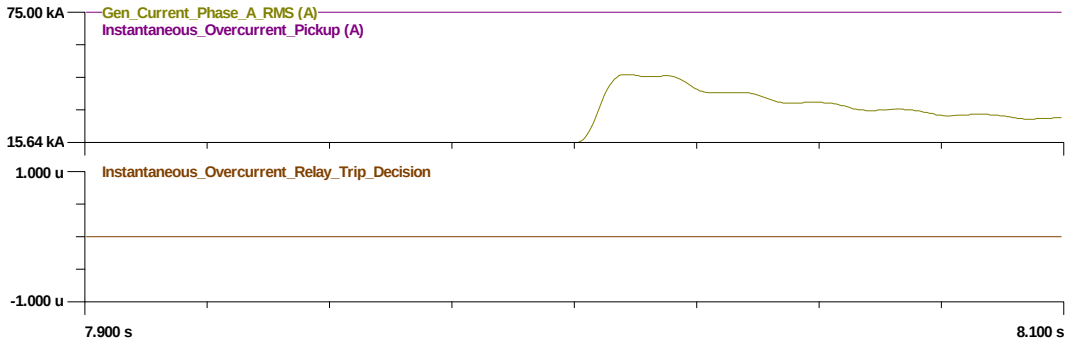

Figure 7.5. Instantaneous Overcurrent Protection Result for Event 1

The instantaneous overcurrent protection sees that the phase A current is less than the pickup current, so the generator will not be tripped. It is because the external fault location is far from the generator and it does not have much impact on the generator.

7.4.4 Negative-sequence Current Protection

As mentioned in Section 7.3, the negative-sequence current protection setting k in the equation $I_2^2 t \le k$ is set to be 7.

The negative-sequence current protection result is shown in Figure 7.6.

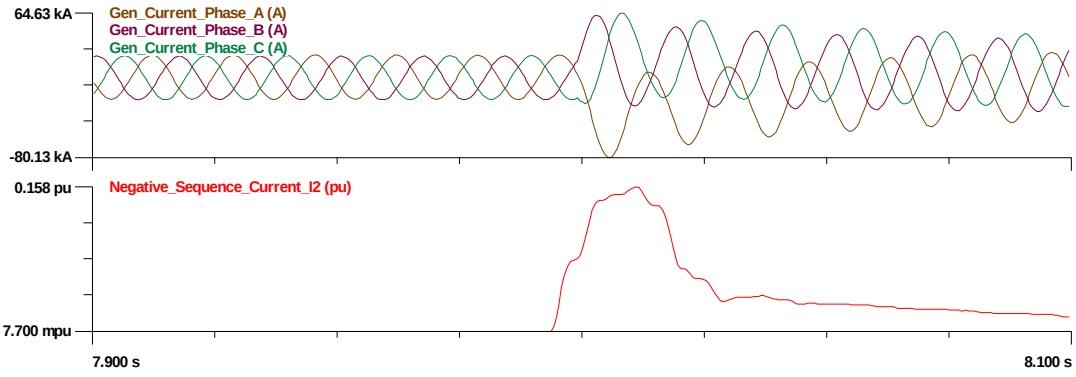

Figure 7.6. Negative-sequence Current Protection Result for Event 1

In the case, the negative-sequence current is 0.158 pu for a short period. According to the equation $I_2^2 t \le k$, where k equals to 7, the negative-sequence current protection will trip the generator in 16k cycles based on calculation. However, the negative-sequence current drops to a very low value very fast, so the relay will not trip.

7.4.5 Third-harmonic Neutral Undervoltage Protection

As mentioned in Section 7.3, the third-harmonic neutral undervoltage protection setting, the pickup voltage, is set to be $V_{pickup} = 40\% * V_{3rd\_neutral\_normal} = 224\ V$.

The third-harmonic neutral undervoltage protection result is shown in Figure 7.7.

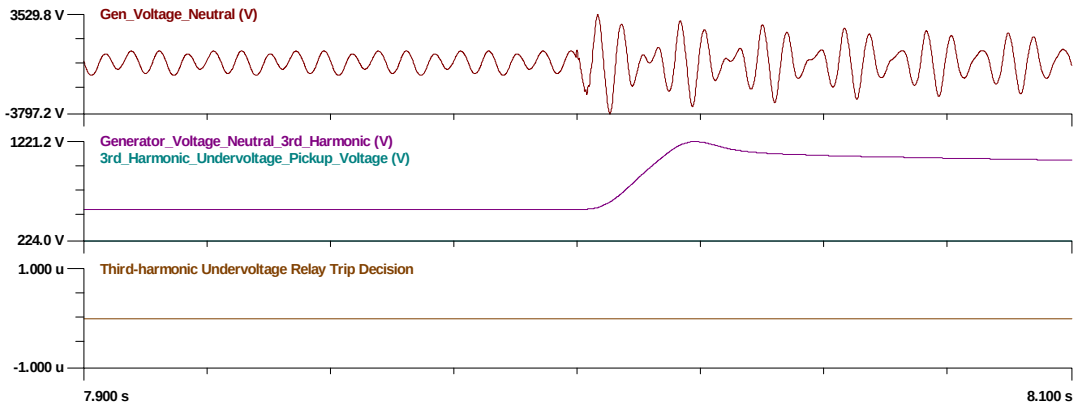

Figure 7.7. Third-harmonic Neutral Undervoltage Protection Result for Event 1

The third-harmonic voltage at neutral point increases during the fault. So the third-harmonic neutral undervoltage relay does not trip the generator for this external fault.

7.5 Results for Event 2: Internal Fault Near Neutral

For the internal fault near neutral, the measurements from 15.0 second to 15.2 second are depicted in Figure 7.8. Three phase terminal voltages, three phase terminal

currents, mechanical speed of the shaft, excitation voltage and current are shown in the figure.

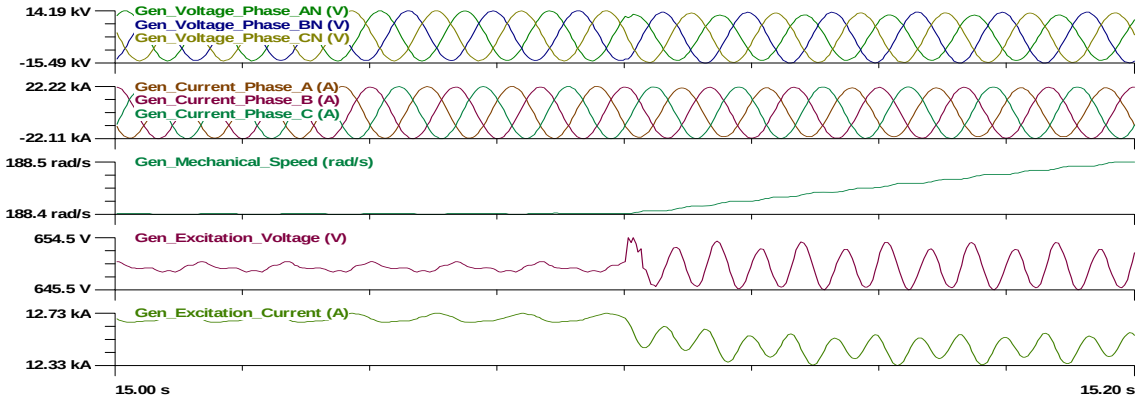

Figure 7.8. Measurements From 15.0 Second to 15.2 Second

7.5.1 Estimation Based Protection

The same settings are used in the case, which is 2 cycles for the length of the integral time window and 50% for confidence level threshold. These settings mean that when the confidence level drops to 0, the EBP will issue the trip signal in one cycle.

The estimation based protection result is shown in Figure 7.9.

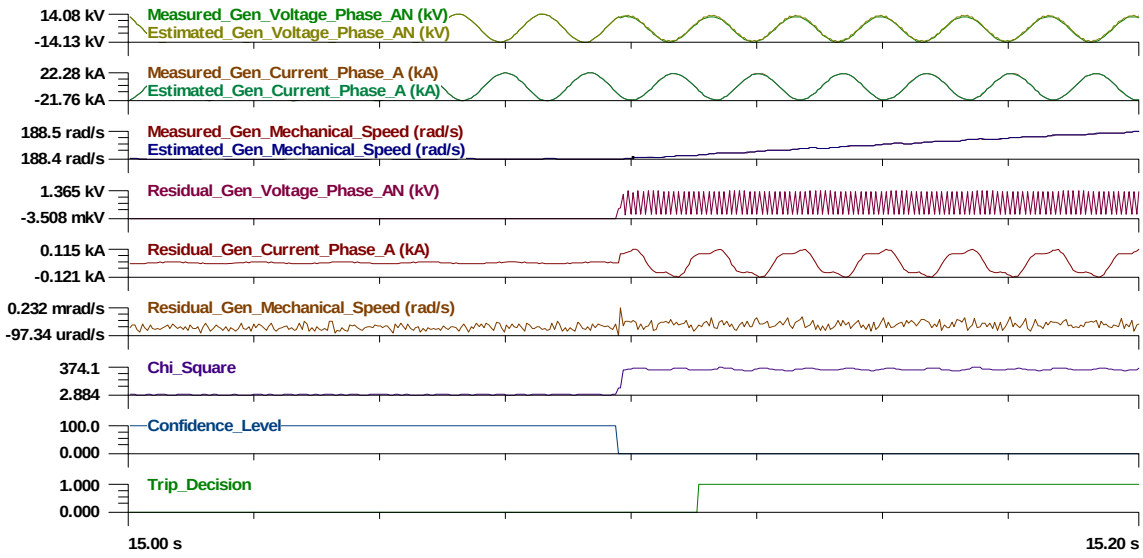

Figure 7.9. Estimation Based Protection Result for Event 2

Figure 7.9 shows 9 sets of traces. The first three sets are the measured and estimated voltages of Phase AN, currents of Phase A and mechanical speed, respectively. Their residuals are shown in the fourth, fifth and sixth sets. The seventh trace is the chi square value and the eighth trace is the confidence level. The last trace is the EBP trip decision. Notice that when the internal fault occurs the confidence level drops to zero and remains zero during the fault. The EBP detects the internal fault in 2 samples after the fault and trips the generator in one cycle.

7.5.2 Differential Protection

Same as the external fault, the minimum operating current is 8% of the generator rated current (26kA), so $I_{\min} = 2.08\ kA$. The slope setting (percentage) is 15% in this case.

The differential protection result is shown in Figure 9.10.

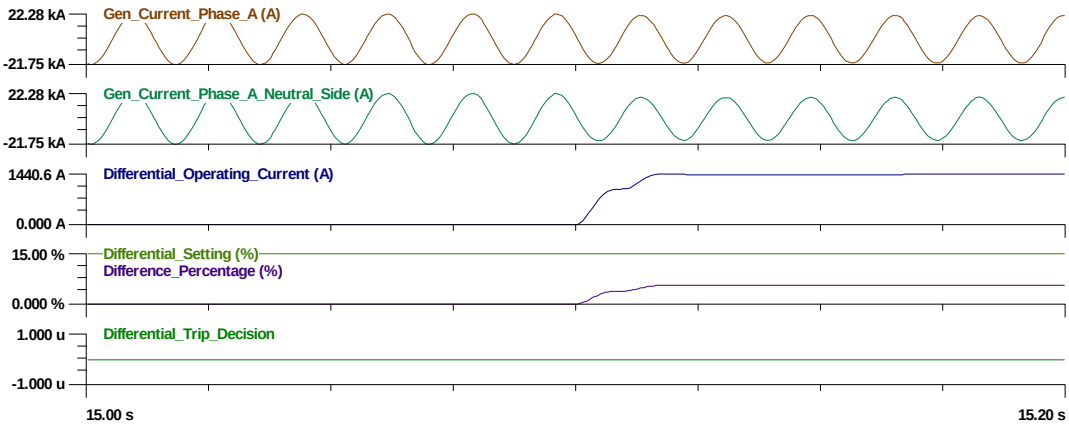

Figure 7.10. Differential Protection Result for Event 2

The differential protection sees the operating current to be 1.4 kA, which is less than the minimum operating current. Also the differential percentage is 5%, which is less than the slope setting (15%). So the differential protection misses the internal fault.

7.5.3 Instantaneous Overcurrent Protection

Recall that the pickup current is set to be about 300% of the generator rated current, so $I_{pickup} = 75\ kA$.

The instantaneous overcurrent protection result is shown in Figure 7.11.

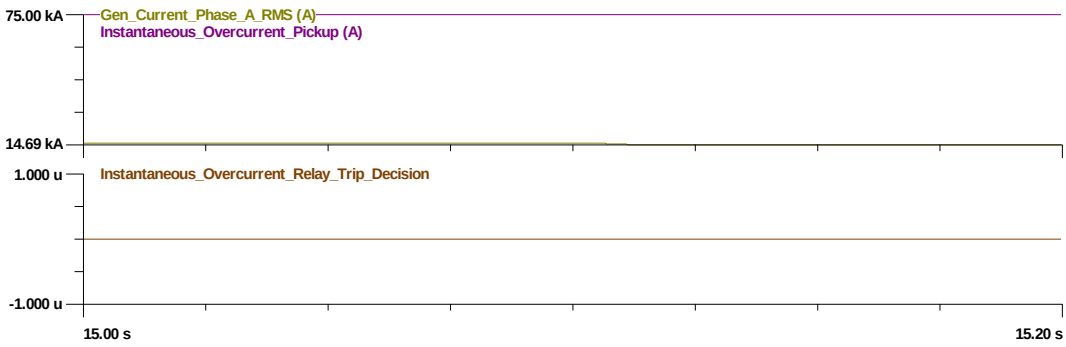

Figure 7.11. Instantaneous Overcurrent Protection Result for Event 2

The instantaneous overcurrent protection sees that the phase A current is less than the pickup current, so the generator will not be tripped. It is because only a very small portion of the Phase A stator winding is shorted, so the phase current does not change much.

7.5.4 Negative-sequence Current Protection

Same settings are used as in the external fault event. The negative-sequence current protection setting k in the equation $I_2^2 t \le k$ is set to be 7.

The negative-sequence current protection result is shown in Figure 7.12.

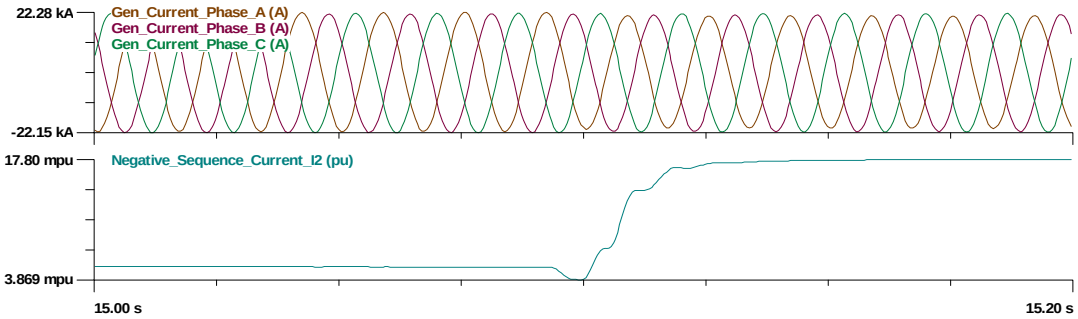

Figure 7.12. Negative-sequence Current Protection Result for Event 2

In the case, the negative-sequence current is 0.0178 pu. According to the equation $I_2^2 t \le k$, where k equals to 7, it takes more than 1000k cycles to meet the inequality. Since it is more than the maximum trip time, the negative-sequence current protection fails to trip the generator.

7.5.5 Third-harmonic Neutral Undervoltage Protection

The third-harmonic neutral undervoltage protection setting, the pickup voltage, is set to be $V_{pickup} = 40\% * V_{3rd\_neutral\_normal} = 224\ V$.

The third-harmonic neutral undervoltage protection result is shown in Figure 7.13.

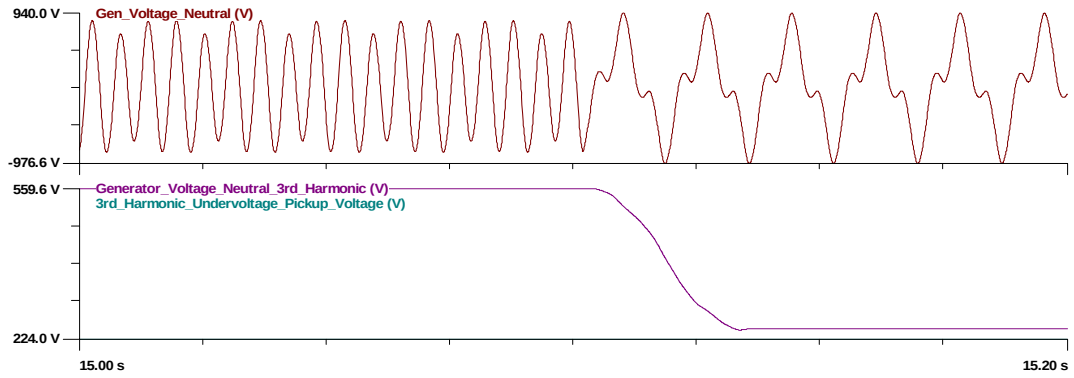

Figure 7.13. Third-harmonic Neutral Undervoltage Protection Result for Event 2

As expected, the third-harmonic voltage at neutral point drops when the internal fault occurs. However, it is still higher than the pickup voltage (224V) which makes the third-harmonic neutral undervoltage protection fail to detect the internal fault.

7.6 Results for Event 3: Internal Turn-To-Turn Fault

For the internal turn-to-turn fault, 5% of the stator phase A winding is shorted. The measurements from 18.4 second to 18.6 second are depicted in Figure 7.14. Three phase terminal voltages, three phase terminal currents, mechanical speed of the shaft, excitation voltage and current are shown in the figure.

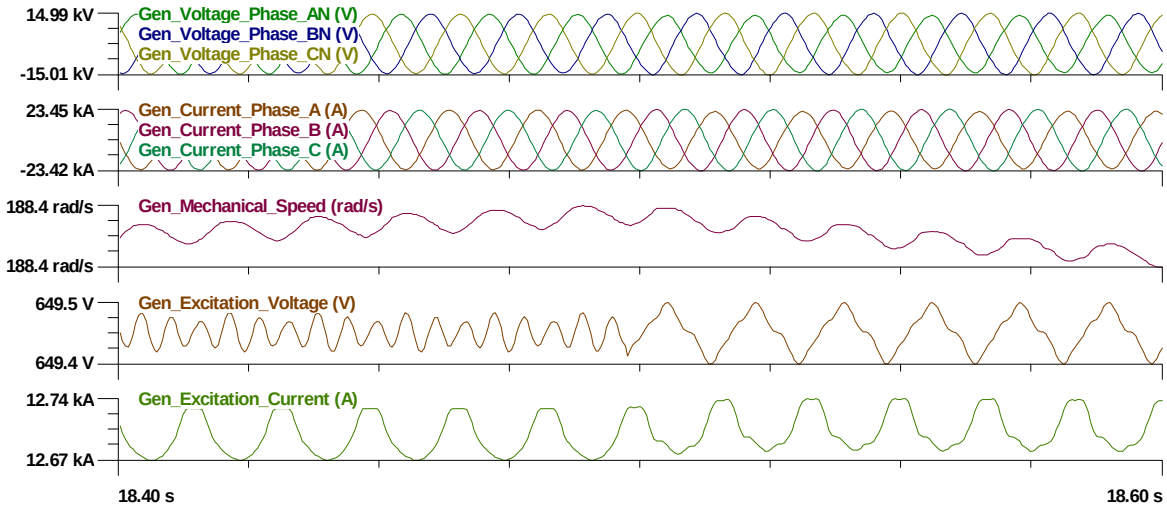

Figure 7.14. Measurements From 18.4 Second to 18.6 Second

7.6.1 Estimation Based Protection

The same settings are used in the case, which is 2 cycles for the length of the integral time window and 50% for confidence level threshold. These settings mean that when the confidence level drops to 0, the EBP will issue the trip signal in one cycle.

The estimation based protection result is shown in Figure 7.15.

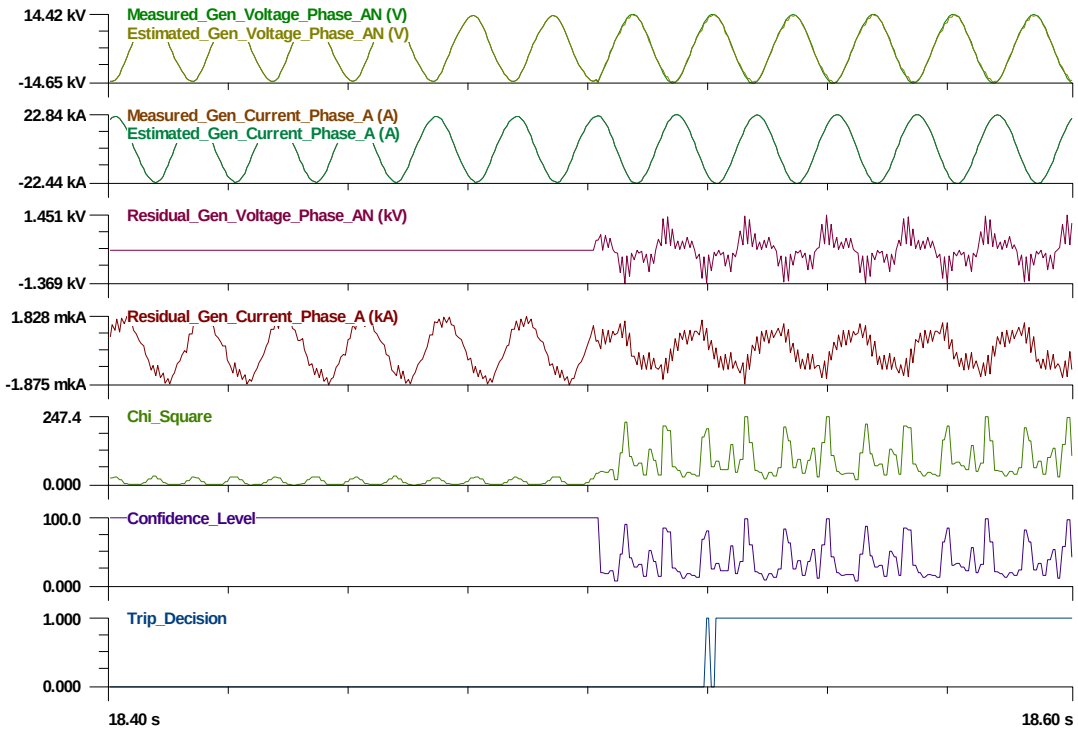

Figure 7.15. Estimation Based Protection Result for Event 3

Figure 7.15 shows 7 sets of traces. The first two sets are the measured and estimated voltages of Phase AN and currents of Phase A, respectively. Their residuals are shown in the third and fourth sets. The fifth trace is the chi square value and the sixth trace is the confidence level. The last trace is the EBP trip decision. Notice that when the internal fault occurs the confidence level drops to zero and remains zero during the fault. The

EBP detects the internal fault in 2 samples after the fault and trips the generator in one cycle.

7.6.2 Differential Protection

Same settings are used in this event. The minimum operating current is 8% of the generator rated current (26kA), so $I_{\min} = 2.08\ kA$. The slope setting (percentage) is 15% in this case.

The differential protection result is shown in Figure 9.16.

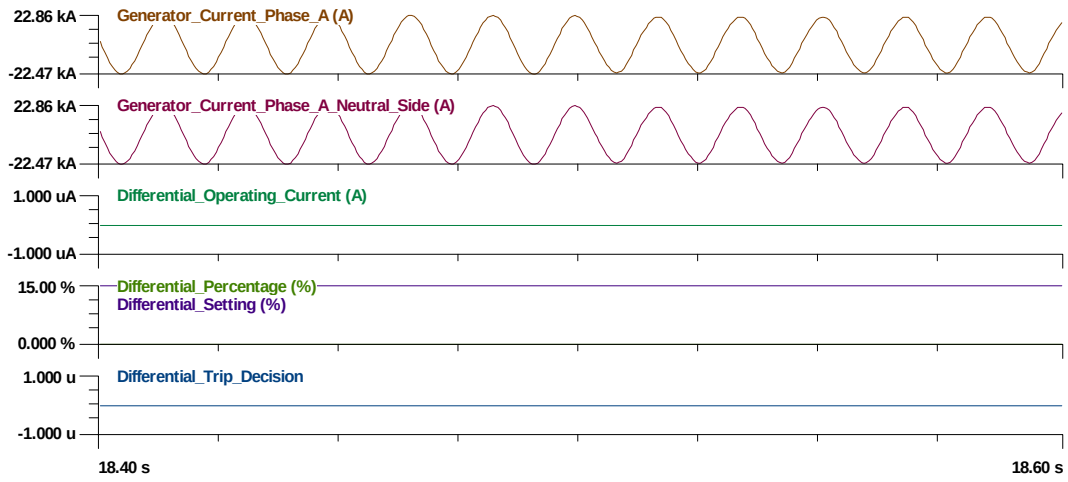

Figure 7.16. Differential Protection Result for Event 3

Since it is the turn-to-turn fault, the currents at the terminal and neutral side are the same. So the differential protection does not see any operating current, thus it misses the internal fault.

7.6.3 Instantaneous Overcurrent Protection

Recall that the pickup current is set to be about 300% of the generator rated current, so $I_{pickup} = 75\ kA$.

The instantaneous overcurrent protection result is shown in Figure 7.17.

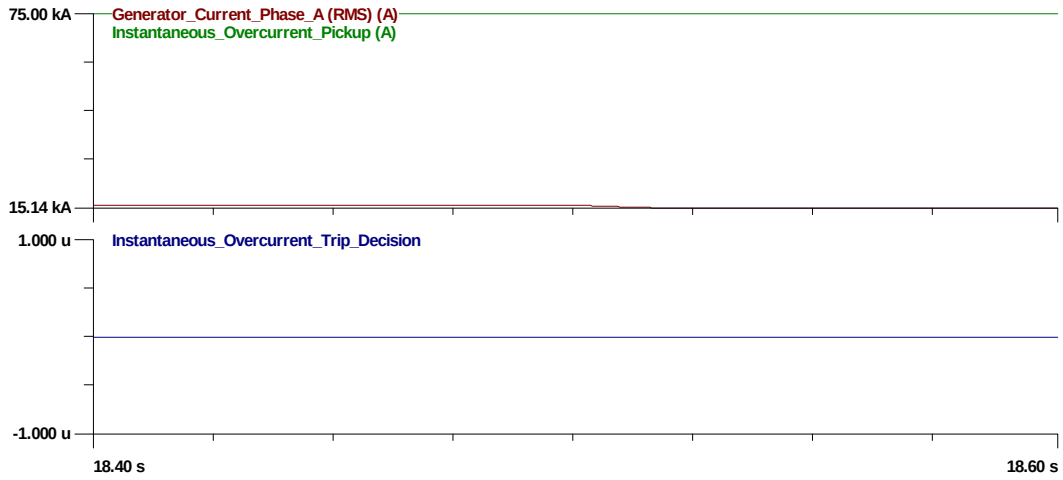

Figure 7.17. Instantaneous Overcurrent Protection Result for Event 3

The instantaneous overcurrent protection sees that the phase A current is less than the pickup current, so the generator will not be tripped. It is because only a very small portion of the Phase A stator winding is shorted, so the phase current does not change much.

7.6.4 Negative-sequence Current Protection

Recall that the negative-sequence current protection setting k in the equation $I_2^2 t \le k$ is set to be 7.

The negative-sequence current protection result is shown in Figure 7.18.

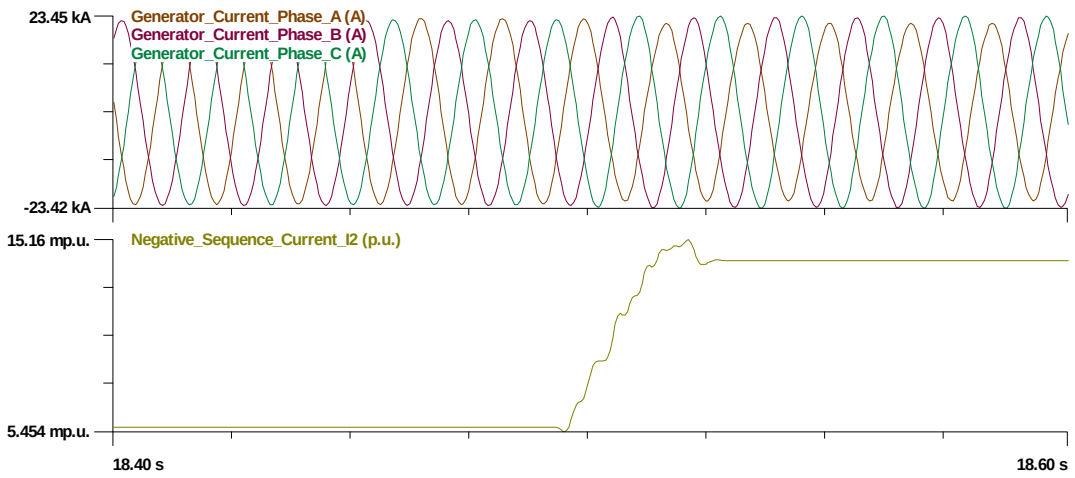

Figure 7.18. Negative-sequence Current Protection Result for Event 3

In the case, the negative-sequence current is 0.015 pu. According to the equation $I_2^2 t \le k$, where k equals to 7, it takes more than 1000k cycles to meet the inequality. Since it is more than the maximum trip time, the negative-sequence current protection fails to trip the generator.

7.6.5 Third-harmonic Neutral Undervoltage Protection

The third-harmonic neutral undervoltage protection setting, the pickup voltage, is set to be $V_{pickup} = 40\% * V_{3rd\_neutral\_normal} = 224\ V$.

The third-harmonic neutral undervoltage protection result is shown in Figure 7.19.

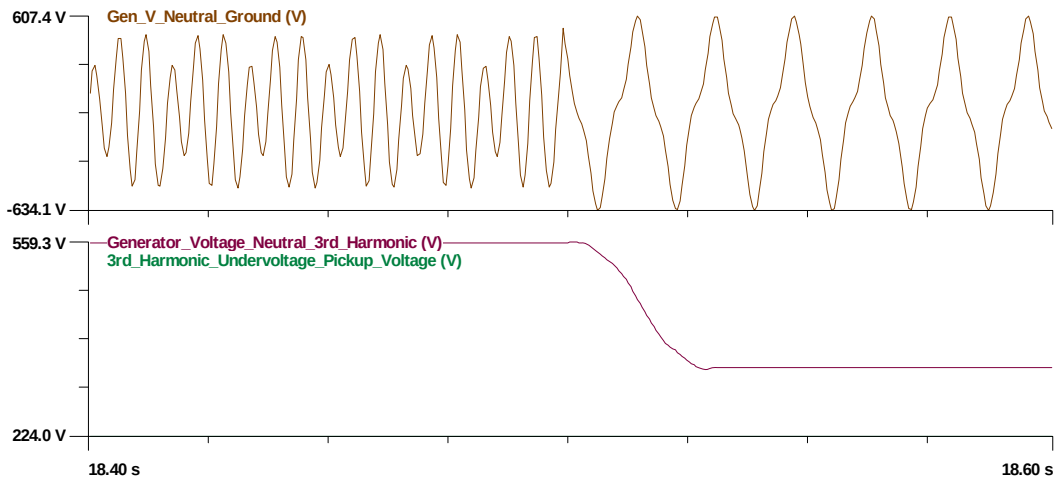

Figure 7.19. Third-harmonic Neutral Undervoltage Protection Result for Event 3

As expected, the third-harmonic voltage at neutral point drops when the internal fault occurs. However, it is still higher than the pickup voltage (224V) which makes the third-harmonic neutral undervoltage protection fail to detect the internal fault.

7.7 Summary

This chapter presented several numerical cases for the machine estimation based protection. Specifically, one external fault and two internal faults are utilized as test cases. For the external fault case, the proposed estimation based protection correctly ignores the external fault. For the internal faults, both the fault near neutral and turn-to-turn fault are very difficult to be detected with the present technology. The demonstration of legacy protective functions also show that none of the legacy protective functions detects the internal faults. However, the proposed estimation based protection detects both faults and trips the generator from further damage. All three cases show that the proposed EBP method is secure and dependable.

CHAPTER 8 MODEL VALIDATION - PARAMETER ESTIMATION

8.1 Overview

Modeling accuracy and fidelity are fundamental in the proposed protection algorithm. For success the model must be high fidelity so that the dynamic state estimation can securely and dependably monitor the health status of the device under protection.

For many power system components, high-fidelity models exist. For some new components such as inverter-interfaced power components, the modeling accuracy may not be as high as that of other components as a result of model parameter uncertainty. In both cases the dynamic state estimation can be utilized to fine tune the models and/or determine the parameters of the model with greater accuracy. The basic approach is to expand the dynamic state estimation to include some key parameters of the power component as unknown states. This is a procedure of parameters estimation and model validation. Therefore the proposed overall approach can also provide better models with field-validated parameters compared with traditional approaches.

The object-oriented, unified, and seamless interoperable device model SAQCF syntax described in Chapter 4 is used to guarantee that the high-fidelity model can be seamlessly used across the dynamic state estimation procedure. Section 8.2 provides the mathematical formulation of the synchronous generator physical parameters estimation problem, to illustrate the procedure of expanding the dynamic state estimation to include some key parameters as unknown states.

8.2 Synchronous Generator Physical Parameters Estimation Model

The SAQCF device model introduced in Chapter 4 can be augmented to include some key parameters of a component as unknown states to perform the dynamic state estimation so that the values of those key parameters can be estimated together with the other states of the component. Here an example of this kind of model parameters validation is provided. A physically-based synchronous generator model expressed in terms of the self and mutual inductances of the generator windings as a function of the rotor position, is proposed for the purpose of synchronous-machine parameters identification. This model accounts for the different impedances along the two axes of the synchronous generator as well as the generation of harmonics in the unit. Compared with the traditional parameters identification methods discussed in Section 2.4, the physical parameters based synchronous generator model used here has the following advantages: (1) there are no simplification assumptions for the proposed dynamic generator model, such as the park's transformation or dynamic order reduction, which is suitable for the situation of sudden application and removal of balanced and unbalanced loads, rectifier loads, and also symmetrical and asymmetrical faults; (2) the model is accurate for both round rotor machines and salient pole machines; (3) rotor angle and the physical parameters of the synchronous generator can be estimated together at the same time.

As discussed in Chapter 4, the quadratized device model of the synchronous generator model with parameters as unknown states are introduced first and then the quadratic integration algorithm is applied to this quadratized device model to obtain the SAQCF synchronous generator model with parameters. The derivation from quadratized device model to SAQCF model is automatically done so in this section only the

quadratized device model of the synchronous generator model with parameters is shown in this section.

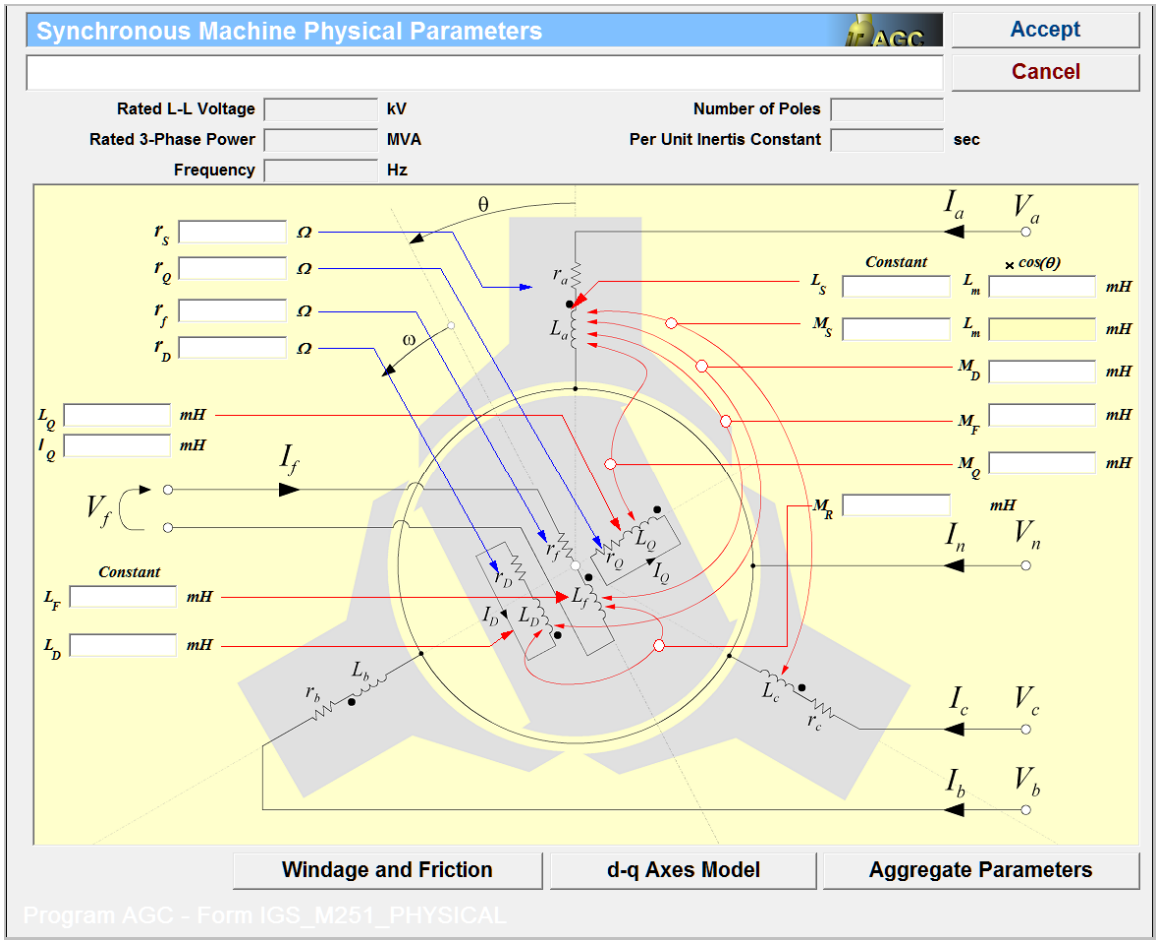

Figure 8.1. Synchronous Generator Physical Parameter Interface

Figure 8.1 shows the parameters for a synchronous generator. The basic independent parameters that can be estimated for the synchronous generator are summarized in Table 8.1.

Table 8.1 Physical Independent Parameters of the Synchronous Generator.

Parameters	Description
L_s	Stator self-inductance constant part
L_m	Stator self-inductance varying part

Table 8.1 continued

Parameters	Description
L_f	Field self-inductance
L_D	D damper self-inductance
L_Q	Q damper self-inductance
M_S	Stator mutual inductance
M_F	Field D damper mutual inductance
M_R	Stator field mutual inductance
M_D	Stator D damper mutual inductance
M_Q	Stator Q damper mutual inductance
H	Generator inertia constant

The electric circuit model of the synchronous generator is illustrated in Figure 8.2. The quadratized device model of the synchronous generator with parameters is derived based on this circuit.

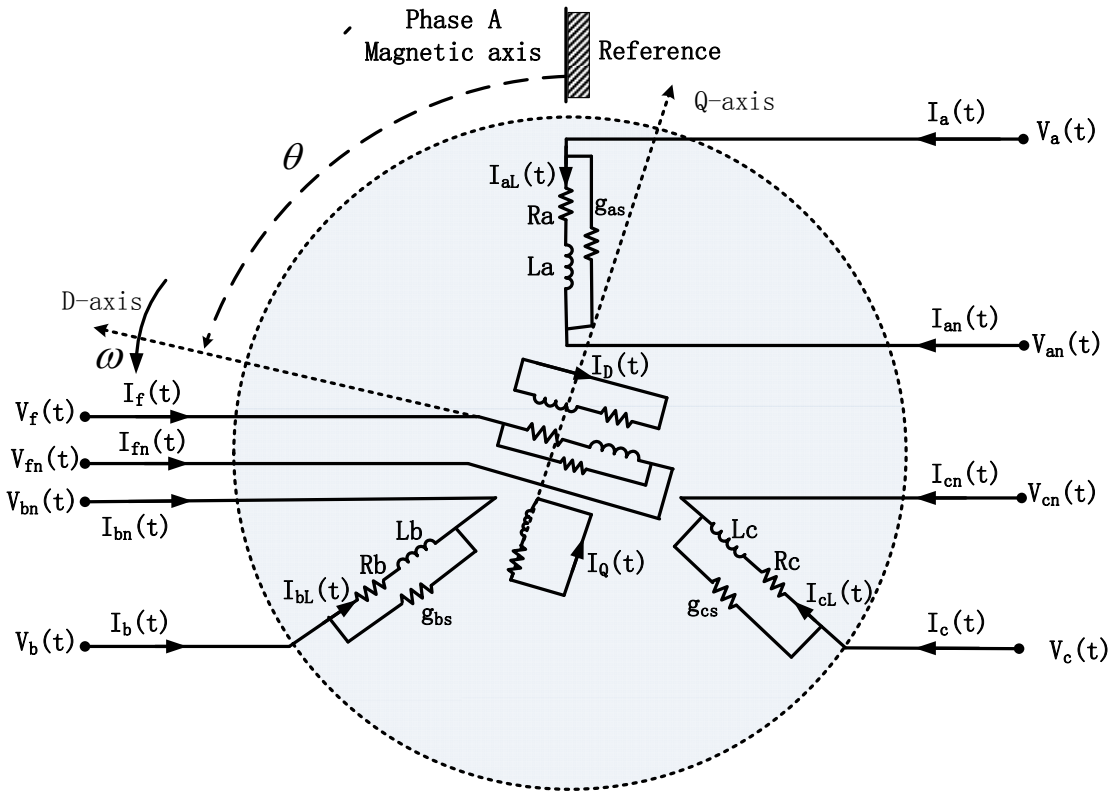

Figure 8.2. Synchronous Generator Electric Circuit Model

The model can be expressed with the following equations:

Equation Set 1:

$$i_{abc}(t) = i_{aL\ bL\ cL}(t) + g_{as,bs,cs} \cdot (v_{abc}(t) - v_{an\ bn\ cn}(t)) \qquad \{v_{abc}(t)\}$$

$$i_{an\ bn\ cn}(t) = -i_{aL\ bL\ cL}(t) + g_{as,bs,cs} \cdot (v_{an\ bn\ cn}(t) - v_{abc}(t)) \qquad \{v_{an\ bn\ cn}(t)\}$$

$$i_f(t) = i_{fL}(t) + g_{fs} \cdot (v_f(t) - v_{fn}(t)) \qquad \{v_f(t)\}$$

$$i_{fn}(t) = -i_{fL}(t) + g_{fs} \cdot (v_{fn}(t) - v_f(t)) \qquad \{v_{fn}(t)\}$$

$$T_m(t) = T_{acc}(t) + T_e(t) + T_{wf}(t) \qquad \{T_{acc}(t)\}$$

Equation Set 2:

$$0 = v_{abc}(t) - v_{an\ bn\ cn}(t) - R_{abc} i_{aL\ bL\ cL}(t) + e_{abc}(t) \qquad \{i_{aL\ bL\ cL}(t)\}$$

$$0 = v_f(t) - v_{fn}(t) - R_f i_{fL}(t) - e_f(t) \qquad \{i_{fL}(t)\}$$

$$0 = R_{DQ} i_{DQ}(t) + e_{DQ}(t) \qquad \{i_{DQ}(t)\}$$

$$0 = \theta(t) - \frac{p}{2}\theta_m(t) \qquad \{\theta(t)\}$$

$$0 = \omega(t) - \frac{p}{2}\omega_m(t) \qquad \{\omega(t)\}$$

$$0 = \frac{d\theta_m(t)}{dt} - \omega_m(t) \qquad \{\theta_m(t)\}$$

$$0 = \frac{d\lambda_{abc}(t)}{dt} - e_{abc}(t) \qquad \{e_{abc}(t)\}$$

$$0 = \frac{d\lambda_{fDQ}(t)}{dt} - e_{fDQ}(t) \qquad \{e_{fDQ}(t)\}$$

$$0 = \frac{dc(t)}{dt} - y_1(t) \qquad \{c(t)\}$$

$$0 = \frac{ds(t)}{dt} - y_2(t) \qquad \{s(t)\}$$

$$0 = \frac{d\omega_m(t)}{dt} - \omega_m^{'}(t) \qquad \{\omega_m(t)\}$$

$$0 = J(t) - \frac{2H(t) \cdot S_{base}}{\omega_s^2} \qquad \{J(t)\}$$

(The following equations can be added considering the parameters remain the same during the state estimation procedure)

$$0 = \frac{dL_s(t)}{dt}$$

$$0 = \frac{dL_m(t)}{dt}$$

$$0 = \frac{dL_f(t)}{dt}$$

$$0 = \frac{dL_D(t)}{dt}$$

$$0 = \frac{dL_Q(t)}{dt}$$

$$0 = \frac{dM_S(t)}{dt}$$

$$0 = \frac{dM_R(t)}{dt}$$

$$0 = \frac{dM_F(t)}{dt}$$

$$0 = \frac{dM_D(t)}{dt}$$

$$0 = \frac{dM_Q(t)}{dt}$$

$$0 = \frac{dH(t)}{dt}$$

Equation Set 3:

$$0 = T_{wf}(t) - \left(D_{fw} + D'_{fw} \cdot \omega_m(t) + D''_{fw} \cdot \omega_m(t)^2 \right) \qquad \{T_{wf}(t)\}$$

$$0 = P_{em}(t) - e_{abc}(t)^T i_{aL\ bL\ cL}(t) \qquad \{P_{em}(t)\}$$

$$0 = P_{em}(t) - T_e(t) \cdot \omega(t) \qquad \{T_e(t)\}$$

$$0 = T_{acc}(t) - J(t) \cdot \omega'_m(t) \qquad \{\omega'_m(t)\}$$

$$0 = y_1(t) + s(t) \cdot \omega(t) \qquad \{y_1(t)\}$$

$$0 = 1 - c^2(t) - s^2(t) \qquad \{y_2(t)\}$$

$$0 = c_2(t) - c^2(t) + s^2(t) \qquad \{c_2(t)\}$$

$$0 = s_2(t) - 2c(t)s(t) \qquad \{s_2(t)\}$$

$$0 = z_1(t) - L_m(t) \cdot c_2(t) \qquad \{z_1(t)\}$$

$$0 = z_2(t) - L_m(t) \cdot s_2(t) \qquad \{z_2(t)\}$$

$$0 = z_3(t) - M_F(t) \cdot c(t) \qquad \{z_3(t)\}$$

$$0 = z_4(t) - M_F(t) \cdot s(t) \qquad \{z_4(t)\}$$

$$0 = z_5(t) - M_D(t) \cdot c(t) \qquad \{z_5(t)\}$$

$$0 = z_6(t) - M_D(t) \cdot s(t) \qquad \{z_6(t)\}$$

$$0 = z_7(t) - M_Q(t) \cdot c(t) \qquad \{z_7(t)\}$$

$$0 = z_8(t) - M_Q(t) \cdot s(t) \qquad \{z_8(t)\}$$

$$0 = -\begin{bmatrix} \lambda_{abc}(t) \\ \lambda_{fDQ}(t) \end{bmatrix} + A \cdot \begin{bmatrix} i_{aL,bL,cL}(t) \\ i_{fL,D,Q}(t) \end{bmatrix} + B \cdot \begin{bmatrix} i_{aL,bL,cL}(t) \\ i_{fL,D,Q}(t) \end{bmatrix} \qquad \begin{Bmatrix} \lambda_{abc}(t) \\ \lambda_{fDQ}(t) \end{Bmatrix}$$

where the following definitions hold:

$$c(t) = \cos\left(\theta(t)\right)$$

$$s(t) = \sin\left(\theta(t)\right)$$

$$c_2(t) = \cos(2 \cdot \theta(t))$$

$$s_2(t) = \sin(2 \cdot \theta(t))$$

$$A = \begin{bmatrix} z_1(t) & -\frac{1}{2}z_1(t) + \frac{\sqrt{3}}{2}z_2(t) & -\frac{1}{2}z_1(t) - \frac{\sqrt{3}}{2}z_2(t) & -z_3(t) & -z_5(t) & -z_8(t) \\ -\frac{1}{2}z_1(t) + \frac{\sqrt{3}}{2}z_2(t) & -\frac{1}{2}z_1(t) - \frac{\sqrt{3}}{2}z_2(t) & z_1(t) & \frac{1}{2}z_3(t) - \frac{\sqrt{3}}{2}z_4(t) & \frac{1}{2}z_5(t) - \frac{\sqrt{3}}{2}z_6(t) & \frac{\sqrt{3}}{2}z_7(t)\frac{1}{2}z_8(t) \\ -\frac{1}{2}z_1(t) - \frac{\sqrt{3}}{2}z_2(t) & z_1(t) & -\frac{1}{2}z_1(t) + \frac{\sqrt{3}}{2}z_2(t) & \frac{1}{2}z_3(t) + \frac{\sqrt{3}}{2}z_4(t) & \frac{1}{2}z_5(t) + \frac{\sqrt{3}}{2}z_6(t) & -\frac{\sqrt{3}}{2}z_7(t) + \frac{1}{2}z_8(t) \\ z_3(t) & -\frac{1}{2}z_3(t) + \frac{\sqrt{3}}{2}z_4(t) & -\frac{1}{2}z_3(t) - \frac{\sqrt{3}}{2}z_4(t) & 0 & 0 & 0 \\ z_5(t) & -\frac{1}{2}z_5(t) + \frac{\sqrt{3}}{2}z_6(t) & -\frac{1}{2}z_5(t) - \frac{\sqrt{3}}{2}z_6(t) & 0 & 0 & 0 \\ z_8(t) & -\frac{\sqrt{3}}{2}z_7(t) - \frac{1}{2}z_8(t) & \frac{\sqrt{3}}{2}z_7(t) - \frac{1}{2}z_8(t) & 0 & 0 & 0 \end{bmatrix}$$

$$B = \begin{bmatrix} L_s(t) & -M_s(t) & -M_s(t) & 0 & 0 & 0 \\ -M_s(t) & L_s(t) & -M_s(t) & 0 & 0 & 0 \\ -M_s(t) & -M_s(t) & L_s(t) & 0 & 0 & 0 \\ 0 & 0 & 0 & L_f(t) & M_R(t) & 0 \\ 0 & 0 & 0 & M_R(t) & L_D(t) & 0 \\ 0 & 0 & 0 & 0 & 0 & L_Q(t) \end{bmatrix}$$

The external states, internal states and through variables of the synchronous generator model are listed in Table 8.2, Table 8.3, Table 8.4.

Table 8.2. External States of the Generator Parameters Estimation Model.

Index	Variable	Description
0	$v_a(t)$	stator phase A terminal voltage (V)

Table 8.2 continued

Index	Variable	Description
1	$v_b(t)$	stator phase B terminal voltage (V)
2	$v_c(t)$	stator phase C terminal voltage (V)
3	$v_{an}(t)$	stator phase A neutral voltage (V)
4	$v_{bn}(t)$	stator phase B neutral voltage (V)
5	$v_{cn}(t)$	stator phase C neutral voltage (V)
6	$v_f(t)$	rotor field winding terminal voltage (V)
7	$v_{fn}(t)$	rotor field winding neutral voltage (V)
8	$\omega_m(t)$	machine mechanical shaft speed (rad/s)

Table 8.3. Internal States of the Generator Parameters Estimation Model.

Index	Variable	Description
9	$i_{aL}(t)$	current through the inductance of stator phase A (A)
10	$i_{bL}(t)$	current through the inductance of stator phase B (A)
11	$i_{cL}(t)$	current through the inductance of stator phase C (A)
12	$i_{fL}(t)$	current through the inductance of field winding (A)
13	$i_D(t)$	current through rotor d-axis damper-winding (A)
14	$i_Q(t)$	current through rotor q-axis damper-winding (A)
15	$\theta_m(t)$	rotor angular position (rad)
16	$\theta(t)$	electrical rotor position angle (rad)
17	$\omega(t)$	machine electrical shaft speed (rad/s)
18	$T_{fw}(t)$	friction and windage torque (Nm)
19	$P_{em}(t)$	internal electrical power (W)
20	$T_e(t)$	machine electrical torque (Nm)
21	$e_a(t)$	stator winding internal EMF, phase A (V)
22	$e_b(t)$	stator winding internal EMF, phase B (V)
23	$e_c(t)$	stator winding internal EMF, phase C (V)

Table 8.3 continued

Index	Variable	Description
24	$e_f(t)$	field winding internal EMF (V)
25	$e_D(t)$	D-damper winding internal EMF (V)
26	$e_Q(t)$	Q-damper winding internal EMF (V)
27	$\lambda_a(t)$	flux linkage through stator winding of phase A (Wb)
28	$\lambda_b(t)$	flux linkage through stator winding of phase B (Wb)
29	$\lambda_c(t)$	flux linkage through stator winding of phase C (Wb)
30	$\lambda_f(t)$	flux linkage through rotor field winding (Wb)
31	$\lambda_D(t)$	flux linkage through rotor d-axis damper-winding (Wb)
32	$\lambda_Q(t)$	flux linkage through rotor q-axis damper-winding (Wb)
33	$T_{acc}(t)$	machine accelerating torque (Nm)
34	$J(t)$	moment of inertia (kg*m^2)
35	$\omega_m^{'}(t)$	dirivative of machine mechanical shaft speed (rad/s)
36	$c(t)$	cos($\theta(t)$) [state 16]
37	$s(t)$	sin($\theta(t)$) [state 16]
38	$y_1(t)$	internal variable y1 (rad/s)
39	$y_2(t)$	internal variable y2 (rad/s)
40	$c_2(t)$	cos($2\theta(t)$) [state 16]
41	$s_2(t)$	sin($2\theta(t)$) [state 16]
42	$z_1(t)$	auxiliary state (mH)
43	$z_2(t)$	auxiliary state (mH)
44	$z_3(t)$	auxiliary state (mH)
45	$z_4(t)$	auxiliary state (mH)
46	$z_5(t)$	auxiliary state (mH)
47	$z_6(t)$	auxiliary state (mH)
48	$z_7(t)$	auxiliary state (mH)
49	$z_8(t)$	auxiliary state (mH)
50	$L_s(t)$	self-inductance (mH)

Table 8.3 continued

Index	Variable	Description
51	$L_m(t)$	mutual inductance (mH)
52	$L_f(t)$	field self-inductance (mH)
53	$L_D(t)$	D damper self-inductance (mH)
54	$L_Q(t)$	Q damper self-inductance (mH)
55	$M_S(t)$	Stator mutual inductance (mH)
56	$M_R(t)$	field D damper mutual inductance (mH)
57	$M_F(t)$	stator field mutual inductance (mH)
58	$M_D(t)$	stator D damper mutual inductance (mH)
59	$M_Q(t)$	stator Q damper mutual inductance (mH)
60	$H(t)$	inertia constant (s)

Table 8.4. Through Variables of the Generator Parameters Estimation Model.

Index	Variable	Description
0	$i_a(t)$	current through stator phase A (A)
1	$i_b(t)$	current through stator phase B (A)
2	$i_c(t)$	current through stator phase C (A)
3	$i_{an}(t)$	current through stator phase A from neutral (A)
4	$i_{bn}(t)$	current through stator phase B from neutral (A)
5	$i_{cn}(t)$	current through stator phase C from neutral (A)
6	$i_f(t)$	current through rotor field winding (A)
7	$i_{fn}(t)$	current through rotor field winding from neutral (A)
8	$T_m(t)$	mechanical torque applied on the machine shaft (Nm)

It is easy to write the above three equations sets into the standard quadratized device model format, which is:

$$\mathbf{i}(t) = Y_{eqx1}\mathbf{x}(t) + D_{eqxd1}\frac{d\mathbf{x}(t)}{dt} + C_{eqc1}$$

$$0 = Y_{eqx2}\mathbf{x}(t) + D_{eqxd2}\frac{d\mathbf{x}(t)}{dt} + C_{eqc2}$$

$$0 = Y_{eqx3}\mathbf{x}(t) + \left\{ \begin{array}{c} \vdots \\ \mathbf{x}(t)^T \left\langle F^i_{eqxx3} \right\rangle \mathbf{x}(t) \\ \vdots \end{array} \right\} + C_{eqc3}$$

The matrices of the quadratized device model are not listed here since they are too big. There is no controls for the synchronous generator parameter estimation model.

This three phase detailed generator model with parameters can be connected either in Y connection or Δ connection. Y connection is used here as an example. If the three phases of the generator are connected in Y connection, the three neutral points of each phase are connected together. Thus the three neutral voltage states, $v_{an}(t)$, $v_{bn}(t)$ and $v_{cn}(t)$, become one shared state $v_n(t)$. Follow this rule, there are 59 equations and 59 states (including 11 parameters as unknown states) for the quadratized model. After applying the quadratic integration, there are 118 equations and 118 states for the SAQCF model (it uses the states and measurements at time t and time t_m, so everything is doubled).

For the estimation process we assume that the following measurements are available. The actual measurements are listed in Table 8.5. The pseudo measurements are listed in Table 8.6. The derived measurements are listed in Table 8.7. The virtual measurements are not listed here. The virtual measurements are the zeros on the left side of the equations in the SAQCF model (104 zero equations in SAQCF model). So the total number of measurements at time t and time t_m is 130.

Table 8.5. Actual Measurements for the Generator Parameters Estimation.

Index	Variable	Description
0	$v_{an}(t)$	stator phase AN terminal voltage (V)
1	$v_{bn}(t)$	stator phase BN terminal voltage (V)
2	$v_{cn}(t)$	stator phase CN terminal voltage (V)
3	$v_{f1}(t)$	rotor field winding F1 terminal voltage (V)
4	$v_{f2}(t)$	rotor field winding F2 terminal voltage (V)
5	$i_a(t)$	current through stator phase A (A)
6	$i_b(t)$	current through stator phase B (A)
7	$i_c(t)$	current through stator phase C (A)
8	$i_f(t)$	current through rotor field winding (A)
9	$i_{fn}(t)$	current through rotor field winding from neutral (A)
10	$T_m(t)$	mechanical torque applied on the machine shaft (Nm)
11	$\omega_m(t)$	machine mechanical shaft speed (rad/s)

Table 8.6. Pseudo Measurements for the Generator Parameters Estimation.

Index	Variable	Description
0	$v_n(t)$	stator neutral voltage (V)

Since the mechanical speed is actual measurement, thus the electrical speed can be derived as a derived measurement according to the relationship of $0 = \omega(t) - \frac{p}{2}\omega_m(t)$, p is the number of poles.

Table 8.7. Derived Measurements for the Generator Parameters Estimation.

Index	Variable	Description
0	$\omega(t)$	machine electrical shaft speed (rad/s)

As a summary, totally there are 118 states for the model and 130 measurements so the system is observable, which makes the parameters can be successfully estimated by performing dynamic state estimation. Several demonstration examples will be shown in the next chapter.

8.3 Summary

This chapter presented the general idea of using the dynamic state estimation to estimate the model parameters. The idea is to express the key independent parameters as unknown states in the device model, thus these unknown states can be estimated during the state estimation procedure. In order to successfully perform the state estimation, the system needs to be observable, which means the number of measurements should be more than the number of states. An example of synchronous generator parameter estimation model was shown in this chapter. 11 parameters are treated as unknown states in the model and the observability of the synchronous generator parameter estimation problem is analyzed. Several numerical cases will be presented in the next chapter.

CHAPTER 9 SYNCHRONOUS GENERATOR MODEL VALIDATION CASES

9.1 Overview

In this chapter, two synchronous generator model validation cases are described. For the first case, it is actually a generator model calibration case from NERC. NERC provides the measurement data with disturbance and the corrupt generator parameters. The proposed parameter estimation algorithm is applied to estimate the generator parameters and then NERC provides the actual values for each parameter for comparison. The data NERC provided are phasors so the conversion and interpolation are needed to convert the phasor data to sampled value data. For the second case, we use our own simulation results from the known parameter model and perform the dynamic state estimation. The estimated parameters are then compared with the known parameter values.

9.2 Case 1: NERC Provided Data

The proposed parameter identification method requires three phase measurements at the terminals of the generator, measurements at the exciter terminals and measurements of the generator speed. The NERC provided data are positive sequence voltage phasors at the high side of the step up transformer, real and reactive power as well as frequency (see Figure 9.1).

In order to apply the proposed method, the given data are converted into time domain three-phase voltage and current measurements at the terminal of the generator, the

frequency on the high side of the transformer was assumed to be the speed of the generator. In creating the three-phase data, it was assumed that the system operates in balanced conditions. A set of exciter voltage and current measurements are also created by the use of a simplified model.

Using the created data, the state estimator is performed for the simple system provided by NERC. Initially the NERC provided generator parameters is used. The confidence level was very low indicating mismatch between the generator parameters and the provided data.

Subsequently, we run the generator parameter estimation method until we had the maximum improvement to the confidence level of the state estimation. Note that the criterion we use to estimate the generator parameters is the confidence level (or the goodness of fit of the data with the generator model). The results are provided in this section.

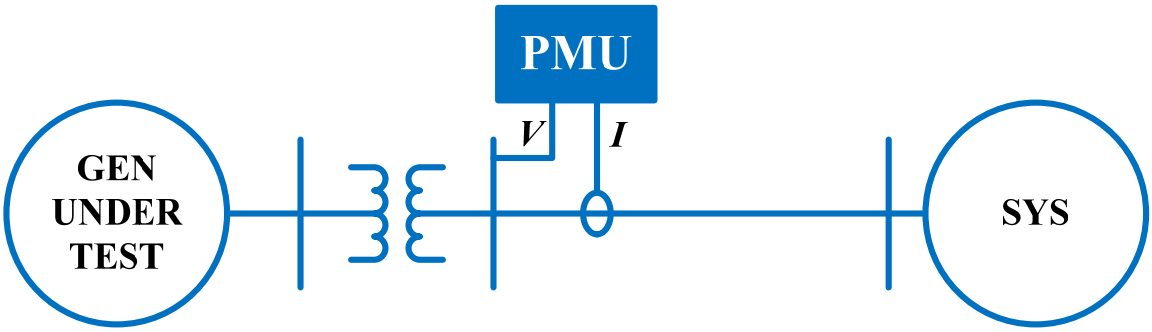

Figure 9.1. NERC Case Test System and Measurement Location [58]

9.2.1 Provided Event Measurement Data

Six measurement quantities are provided: Time (sec), Bus L-L Voltage Magnitude (kV), Bus Frequency (Hz), Active Power Output (MW), Reactive Power Output (MVAR) and Bus Voltage Angle (Deg). The sampling rate is 30 samples/sec.

The first few samples in the provided file are shown in Table 2.1.

Table 9.1. First Few Samples of the Provided Data.

Time	V Mag	Freq	P	Q	Angle
0	547.4673	60.00002	150.008	-1.95556	69.54119
0.033333	547.456	60.00002	149.9997	-1.90678	69.54133
0.066667	547.4366	60.00003	149.9842	-1.90205	69.54166
0.1	547.4335	60.00004	149.9935	-1.90506	69.54196
0.133333	547.4307	60.00001	150.003	-1.90988	69.54157
0.166667	547.4285	59.99997	150.0277	-1.87552	69.54057
0.2	547.4281	59.99995	150.0378	-1.88188	69.5396
0.233333	547.4366	59.99995	150.0351	-1.92892	69.53866
0.266667	547.4299	59.99993	150.0382	-1.88758	69.53742
0.3	547.4277	59.9999	150.0477	-1.89582	69.53572
0.333333	547.4307	59.99988	150.0485	-1.90078	69.53383
0.366667	547.4308	59.99984	150.0637	-1.8666	69.53132
0.4	547.4241	59.99981	150.0617	-1.87419	69.52841
0.433333	547.4166	59.99978	150.0596	-1.88217	69.52535
0.466666	547.4108	59.99974	150.0731	-1.85131	69.52157
0.5	547.4031	59.9997	150.0607	-1.85849	69.51737
0.533333	547.4039	59.99968	150.0403	-1.86198	69.51313
0.566666	547.4205	59.99968	150.0193	-1.90959	69.50908
0.6	547.4301	59.99968	149.9913	-1.90856	69.50512
0.633333	547.4187	59.99969	149.9829	-1.87043	69.5012
0.666666	547.4078	59.99966	149.9696	-1.87817	69.49677
0.7	547.4105	59.99964	149.9803	-1.89471	69.49191

A graphical view of the provided data is shown in Figure 9.2. Note that the data span a period of 90 seconds and an event was initiated at time 14.7 seconds.

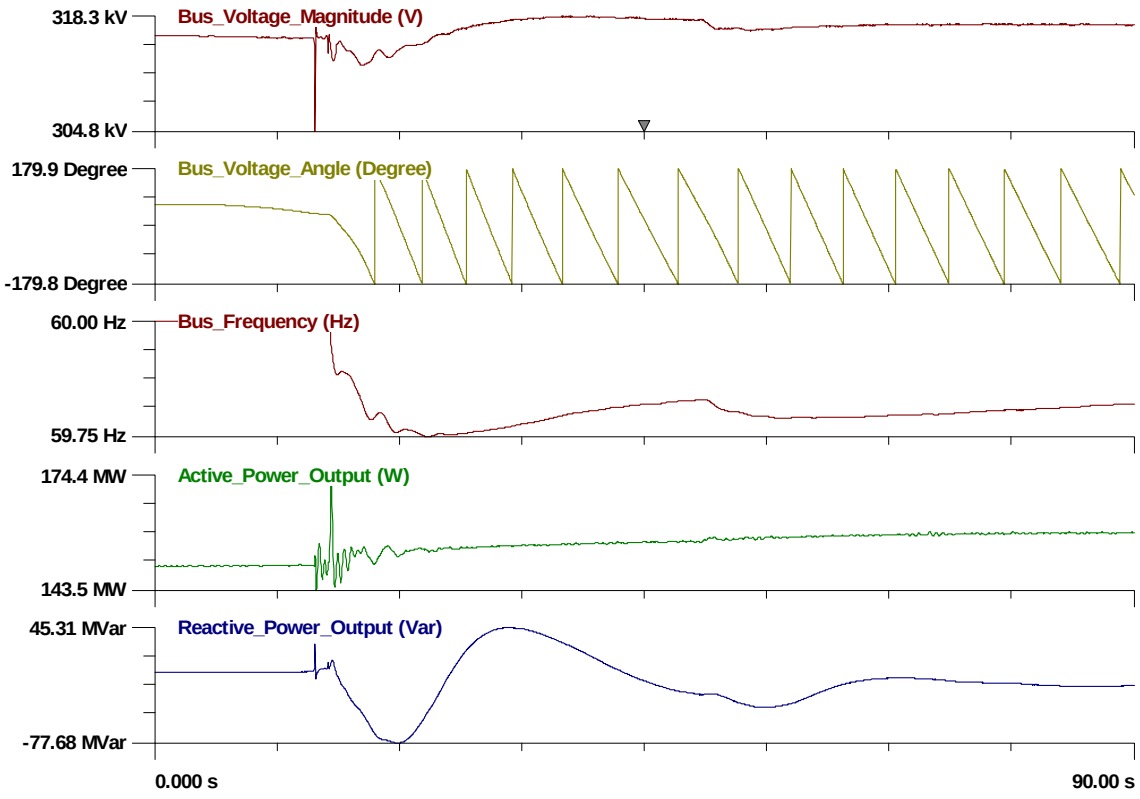

Figure 9.2. Graphical Presentation of the Provided Data

9.2.2 Conversion of Provided Data into Three-Phase Voltage and Current Phasor Measurements

The provided data are converted into three-phase voltage and current phasor measurements. The frequency is used to provide the speed of the generator. Note that since the frequency is measured at the high side of the transformer, it may not be exactly the speed of the generator. However, we believe that our assumption is reasonable.

The problem is posted as follows:

Given $V_{L-L,mag}$, θ_{Va}, P_{3p} and Q_{3p},

Compute:

1. Phase A Current Magnitude, Phase A Current Phase Angle,

2. Phase B Current Magnitude, Phase B Current Phase Angle,
3. Phase C Current Magnitude, Phase C Current Phase Angle,
4. Phase A Voltage Magnitude, Phase A Voltage Phase Angle,
5. Phase B Voltage Magnitude, Phase B Voltage Phase Angle,
6. Phase C Voltage Magnitude, Phase C Voltage Phase Angle

The calculations are shown below:

$$\tilde{I}_a = \left(\frac{P_{3p} + jQ_{3p}}{\sqrt{3} V_{L-L,mag} e^{j\theta_{VA}}} \right)^*$$

$$V_{amag} = V_{bmag} = V_{cmag} = \frac{V_{L-L,mag}}{\sqrt{3}}$$

$$I_{mag} = I_{amag} = I_{bmag} = I_{cmag} = abs\left(\tilde{I}_a\right)$$

$$\theta_{Vb} = \theta_{Va} - 120^\circ, \theta_{Vc} = \theta_{Va} - 240^\circ$$

$$\theta_{Ia} = phase\left(\tilde{I}_a\right),\ \theta_{Ib} = \theta_{Ia} - 120^\circ, \theta_{Ic} = \theta_{Ia} - 240^\circ$$

The results are shown in Figure 9.3.

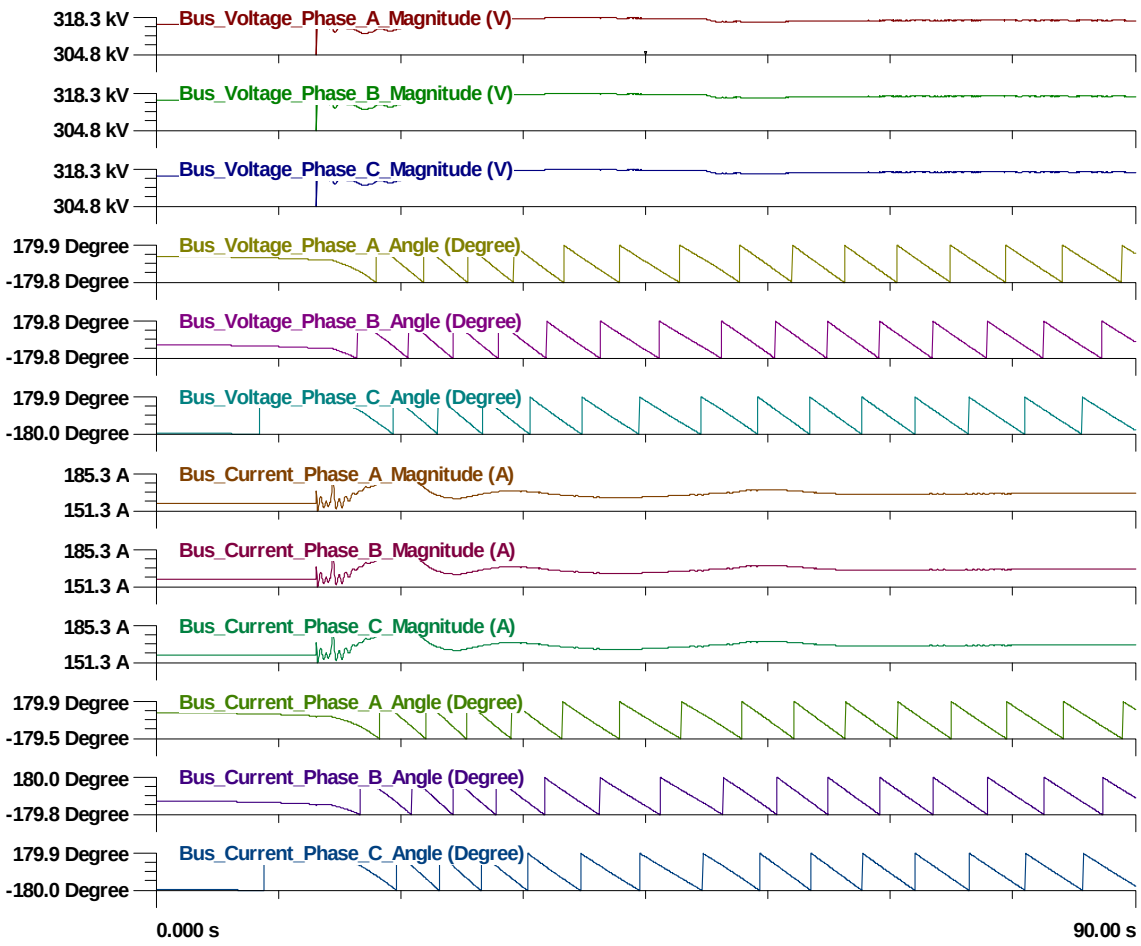

Figure 9.3. Three Phase Voltage and Current Phasor Measurements and Frequency on the Transformer High Side

9.2.3 Data Conversion to Generator Side

The data created in last section are converted to the generator bus. For this purpose, the step up transformer model is used to compute. Specifically, the problem is posted as follows:

Given the voltage and current phasor measurements on the high side of the step up transformer, compute the voltage and current phasors at the terminal of the generator. Note that we assume that there are no auxiliaries at the terminals of the generator that may draw some current.

The computations are performed as follows. The step up transformer is delta-wye connected. The circuit is shown below.

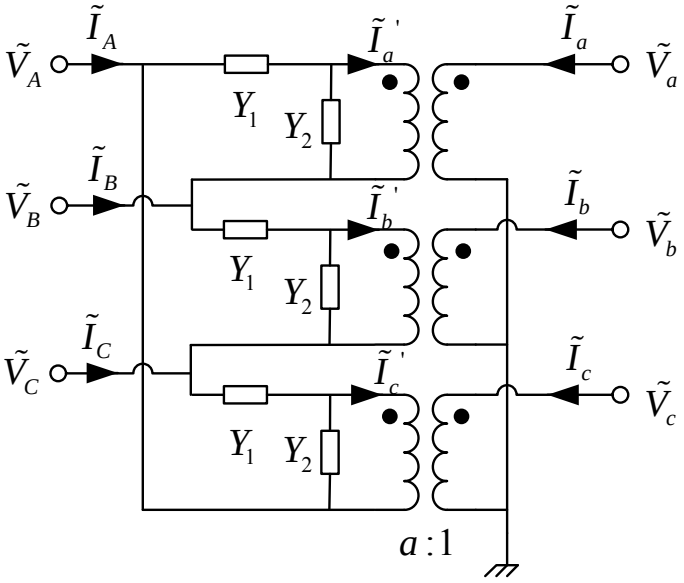

Figure 9.4. Step Up Transformer Circuit

Given transformer rating S, ratio a, leakage reactance X, winding resistance R, magnetizing admittance G and B, the following parameters can be calculated:

$$Y_{base} = \frac{S}{V^2_{L-L,low}} \quad , \qquad Y_1 = \frac{1}{R + jx} \cdot Y_{base} , \qquad Y_2 = (G - jB) \cdot Y_{base}$$

From the circuit, the following relationships are valid:

$$\tilde{I}_a' = (\tilde{V}_A - \tilde{V}_B - a\tilde{V}_a)Y_1 - a\tilde{V}_a Y_2 \qquad \tilde{I}_a = -a\tilde{I}_a'$$

$$\tilde{I}_b' = (\tilde{V}_B - \tilde{V}_C - a\tilde{V}_b)Y - a\tilde{V}_b Y_2 \qquad \tilde{I}_b = -a\tilde{I}_b'$$

$$\tilde{I}_c' = (\tilde{V}_C - \tilde{V}_A - a\tilde{V}_c)Y - a\tilde{V}_c Y_2 \qquad \tilde{I}_c = -a\tilde{I}_c'$$

$$\tilde{I}_A = \tilde{I}_a' + aV_a Y_2 - \tilde{I}_c' - aV_c Y_2$$

$$\tilde{I}_B = \tilde{I}_b' + aV_b Y_2 - \tilde{I}_a' - aV_a Y_2$$

$$\tilde{I}_C = \tilde{I}_c' + aV_c Y_2 - \tilde{I}_b' - aV_b Y_2$$

Expressing the low voltage side quantities as a function of the high voltage side quantities, we obtain a set of six equations which is written in the following matrix notation:

$$\begin{bmatrix} 1 & 0 & 0 & 0 & 0 & 0 \\ 0 & 1 & 0 & 0 & 0 & 0 \\ 0 & 0 & 1 & 0 & 0 & 0 \\ 0 & 0 & 0 & Y_1 & -Y_1 & 0 \\ 0 & 0 & 0 & 0 & Y_1 & -Y_1 \\ 0 & 0 & 0 & -Y_1 & 0 & Y_1 \end{bmatrix} \begin{bmatrix} \tilde{I}_A \\ \tilde{I}_B \\ \tilde{I}_C \\ \tilde{V}_A \\ \tilde{V}_B \\ \tilde{V}_C \end{bmatrix} = \begin{bmatrix} 1 & 0 & -1 & aY_2 & 0 & -aY_2 \\ -1 & 1 & 0 & -aY_2 & aY_2 & 0 \\ 0 & -1 & 1 & 0 & -aY_2 & aY_2 \\ -a & 0 & 0 & aY_1 + aY_2 & 0 & 0 \\ 0 & -a & 0 & 0 & aY_1 + aY_2 & 0 \\ 0 & 0 & -a & 0 & 0 & aY_1 + aY_2 \end{bmatrix} \begin{bmatrix} \tilde{I}_a \\ \tilde{I}_b \\ \tilde{I}_c \\ \tilde{V}_a \\ \tilde{V}_b \\ \tilde{V}_c \end{bmatrix}$$

$$\begin{bmatrix} \tilde{I}_A \\ \tilde{I}_B \\ \tilde{I}_C \\ \tilde{V}_A \\ \tilde{V}_B \\ \tilde{V}_C \end{bmatrix} = \begin{bmatrix} 1 & 0 & 0 & 0 & 0 & 0 \\ 0 & 1 & 0 & 0 & 0 & 0 \\ 0 & 0 & 1 & 0 & 0 & 0 \\ 0 & 0 & 0 & Y_1 & -Y_1 & 0 \\ 0 & 0 & 0 & 0 & Y_1 & -Y_1 \\ 0 & 0 & 0 & -Y_1 & 0 & Y_1 \end{bmatrix}^{-1} \begin{bmatrix} 1 & 0 & -1 & aY_2 & 0 & -aY_2 \\ -1 & 1 & 0 & -aY_2 & aY_2 & 0 \\ 0 & -1 & 1 & 0 & -aY_2 & aY_2 \\ -a & 0 & 0 & aY_1 + aY_2 & 0 & 0 \\ 0 & -a & 0 & 0 & aY_1 + aY_2 & 0 \\ 0 & 0 & -a & 0 & 0 & aY_1 + aY_2 \end{bmatrix} \begin{bmatrix} \tilde{I}_a \\ \tilde{I}_b \\ \tilde{I}_c \\ \tilde{V}_a \\ \tilde{V}_b \\ \tilde{V}_c \end{bmatrix}$$

The computed data are illustrated in Figure 9.5.

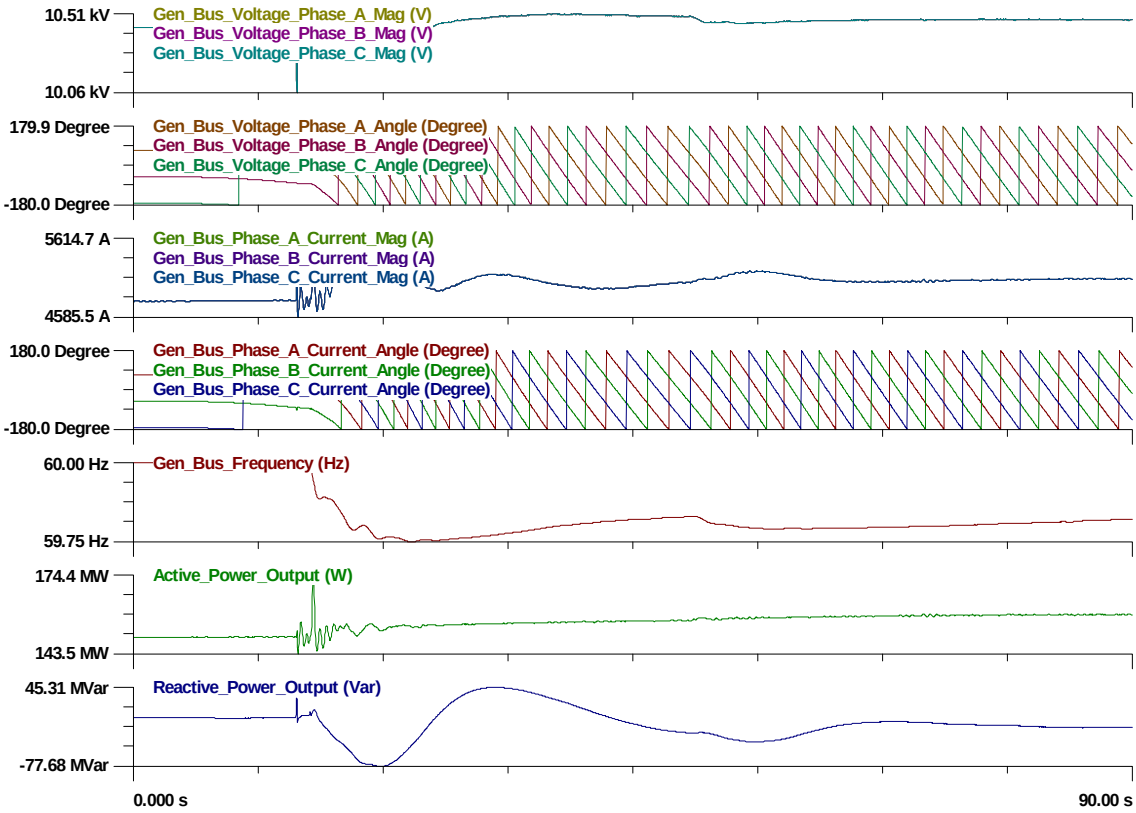

Figure 9.5. Computed Voltage and Current Phasor Data and Frequency Computed at the Terminals of the Generator

Note that the data include the following quantities:

Generator bus voltage phase A magnitude;

Generator bus voltage phase B magnitude;

Generator bus voltage phase C magnitude;

Generator bus voltage phase A angle;

Generator bus voltage phase B angle;

Generator bus voltage phase C angle;

Generator phase A current magnitude;

Generator phase B current magnitude;

Generator phase C current magnitude;

Generator phase A current angle;

Generator phase B current angle;

Generator phase C current angle;

Generator bus frequency;

Generator active power output;

Generator reactive power output;

9.2.4 Measurement Data Conversion into Time Domain Sampled Value Data

The phasor data are converted into time domain sampled value data. The selected sampling rate is 4800 samples/s.

The computational procedure is given below:

$$V_A(t) = V_{Amag} \cos(2\pi f_0 \cdot t + \theta_{VA})$$

$$V_B(t) = V_{Bmag} \cos(2\pi f_0 \cdot t + \theta_{VB})$$

$$V_C(t) = V_{Cmag} \cos(2\pi f_0 \cdot t + \theta_{VC})$$

$$I_A(t) = I_{Amag} \cos(2\pi f_0 \cdot t + \theta_{IA})$$

$$I_B(t) = I_{Bmag} \cos(2\pi f_0 \cdot t + \theta_{IB})$$

$$I_C(t) = I_{Cmag} \cos(2\pi f_0 \cdot t + \theta_{IC})$$

The generator frequency is:

$$\mathrm{f}(t) = f_0 + \frac{1}{2\pi} \frac{1}{6} \frac{d}{dt} (\theta_{VA} + \theta_{VB} + \theta_{VC} + \theta_{IA} + \theta_{IB} + \theta_{IC})$$

$$\omega(t) = 2\pi \mathrm{f}(t)$$

The resulting sampled value data are shown in Figure 9.6.

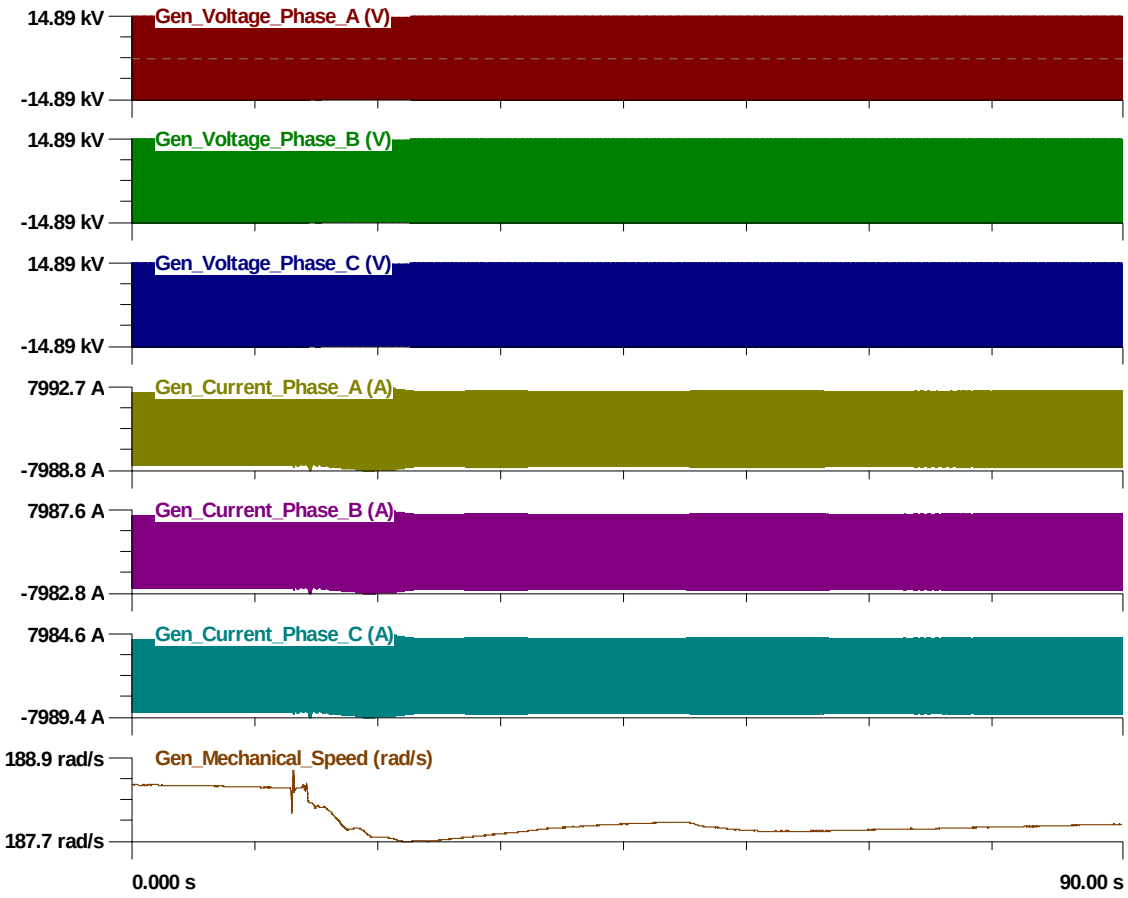

Figure 9.6. Sampled Value Data of Voltage and Current at the Generator Terminals

The data from time 5 seconds to 5.1 seconds are shown in Figure 9.7 for better observance.

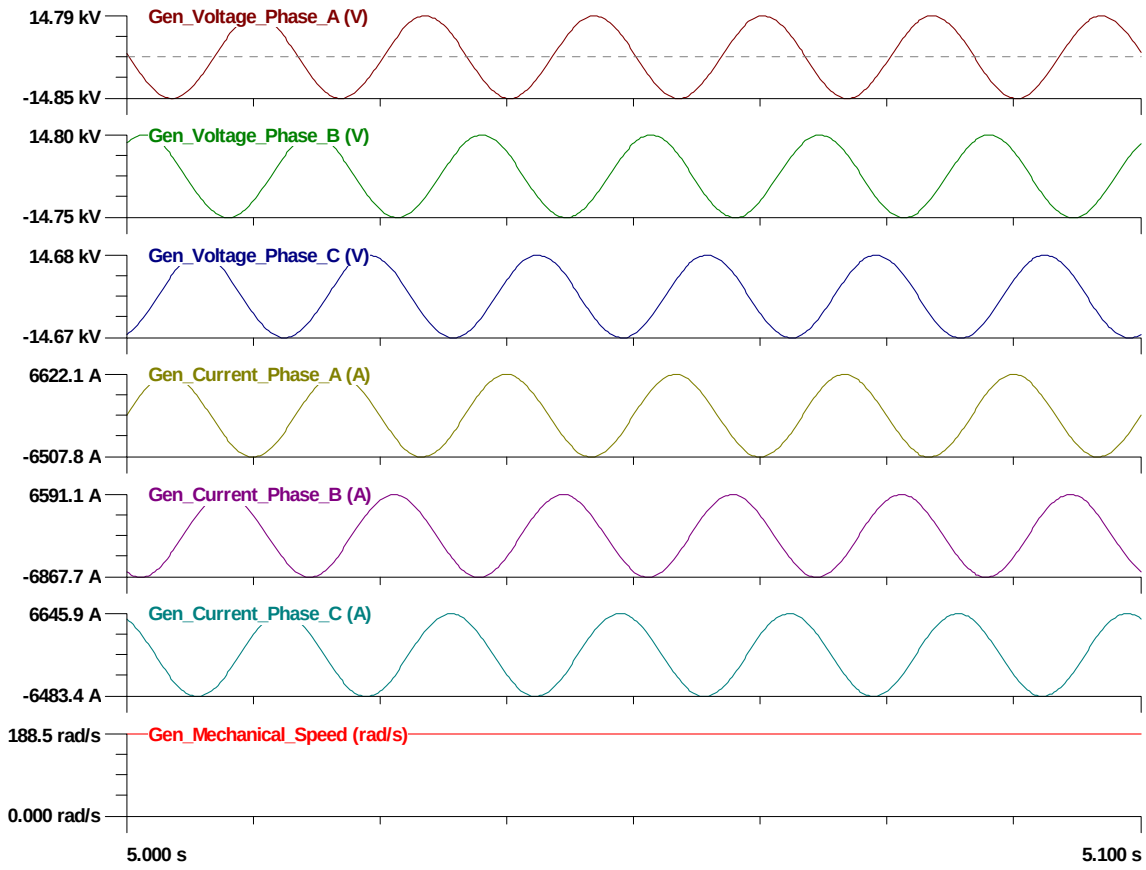

Figure 9.7. Sampled Value Data of Voltage and Current at the Generator Terminals from period of 5.0 seconds to 5.1 seconds

9.2.5 Parameter Calibration Results

The dynamic state estimation results by using the original provided generator parameters are shown in Figure 9.8.

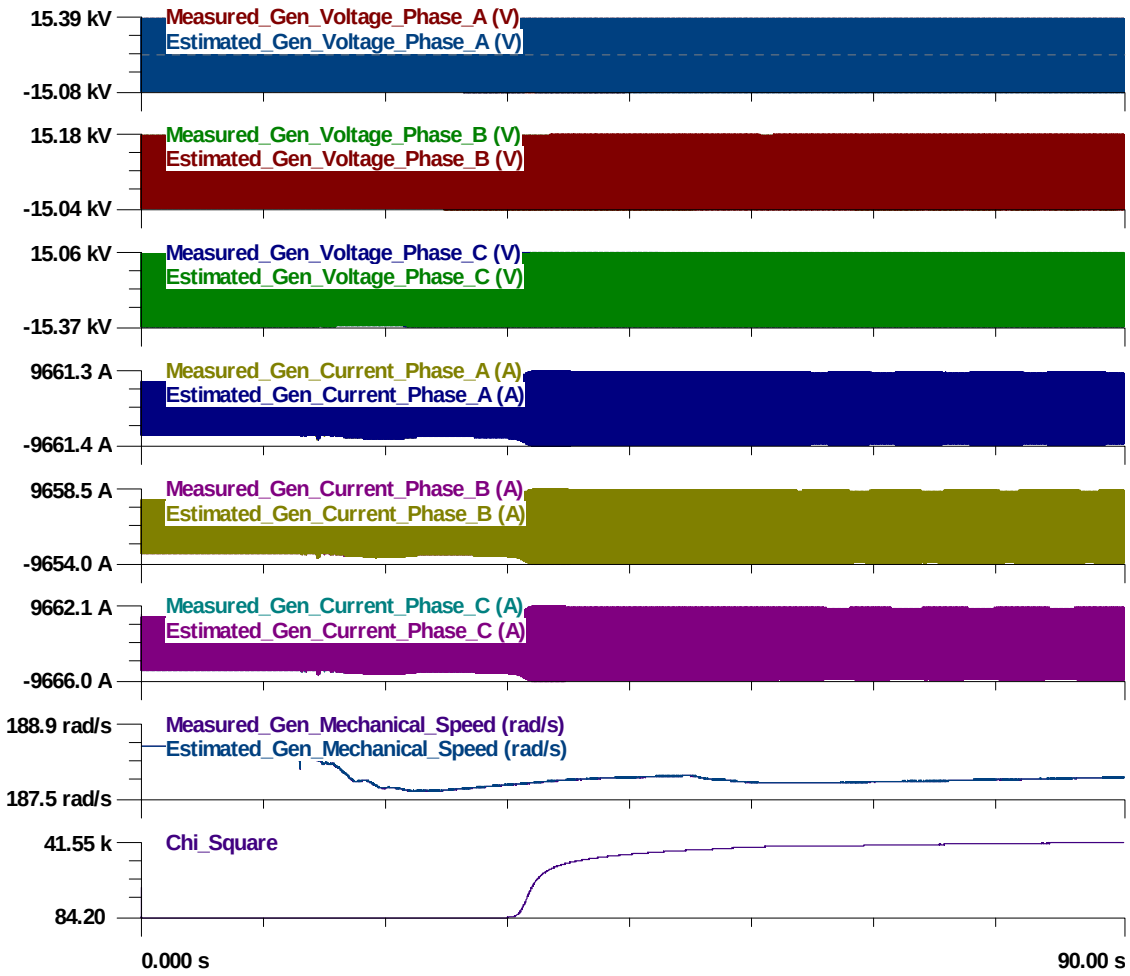

Figure 9.8. Dynamic State Estimation with Generator Provided Parameters

The first six sets of traces are the measured and estimated terminal voltages and currents. The seventh set of traces is the measured and estimated generator mechanical speed. The last trace is the chi-square value. It can be seen that the chi-square value is very large indicating substantial mismatch between the measurements and the generator model when the provided generator parameters are used.

For convenience, two zoomed in views of the data of Figure 9.8 are provided for the time intervals: [10.0s,10.1s] and [40.0s,40.1s]. Specifically, Figure 9.9 provides a

zoomed in view in the time interval [10.0s,10.1s] and Figure 9.10 provides a zoomed in view in the time interval [40.0s,40.1s].

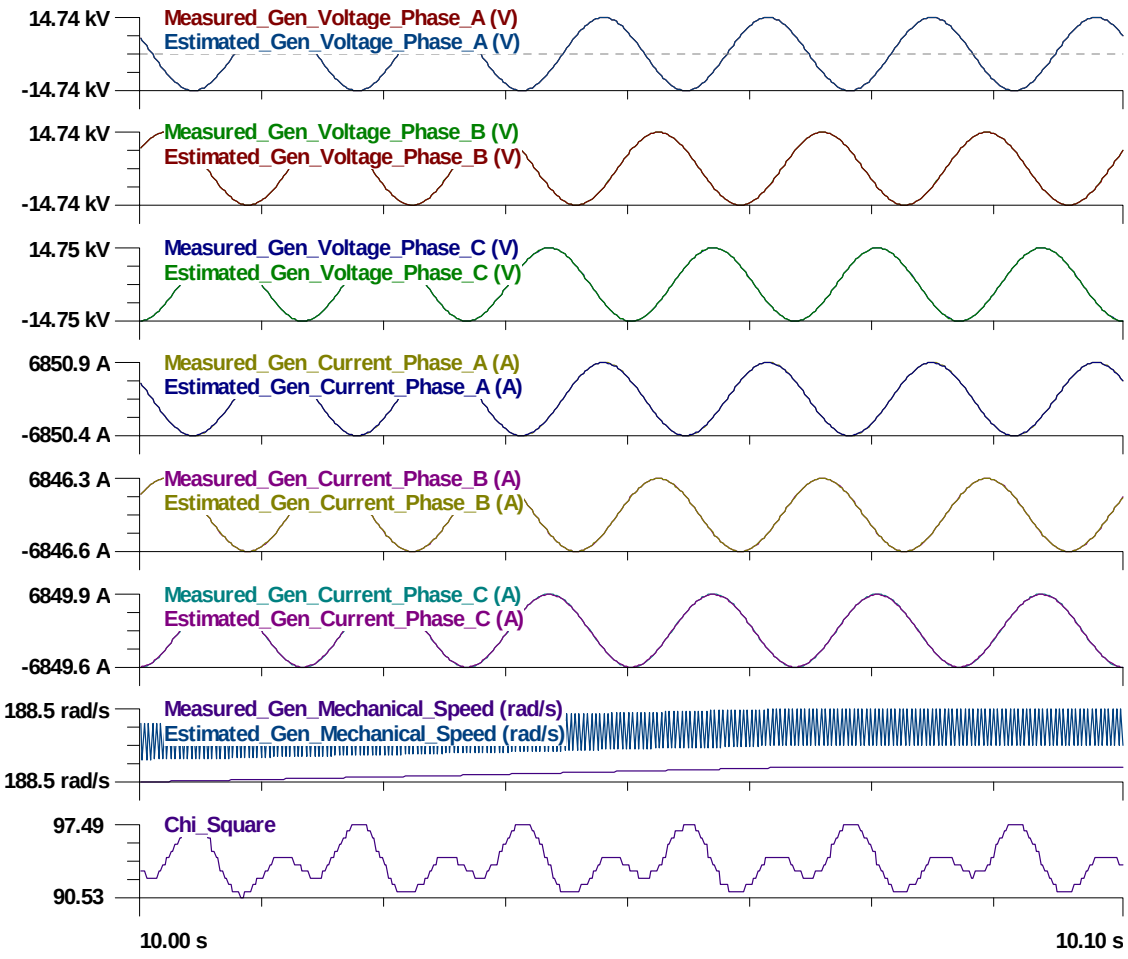

Figure 9.9. Dynamic State Estimation with Generator Provided Parameters – Zoomed-In View, [10.0s,10.1s]

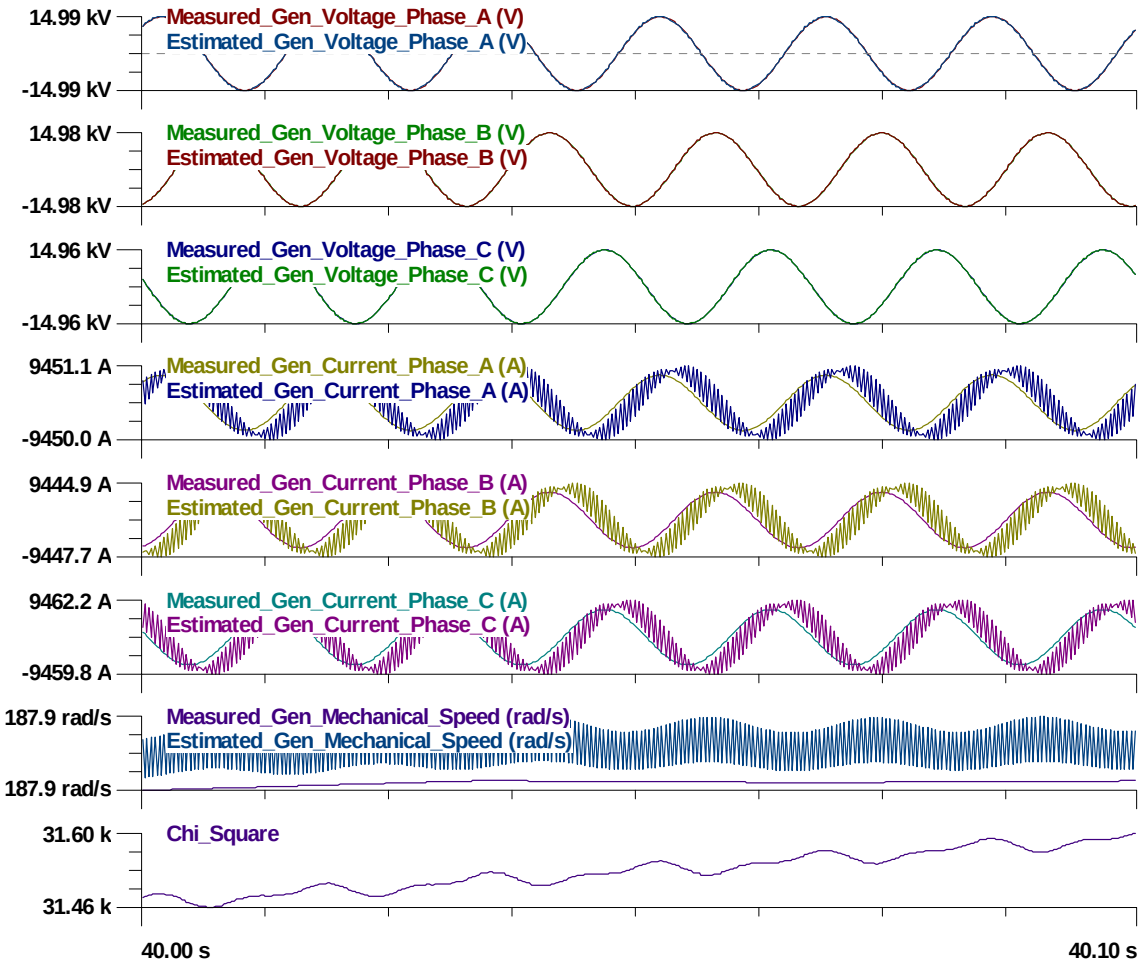

Figure 9.10. Dynamic State Estimation with Generator Provided Parameters – Zoomed-In View, [40.0s,40.1s]

The parameter identification process yielded the estimated parameters in Table 9.2.

Table 9.2. Estimated Generator Physical Parameters.

L_s	L_m	L_f	L_D	L_Q	M_S	M_R	M_F	M_D	M_Q
2.5349 mH	1.2789 mH	78.5663 mH	5.0182 mH	10.8005 mH	1.2674 mH	18.1458 mH	16.2813 mH	4.0827 mH	3.0072 mH

The above estimated physical parameters are converted to the d-q-0 parameters for easier comparison. Table 9.3 shows the initial generator parameters and the estimated parameters.

Table 9.3. Estimated Generator Physical Parameters.

Parameter	Original	Estimated
Xd	1.85	1.75
X'd	0.21	0.21
X"d	0.15	0.15
Xq	1.3	1.70
X'q	0.7	0.60
X"q	0.15	0.20
Xl	0.15	0.15
T'd0	5	9.5
T"d0	0.25	0.12
T'q0	1	1
T"q0	0.05	0.08

The dynamic state estimation results with the tuned parameters are shown in the Figure 9.11.

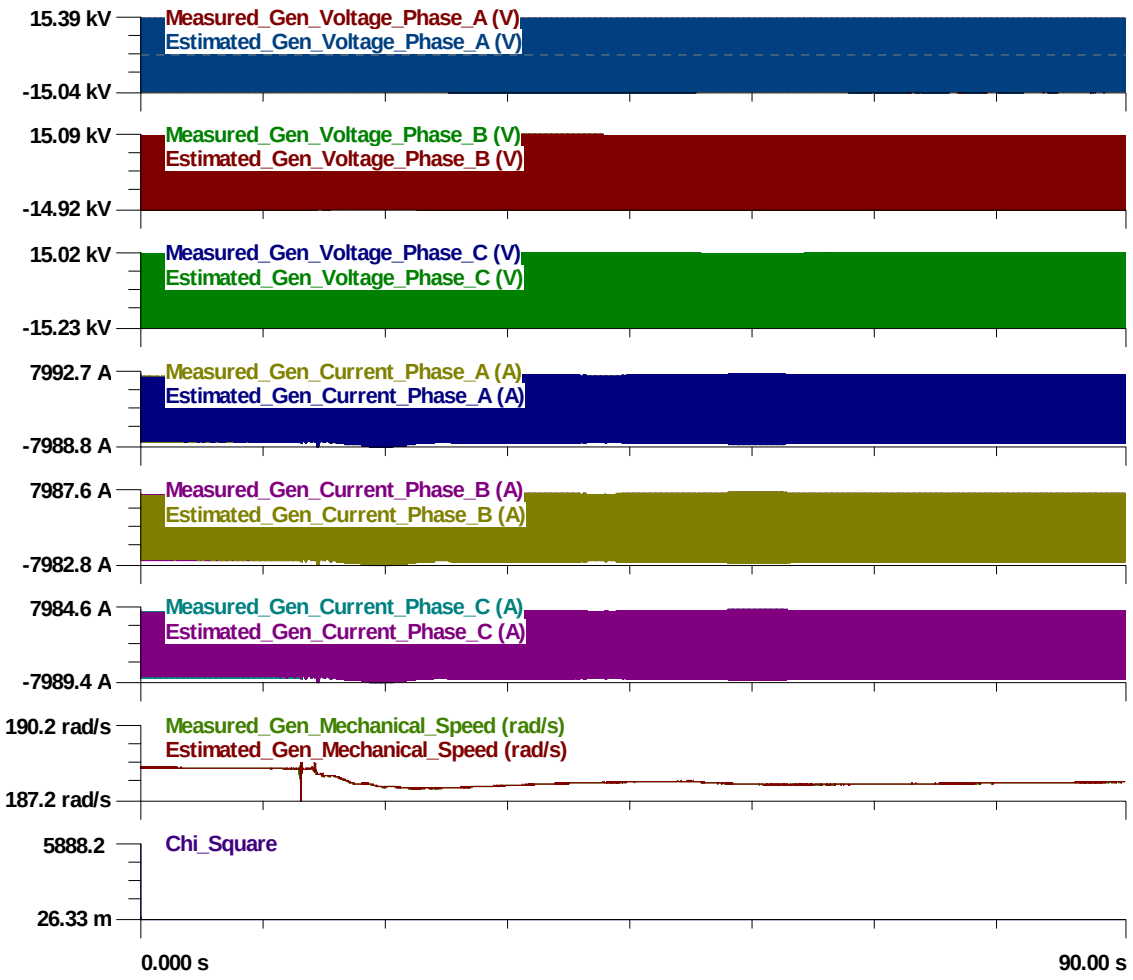

Figure 9.11. Dynamic State Estimation with Tuned Generator Parameters

The first six sets of traces are the measured and estimated terminal voltages and currents. It can be observed that the measured and estimated value are closer, which means the model matches with the measurements. The seventh set of traces is the measured and estimated generator mechanical speed. The last trace is the chi-square value. It can be seen that the chi-square value is relatively small indicating improved fitting between the measurements and the generator model when the estimated generator parameters are used.

For convenience, two zoomed in views of the data of Figure 9.11 are provided for the time intervals: [10.0s,10.1s] and [40.0s,40.1s]. Specifically, Figure 9.12 provides a zoomed in view in the time interval [10.0s,10.1s] and Figure 9.13 provides a zoomed in view in the time interval [40.0s,40.1s].

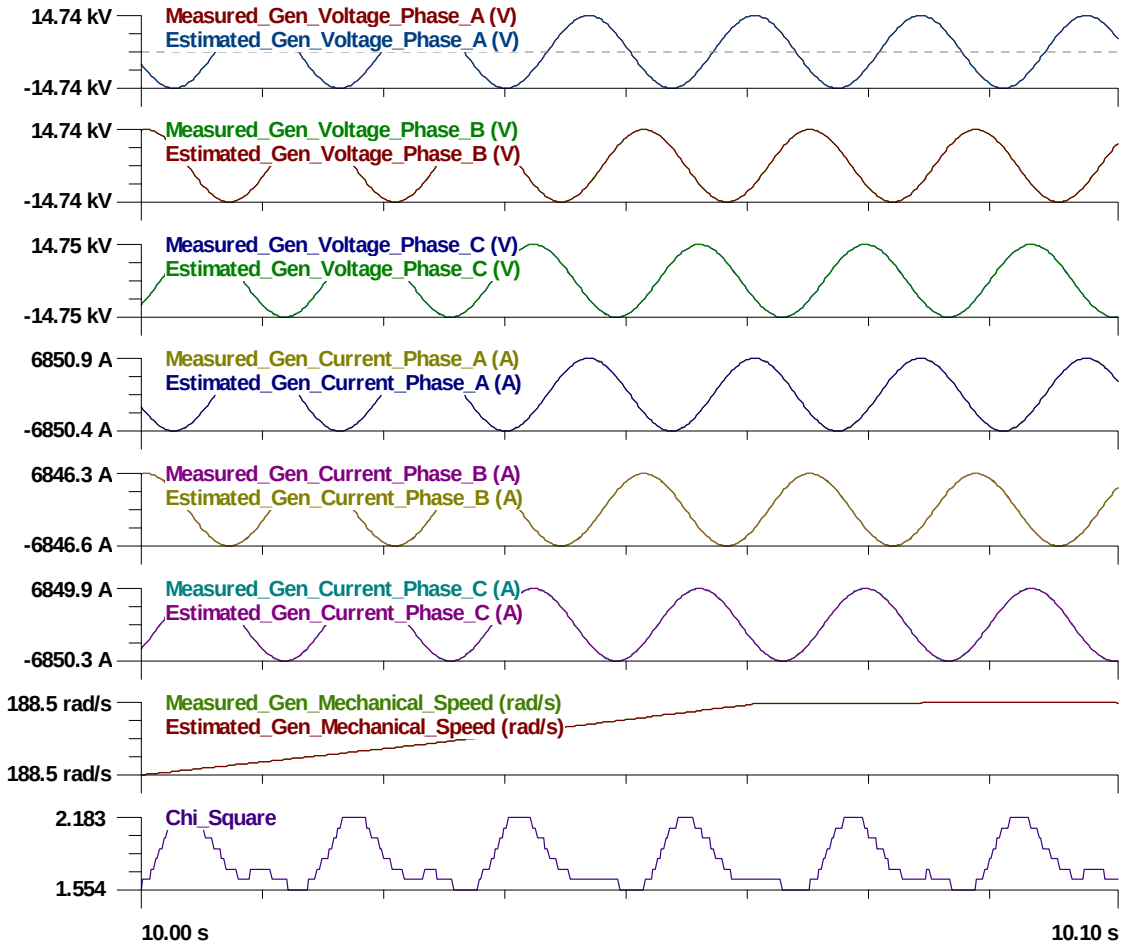

Figure 9.12. Dynamic State Estimation with Tuned Generator Parameters – Zoomed-In View, [10.0s,10.1s]

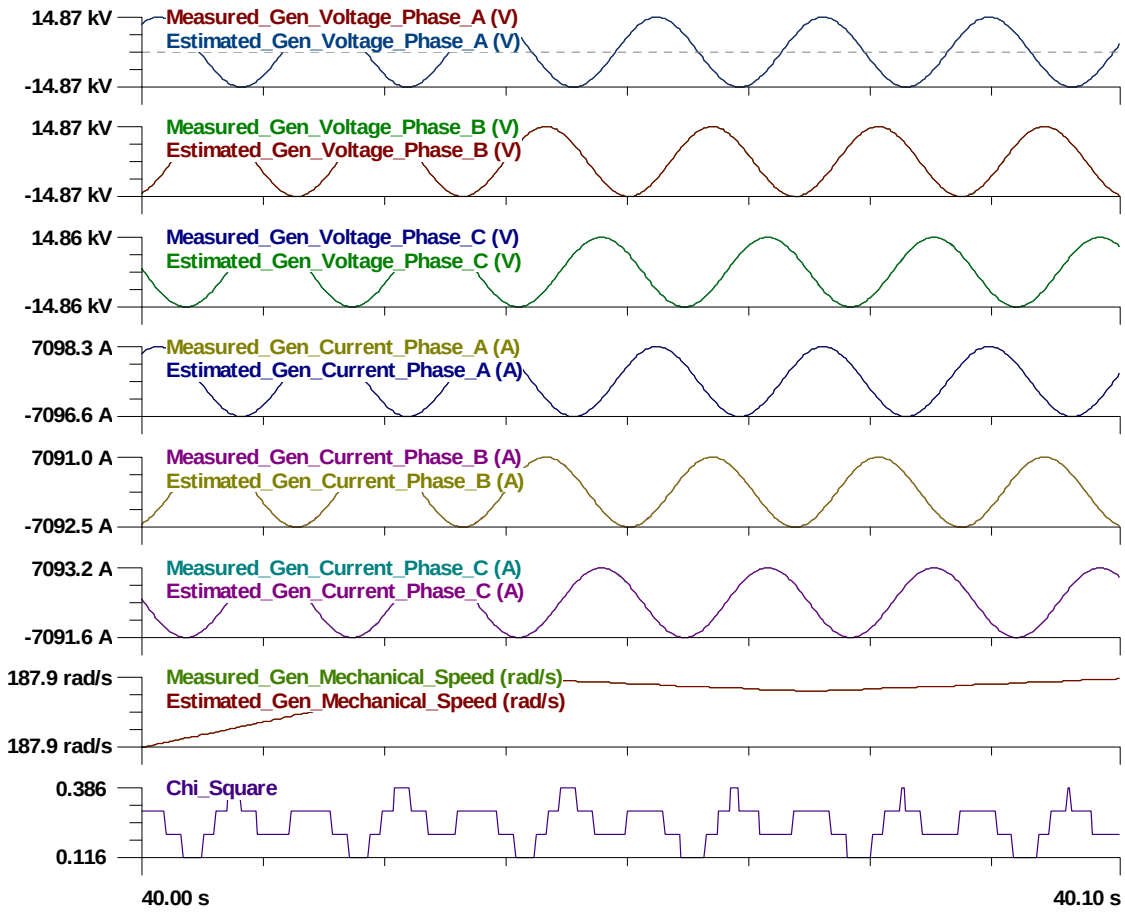

Figure 9.13. Dynamic State Estimation with Tuned Generator Parameters – Zoomed-In View, [40.0s,40.1s]

NERC released the actual parameters later. The results are listed in Table 9.4.

Table 9.4. Summary of Actual, Corrupt and Tuned Parameters.

Parameter	Actual	Corrupt	Estimated
Xd	1.85	1.85	1.75
X'd	0.21	0.21	0.21
X"d	0.15	0.15	0.15
Xq	1.8	1.3	1.7
X'q	0.45	0.7	0.6
X"q	0.15	0.15	0.2
Xl	0.15	0.15	0.15
T'd0	6.5	5	9.5
T"d0	0.05	0.25	0.12
T'q0	1	1	1
T"q0	0.05	0.05	0.08

From the table, it can be seen that compared to the corrupt parameters, the calibrated parameters are close to the actual parameters in the correct direction (highlighted in the table). Although some of the parameters are still not exactly the same as the actual values, the calibrated model is still more suitable to the measurements.

The reasons that cause the imperfect parameter estimation are (1) only phasor measurements are available at the high side of the step-up transformer and we had to convert the phasor measurements to three phase sampled value based on the assumption that the three phases are balanced, and (2) no measurements are available at the exciter and governor terminal sides. For best performance of the proposed method for generator parameter identification, these measurements are required. If there were three phase generator terminal measurements, exciter and governor measurements, the generator parameters can be estimated more accurately.

9.3 Case 2: Simulated Data

In this case, a generator with known parameters is utilized first to perform the simulation and the generator measurements from the simulation are stored. Then a generator model which treats the parameters as unknown states is used to perform the state estimation to obtain the estimated parameters. In this step, some initial parameters are chosen as initial values for the parameters in the state estimation. The generator model using the initial parameters will be used to perform the state estimation first. Then the parameter estimation will be used to estimate the parameters. The last step is to run

the simulation again with the estimated generator parameters and the measurements from the new simulation will be used to compare with the stored measurements.

The test system for the generator parameter estimation is the same as the one used for protection in Chapter 7. Again, the test system is shown in Figure 9.14 where the synchronous generator for the parameter estimation purpose is in the blue block. The ratings of generator are 825 MVA, 18 kV and 60 Hz. The step-up transformer is 725 MVA, 18kV/230kV for the interconnection to the system, which is rated 230 kV. The actual parameters are shown in Table 9.5.

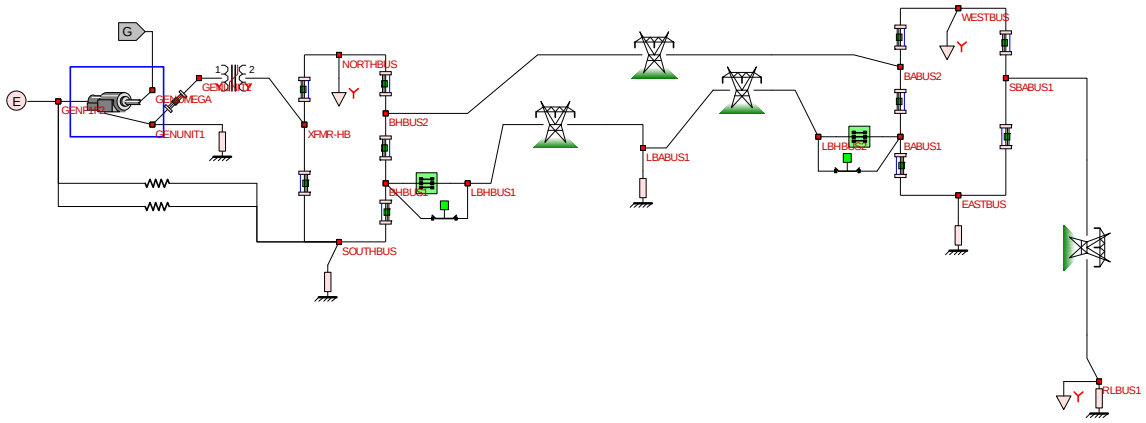

Figure 9.14. Synchronous Generator Parameter Estimation Test System

Table 9.5. Generator Actual Parameters Used in the Simulation.

Parameters	Actual Value
L_s	1.437603 mH
L_m	0.017362 mH
L_f	28.11097 mH
L_D	1.705491 mH
L_Q	1.028648 mH
M_S	0.671923 mH
M_R	6.020414 mH
M_F	5.40181 mH

Table 9.5. continued

M_D	1.354546 mH
M_Q	1.056418 mH
H	2.8 s

The measurements are terminal voltages and currents, excitation voltage and current, shaft torque and mechanical speed. A summary of the measurement list is shown in Table 9.6.

Table 9.6. Measurement List for the Generator Parameters Estimation.

Index	Variable	Description
0	$v_{an}(t)$	stator phase AN terminal voltage (V)
1	$v_{bn}(t)$	stator phase BN terminal voltage (V)
2	$v_{cn}(t)$	stator phase CN terminal voltage (V)
3	$v_{f1}(t)$	rotor field winding F1 terminal voltage (V)
4	$v_{f2}(t)$	rotor field winding F2 terminal voltage (V)
5	$i_a(t)$	current through stator phase A (A)
6	$i_b(t)$	current through stator phase B (A)
7	$i_c(t)$	current through stator phase C (A)
8	$i_f(t)$	current through rotor field winding (A)
9	$i_{fn}(t)$	current through rotor field winding from neutral (A)
10	$T_m(t)$	mechanical torque applied on the machine shaft (Nm)
11	$\omega_m(t)$	machine mechanical shaft speed (rad/s)

Step 1: Simulation using the generator actual parameters

In the first step, a simulation is run by using the generator actual parameters as shown in Table 9.5 to obtain 12 measurements for the generator. These measurements are

stored in a COMTRADE file and they will be used as measurements for the parameter estimation process. These measurements are depicted in Figure 9.15.

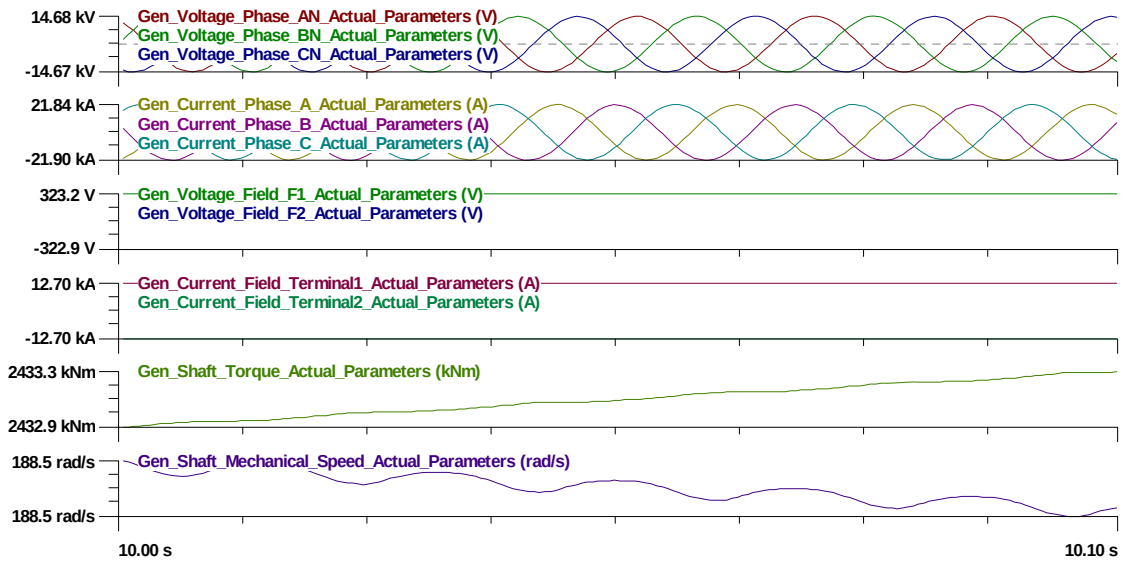

Figure 9.15. Generator Measurements Using Generator Actual Parameters

The first set of the measurements is generator terminal three phase voltages. The second set is three phase currents. The third and fourth sets are field voltages and current. The last two sets are the generator shaft torque and mechanical speed.

Step 2: State estimation using generator initial parameters

To perform the parameter estimation, the parameter initial values are needed. The initial parameters are basically chosen based on generator data sheet and manual. The initial parameters are listed in Table 9.7.

Table 9.7. Generator Initial Parameters Chosen for the Parameter Estimation.

Parameters	Initial Value
L_s	1.88 mH
L_m	0.01 mH
L_f	41.1 mH

Table 9.7. continued

L_D	2.28 mH
L_Q	1.31 mH
M_S	0.83 mH
M_R	8.60 mH
M_F	7.72 mH
M_D	1.93 mH
M_Q	1.46 mH
H	3.0 s

The dynamic state estimation is performed using the generator model with the initial parameters to see how the model fits with the measurements. The results are shown in Figure 9.16.

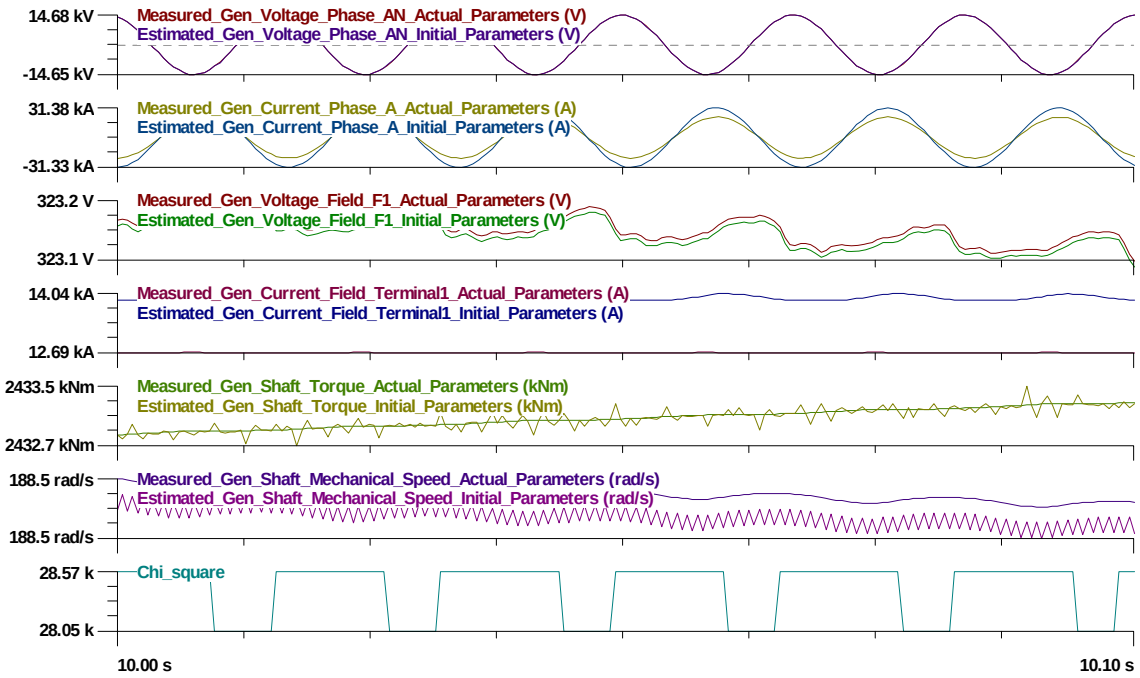

Figure 9.16. State Estimation Results Using Generator Initial Parameters

There are totally seven traces in the figure. The first six traces are the measured and estimated generator terminal voltage, terminal current, field voltage, field current, torque

and mechanical speed. That last trace is the chi square value of the state estimation. It can be seen that the measurements and the model do not fit with each other, which means the initial parameters are not accurate and may contain large errors.

Step 3: Parameter estimation using generator parameter model

In this step, the generator parameters are treated as unknown states in the generator model as described in Chapter 7. The state estimation results are shown in Figure 9.17.

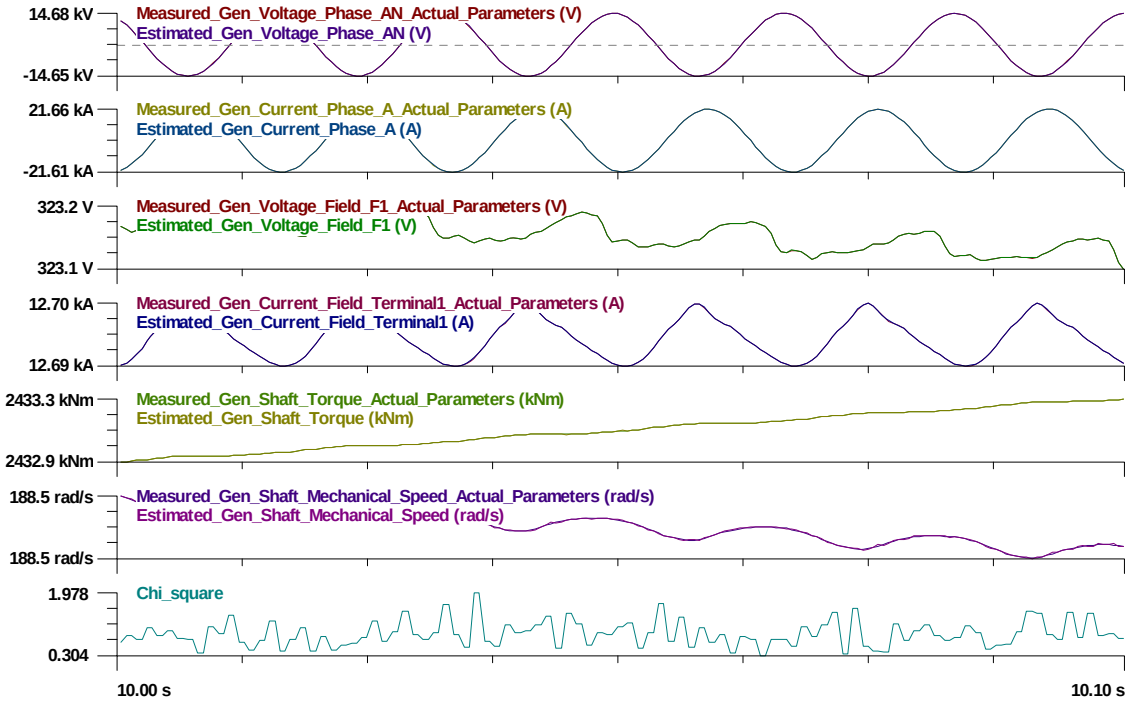

Figure 9.17. State Estimation Results Using Generator Parameter Model

The same as Figure 9.16, measured and estimated generator terminal voltage, terminal current, field voltage, field current, torque and mechanical speed are illustrated in Figure 9.17. It can be seen that different than the previous chi square, the chi square value in this case is very small, which indicates that the measurements fit the model. The generator parameters (treated as states of the model) are estimated by the state estimation. The estimated parameters are shown in Figure 9.18.

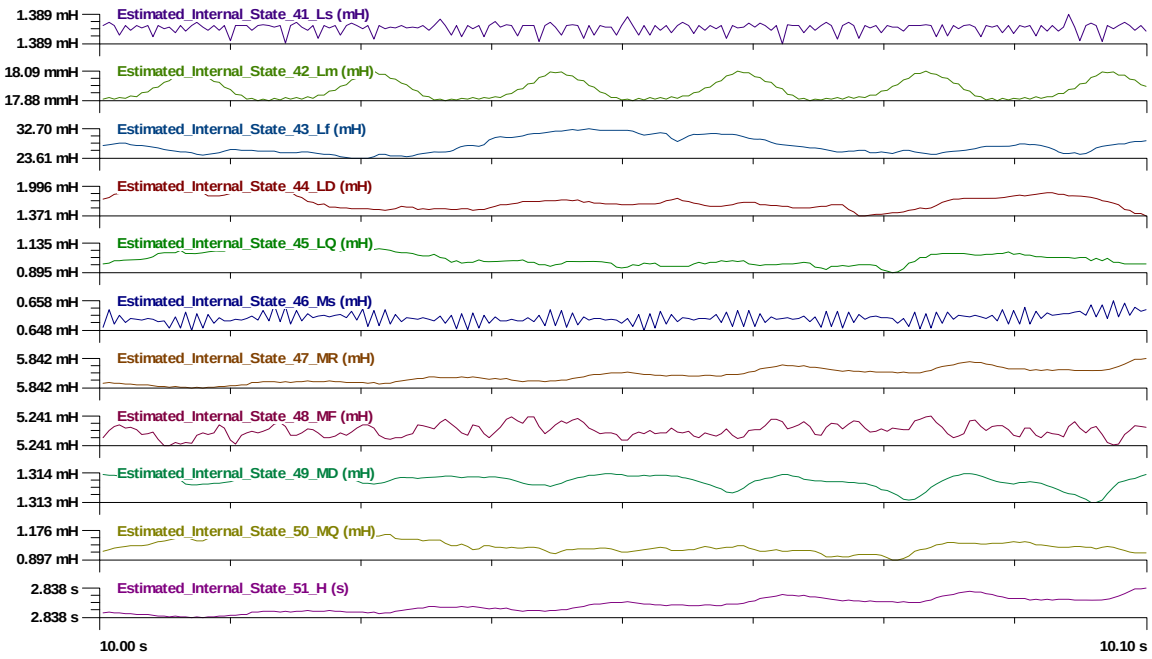

Figure 9.18. Parameter Estimation Results

In Figure 9.18, 11 parameters are estimated by the state estimation. By averaging the values on the waveforms, each of the parameter estimated value can be obtained. Table 9.8 summarizes the actual, initial and estimated parameter values.

Table 9.8. Summary of Generator Actual, Initial and Estimated Parameters.

Parameters	Actual Value	Initial Value	Estimated Value
L_s	1.437603 mH	1.88 mH	1.388915 mH
L_m	0.017362 mH	0.01 mH	0.017964 mH
L_f	28.11097 mH	41.1 mH	27.521038 mH
L_D	1.705491 mH	2.28 mH	1.656319 mH
L_Q	1.028648 mH	1.31 mH	1.010297 mH
M_S	0.671923 mH	0.83 mH	0.652370 mH
M_R	6.020414 mH	8.60 mH	5.841522 mH
M_F	5.40181 mH	7.72 mH	5.241299 mH
M_D	1.354546 mH	1.93 mH	1.314297 mH
M_Q	1.056418 mH	1.46 mH	1.032942 mH
H	2.8 s	3.0 s	2.83752 s

Step 4: Simulation using the generator estimated parameters

A simulation using the generator estimated parameters is performed to check the measurement differences. The measurements from the new simulation are shown in the Figure 9.19.

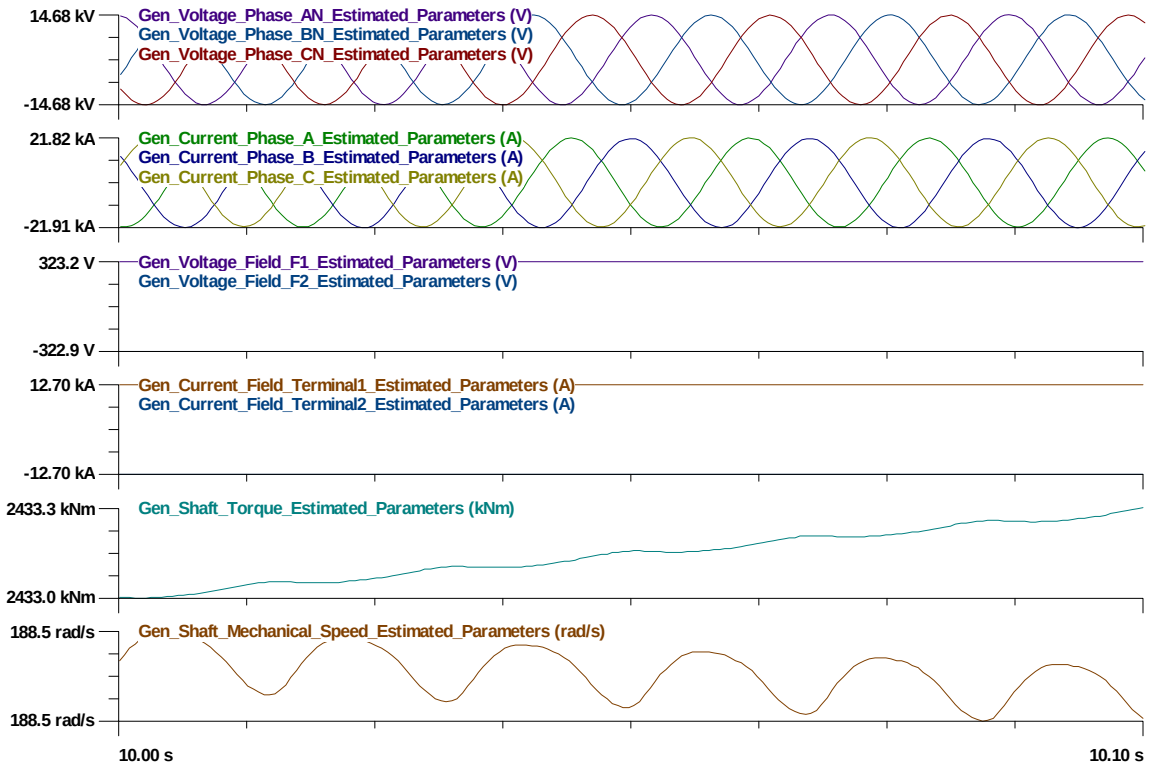

Figure 9.19. Generator Measurements Using Generator Estimated Parameters

The differences between the simulation results from actual parameters and estimated parameters are shown in Figure 9.20.

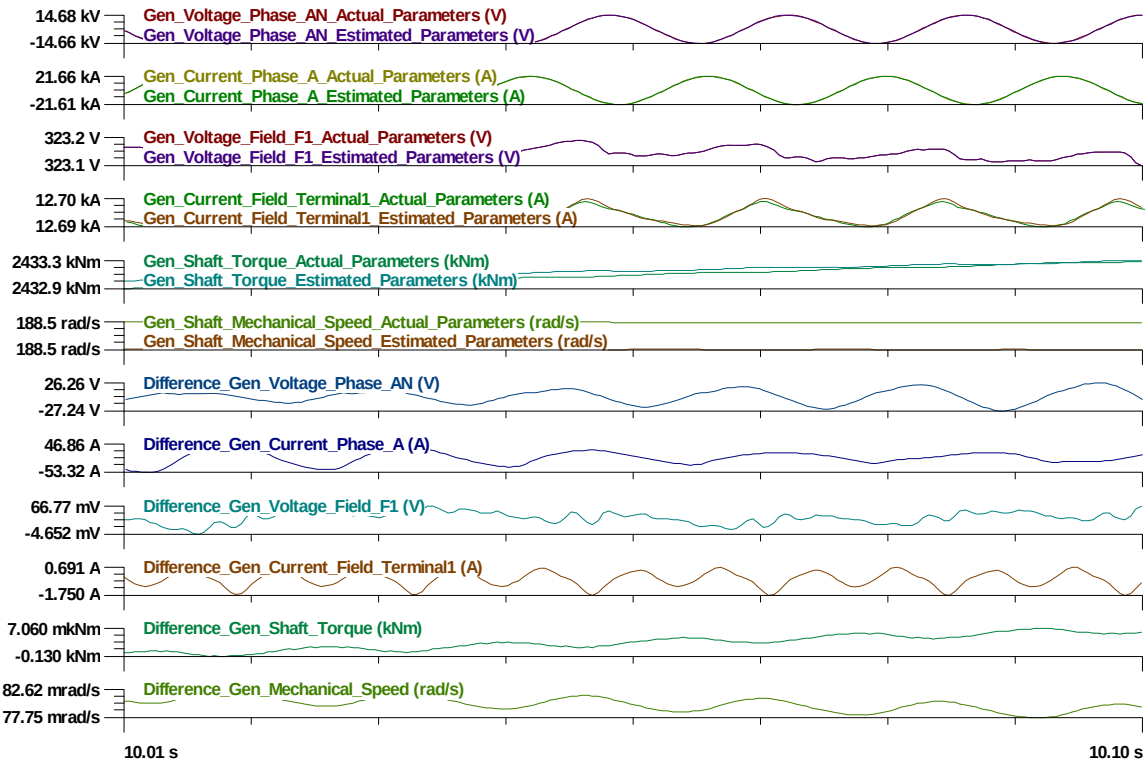

Figure 9.20. Measurement Differences between Using Generator Actual Parameters and Generator Estimated Parameters

In Figure 9.20, the first 6 sets of traces are the measurements for selected phase terminal voltage, phase current, excitation voltage, excitation current, toque and mechanical speed using actual parameters and estimated parameters. The last six traces are the differences between the two models. It is clear that the differences are quite small, which proves that the generator model with estimated parameters are accurate enough to represent the actual generator model. Table 9.9 calculates the parameter estimation errors for each parameter.

Table 9.9. Parameter Estimation Error.

Parameters	Actual Value	Initial Value	Estimated Value	Error
L_s	1.437603 mH	1.88 mH	1.388915 mH	3.38%

Table 9.8. continued

L_m	0.017362 mH	0.01 mH	0.017964 mH	-3.47%
L_f	28.11097 mH	41.1 mH	27.521038 mH	2.09%
L_D	1.705491 mH	2.28 mH	1.656319 mH	2.88%
L_Q	1.028648 mH	1.31 mH	1.010297 mH	1.78%
M_S	0.671923 mH	0.83 mH	0.652370 mH	2.91%
M_R	6.020414 mH	8.60 mH	5.841522 mH	2.97%
M_F	5.40181 mH	7.72 mH	5.241299 mH	2.97%
M_D	1.354546 mH	1.93 mH	1.314297 mH	2.97%
M_Q	1.056418 mH	1.46 mH	1.032942 mH	2.22%
H	2.8 s	3.0 s	2.83752 s	-1.34%

9.4 Summary

Two numerical synchronous generator parameter estimation cases were presented in this chapter. The first case used NERC provided phasor data. Since the proposed method requires time domain sampled valve data, so the conversion from phasor data to sampled valve data was applied and interpolation was done to provide measurements at 4800 samples/second. The second case used the simulation data from the generator model with the actual parameters, which does not have any assumption during the parameter estimation procedure. The results of both cases proves the effectiveness of the proposed parameter estimation method.

CHAPTER 10 CONCLUSION AND FUTURE WORK DIRECTION

10.1 Conclusion

The main contributions of this dissertation include: (1) development of an innovative protection function which is based on the dynamic state estimation of the protection zone, in this case, it is a synchronous generator or an induction generator; (2) development of an interoperable and unified syntax of a protection zone so that the EBP algorithm can be programmed in an object-oriented manner and no specific setting is needed for different types of machines; (3) development of physical based synchronous generator and induction generator models using the above syntax, which have the capability of representing both balanced and unbalanced machine conditions and (4) a model parameter estimation algorithm which leverages the dynamic state estimation to perform model validation.

The dynamic state estimation based protective function uses dynamic state estimation to detect faults in the protection zone. Generally, the EBP method can be utilized to protect any power system apparatus so a general methodology description was introduced in this dissertation. The EBP algorithm monitors the consistency between the real-time measurements for the protection zone and protection zone dynamic model. If they line up with each other, it means the protection zone is healthy and under normal operating condition. Otherwise, any mismatch between the measurements and the model indicates abnormality inside the protection zone. In this case, protection actions are taken to protect the device from further damage. Compared to the legacy protective functions,

the EBP approach only needs very few simple settings, which reduces the relay setting complicity greatly. In addition, the EBP method does not need any coordination with other protective functions, which also decreases the possibility of mis-operations.

In order to make the EBP algorithm applicable to any protection zone, the protection zone model is written in a general format, which makes the entire protective function object oriented. This interoperable and unified syntax of a protection zone is called State Algebraic Quadratic Companion Form (SAQCF). It is derived directly from the protection zone physical model and can represent the dynamics in the protection zone. In this dissertation, the SAQCF model derivation for synchronous generators and induction generators were shown step by step for the purpose of generator and machine protection.

Furthermore, modeling accuracy and fidelity are fundamental for this protection approach. For the synchronous generator and induction generator models, sometimes the generator and machine parameters are difficult to obtain or have been changed due to aging and temperature change, thus the parameters may be inaccurate. To overcome this challenge, a parameter estimation process was introduced by using the same dynamic state estimation algorithm. It treats the uncertain parameters as unknown states during the state estimation process. With the help of redundant measurements, the final state estimation results can provide the estimated parameters for those models.

10.2 Future Work Directions

As mentioned at the beginning of this dissertation, machine needs to be protected when experiencing internal faults and operating abnormally. This dissertation only focused on the internal fault part by applying the dynamic state estimation based

protection. More research need to be done for the abnormal operating protection. Dynamic state estimation has the capability of providing machine operating state values and the operating state values can be utilized for the abnormal operating condition protection. For example, an out-of-step generator protection approach has been proposed in [59]. It uses the dynamic state estimation to get the rotor angle of the generator and then calculates the total energy of the generator during system transitions. If the total energy is higher than a barrier, this generator is going to be unstable so a trip signal will be issued. Dynamic state estimation is a very powerful tool, and many more applications can be explored to provide a better protection for synchronous generators and induction generators.

Furthermore, the protection for renewable energy is still a challenging problem. Doubly-fed induction generator is widely used in the wind power generator, and many converters are involved in the process of wind power generation. The application of Estimation Based Protection to the converters is a very good topic to study.

Last but not least, instrumentation channel saturation may be another interesting topic to investigate. In the real world, CT/PT may experience saturation situation. In this case the measurements are inaccurate, which will impact the accuracy of the proposed Estimation Based Protection. One solution is to include the CT and PT model in the state estimation as well, which means the dynamic model of instrumentation channels are considered during the state estimation so that the saturation can also be modeled and estimated.

PUBLICATIONS

1. A.P.S. Meliopoulos, G. Cokkinides, R. Fan and L. Sun, "Data Attack Detection and Command Authentication via Cyber-Physical Co-Modeling," IEEE Design & Test (accepted)

2. L. Sun, A.P.S. Meliopoulos, Y. Liu, and B. Xie, "Dynamic State Estimation Based Synchronous Generator Model Calibration Using PMU Data," 2017 IEEE Power and Energy Society General Meeting (PES) (accepted)

3. Y. Liu, A.P.S. Meliopoulos, L. Sun and R. Fan, "Dynamic State Estimation Based Protection of Mutually Coupled Transmission Lines," CSEE Journal of Power and Energy Systems, vol. 2, no. 4, pp. 6-14, December 2016

4. Y. Liu, A.P.S. Meliopoulos, R. Fan, L. Sun and Z. Tan, "Dynamic State Estimation Based Protection on Series Compensated Transmission Lines," IEEE Trans. on Power Delivery, 29 Nov 2016

5. A.P.S. Meliopoulos, G. Cokkinides, P. Myrda, Y. Liu, R. Fan, L. Sun, R. Huang and Z. Tan, "Dynamic State Estimation Based Protection: Status and Promise," IEEE Trans. on Power Delivery, 23 Sept 2016

6. L. Sun, R. Fan, A.P.S. Meliopoulos, Y. Liu and Z. Tan, "Capacitor Bank Protection via Constraint WLS Dynamic State Estimation Method (CWLS-DSE)," 2016 North American Power Symposium (NAPS), 18-20 Sept 2016

7. R. Fan, A.P.S. Meliopoulos, L. Sun, Z. Tan and Y. Liu, "Transformer Inter-Turn Faults Detection by Dynamic State Estimation Method," 2016 North American Power Symposium (NAPS), 18-20 Sept 2016

8. Y. Liu, S. Choi, A.P.S. Meliopoulos, R. Fan, L. Sun and Z. Tan, "Dynamic State Estimation Enabled Predictive Inverter Control," 2016 IEEE Power and Energy Society General Meeting (PES), 17-21 July 2016

9. Z. Tan, R. Fan, Y. Liu, and L. Sun, “Microgrid Black-Start After Natural Disaster With Load Restoration Using Spanning Tree Search,” 2016 IEEE Power and Energy Society General Meeting (PES), 17-21 July 2016

10. R. Fan, L. Sun and Z. Tan, “Dynamic Linear Quadratic Control of SSSC to Increase Power Oscillations Damping of HVDC-AC Power System,” 2015 IEEE Power and Energy Society General Meeting (PES), 26-30 July 2015

11. R. Fan, A.P.S. Meliopoulos, G.J. Cokkinides, L. Sun and Y. Liu, “Dynamic State Estimation-based Protection of Power Transformers,” 2015 IEEE Power and Energy Society General Meeting (PES), 26-30 July 2015

12. Y. Liu, A.P.S. Meliopoulos, R. Fan and L. Sun, “Dynamic State Estimation-based Protection of Microgrid Circuits,” 2015 IEEE Power and Energy Society General Meeting (PES), 26-30 July 2015

13. L. Sun, “Real-Time Pricing Algorithm Considering Load Identification for Smart Grid,” 2014 IEEE Power and Energy Society General Meeting (PES), 27-31 July 2014

14. L. Sun, A.P.S. Meliopoulos, R. Fan, R. Huang, “Introduction of Setting-less Protection Relay,” 2014 Protection, Automation & Control World Conference, Croatia, 23-26 June 2014

15. A.P.S. Meliopoulos, L. Sun, R. Fan and P. Myrda, “Update on Object-oriented DSE Based Protection,” 2014 Fault and Disturbance Analysis Conference (FDA), 28-29 April 2014

16. D. Zhao, A.P.S. Meliopoulos and L. Sun, "Cost analysis and optimal kV level selection of alternate wind farms," 2013 North American Power Symposium (NAPS), 22-24 Sept. 2013

17. R.Fan, D. Zhao, Z. Tan, L. Sun and A.P.S. Meliopoulos, "State space based modeling and sensitivity analysis of DFIG in an unbalanced network," 2013 North American Power Symposium (NAPS), 22-24 Sept. 2013

18. L. Sun, Z. Tan, R. Fan and A.P.S. Meliopoulos, "Transient response improvement of doubly-fed induction machine during unbalanced network," 2013 IEEE Power and Energy Society General Meeting (PES), 21-25 July 2013

19. Z. Tan, L. Sun, D. Zhao and A.P.S. Meliopoulos, "Dynamic modeling of doubly fed induction machine during balanced voltage dips with control effects formulation," 2013 IEEE Power and Energy Society General Meeting (PES), 21-25 July 2013

APPENDICES

Appendix A1: Synchronous Generator Modeling in SAQCF Standard

The synchronous generator model is written in the SAQCF format. As mentioned in Chapter 4, SAQCF device model is derived by applying the quadratic integration method to the quadratized device model. Thus, obtaining the quadratized device model is the first step. The quadratized device model is derived from the physically-based machine circuit. The physically-based circuits, the quadratized device model and the SAQCF device model of the synchronous generator is discussed below.

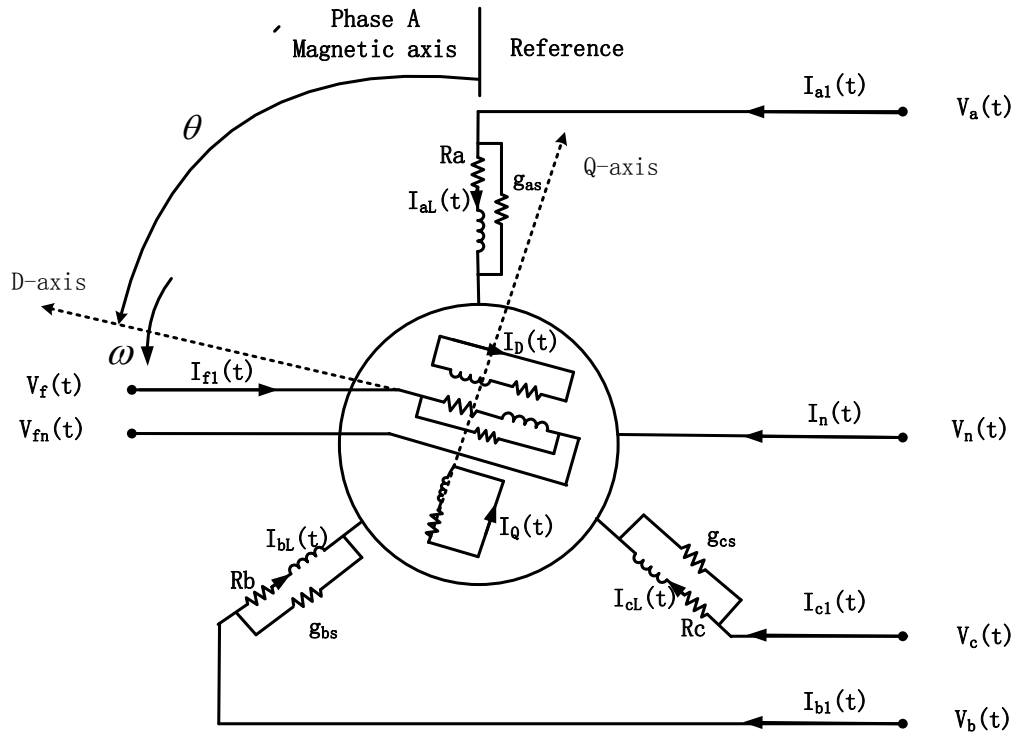

Figure A.1. Physically-Based Circuit of the Synchronous Generator

Quadratized Model:

$$i_{abc}(t) = i_{aL\ bL\ cL}(t) + g_{as,bs,cs} \cdot (v_{abc}(t) - v_{an\ bn\ cn}(t))$$

$$i_{an\ bn\ cn}(t) = -i_{aL\ bL\ cL}(t) + g_{as,bs,cs} \cdot (v_{an\ bn\ cn}(t) - v_{abc}(t))$$

$$i_f(t) = i_{fL}(t) + g_{fs} \cdot (v_f(t) - v_{fn}(t))$$

$$i_{fn}(t) = -i_{fL}(t) + g_{fs} \cdot (v_{fn}(t) - v_f(t))$$

$$T_m(t) = T_{acc} + T_e(t) + T_{wf}(t)$$

$$0 = v_{abc}(t) - v_{an\ bn\ cn}(t) - R_{abc} i_{aL\ bL\ cL}(t) + e_{abc}(t)$$

$$0 = v_f(t) - R_f i_{fL}(t) - e_f(t) - v_{fn}(t)$$

$$0 = R_{DQ} i_{DQ}(t) + e_{DQ}(t)$$

$$0 = \theta(t) - \frac{p}{2}\theta_m(t)$$

$$0 = \omega(t) - \frac{p}{2}\omega_m(t)$$

$$0 = \frac{d\theta_m(t)}{dt} - \omega_m(t)$$

$$0 = \frac{d\lambda_{abc}(t)}{dt} - e_{abc}(t)$$

$$0 = \frac{d\lambda_{fDQ}(t)}{dt} - e_{fDQ}(t)$$

$$0 = \frac{d\omega_m(t)}{dt} - \frac{1}{J}T_{acc}(t)$$

$$0 = \frac{dc(t)}{dt} - y_1(t)$$

$$0 = \frac{ds(t)}{dt} - y_2(t)$$

$$0 = T_{wf}(t) - \left(D_{fw} + D'_{fw} \cdot \omega_m(t) + D''_{fw} \cdot \omega_m(t)^2\right)$$

$$0 = P_{em}(t) - e_{abc}(t)^T i_{aL\ bL\ cL}(t)$$

$$0 = P_{em}(t) - T_e(t) \cdot \omega_m(t)$$

$$0 = y_1(t) + s(t) \cdot \omega(t)$$

$$0 = 1.0 - c^2(t) - s^2(t)$$

$$0 = c_2(t) - c^2(t) + s^2(t)$$

$$0 = s_2(t) - 2c(t)s(t)$$

$$0 = -\begin{bmatrix} \lambda_{abc}(t) \\ \lambda_{fDQ}(t) \end{bmatrix} + \left(A \cdot c(t) + B \cdot s(t) + C \cdot c_2(t) + D \cdot s_2(t) + E \right) \cdot \begin{bmatrix} -i_{aL\ bL\ cL}(t) \\ i_{fL\ DQ}(t) \end{bmatrix}$$

where:

$$A = \begin{bmatrix} 0 & 0 & 0 & M_F & M_D & 0 \\ 0 & 0 & 0 & -\frac{1}{2}M_F & -\frac{1}{2}M_D & -\frac{\sqrt{3}}{2}M_Q \\ 0 & 0 & 0 & -\frac{1}{2}M_F & -\frac{1}{2}M_D & \frac{\sqrt{3}}{2}M_Q \\ M_F & -\frac{1}{2}M_F & -\frac{1}{2}M_F & 0 & 0 & 0 \\ M_D & -\frac{1}{2}M_D & -\frac{1}{2}M_D & 0 & 0 & 0 \\ 0 & -\frac{\sqrt{3}}{2}M_Q & \frac{\sqrt{3}}{2}M_Q & 0 & 0 & 0 \end{bmatrix} \quad B = \begin{bmatrix} 0 & 0 & 0 & 0 & 0 & M_Q \\ 0 & 0 & 0 & \frac{\sqrt{3}}{2}M_F & \frac{\sqrt{3}}{2}M_D & -\frac{1}{2}M_Q \\ 0 & 0 & 0 & -\frac{\sqrt{3}}{2}M_F & -\frac{\sqrt{3}}{2}M_D & -\frac{1}{2}M_Q \\ 0 & \frac{\sqrt{3}}{2}M_F & -\frac{\sqrt{3}}{2}M_F & 0 & 0 & 0 \\ 0 & \frac{\sqrt{3}}{2}M_D & -\frac{\sqrt{3}}{2}M_D & 0 & 0 & 0 \\ M_Q & -\frac{1}{2}M_Q & -\frac{1}{2}M_Q & 0 & 0 & 0 \end{bmatrix}$$

$$C = \begin{bmatrix} L_m & -\frac{1}{2}L_m & -\frac{1}{2}L_m & 0 & 0 & 0 \\ -\frac{1}{2}L_m & -\frac{1}{2}L_m & L_m & 0 & 0 & 0 \\ -\frac{1}{2}L_m & L_m & -\frac{1}{2}L_m & 0 & 0 & 0 \\ 0 & 0 & 0 & 0 & 0 & 0 \\ 0 & 0 & 0 & 0 & 0 & 0 \\ 0 & 0 & 0 & 0 & 0 & 0 \end{bmatrix} \quad D = \begin{bmatrix} 0 & \frac{\sqrt{3}}{2}L_m & -\frac{\sqrt{3}}{2}L_m & 0 & 0 & 0 \\ \frac{\sqrt{3}}{2}L_m & -\frac{\sqrt{3}}{2}L_m & 0 & 0 & 0 & 0 \\ -\frac{\sqrt{3}}{2}L_m & 0 & \frac{\sqrt{3}}{2}L_m & 0 & 0 & 0 \\ 0 & 0 & 0 & 0 & 0 & 0 \\ 0 & 0 & 0 & 0 & 0 & 0 \\ 0 & 0 & 0 & 0 & 0 & 0 \end{bmatrix}$$

$$E=\begin{bmatrix} L_s & -M_s & -M_s & 0 & 0 & 0 \\ -M_s & L_s & -M_s & 0 & 0 & 0 \\ -M_s & -M_s & L_s & 0 & 0 & 0 \\ 0 & 0 & 0 & L_f & M_R & 0 \\ 0 & 0 & 0 & M_R & L_D & 0 \\ 0 & 0 & 0 & 0 & 0 & L_Q \end{bmatrix}$$

It is easy to write the above equations into the matrix format as follows:

$$\mathbf{i}(t) = Y_{eqx1}\mathbf{x}(t) + D_{eqxd1}\frac{d\mathbf{x}(t)}{dt} + C_{eqc1}$$

$$0 = Y_{eqx2}\mathbf{x}(t) + D_{eqxd2}\frac{d\mathbf{x}(t)}{dt} + C_{eqc2}$$

$$0 = Y_{eqx3}\mathbf{x}(t) + \begin{Bmatrix} \vdots \\ \mathbf{x}(t)^T \left\langle F^i_{eqxx3} \right\rangle \mathbf{x}(t) \\ \vdots \end{Bmatrix} + C_{eqc3}$$

where, $\mathbf{i}(t) = [i_{abc}(t)\ \ i_{an\ bn\ cn}(t)\ \ i_f(t)\ \ i_{fn}(t)\ \ T_m(t)]'$,

$\mathbf{x}(t) = [v_{abc}(t)\ \ v_{an\ bn\ cn}(t)\ \ v_f(t)\ \ v_{fn}(t)\ \ \omega_m(t)\ \ i_{abcL}(t)\ \ i_{DQ}(t)\ \ \theta_m(t)\ \ \theta(t)\ \ \omega(t)\ \ T_{fw}(t)\ \ P_{em}(t)$
$T_e(t)\ \ e_{abc}(t)\ \ e_f(t)\ \ e_{DQ}(t)\ \ \lambda_{abc}(t)\ \ \lambda_f(t)\ \ \lambda_{DQ}(t)\ \ T_{acc}(t)\ \ c(t)\ \ s(t)\ \ y_1(t)\ \ y_2(t)\ \ c_2(t)\ \ s_2(t)]'$
Y, D and F are coefficient matrices and C is constant vector.

After applying the quadratic integration method, the SAQCF model is:

$$\begin{Bmatrix} i(t) \\ 0 \\ 0 \\ i(t_m) \\ 0 \\ 0 \end{Bmatrix} = Y_{eqx}\mathbf{x} + \begin{Bmatrix} \vdots \\ \mathbf{x}^T \left\langle F^i_{eqx} \right\rangle \mathbf{x} \\ \vdots \end{Bmatrix} + N_{eqx}\mathbf{x}(t-h) + M_{eq}i(t-h) + K_{eq}$$

where: $Y_{eqx} = \begin{bmatrix} \frac{4}{h}D_{eqxd1} + Y_{eqx1} & -\frac{8}{h}D_{eqxd1} \\ \frac{4}{h}D_{eqxd2} + Y_{eqx2} & -\frac{8}{h}D_{eqxd2} \\ Y_{eqx3} & 0 \\ \frac{1}{2h}D_{eqxd1} & \frac{2}{h}D_{eqxd1} + Y_{eqx1} \\ \frac{1}{2h}D_{eqxd2} & \frac{2}{h}D_{eqxd2} + Y_{eqx2} \\ 0 & Y_{eqx3} \end{bmatrix}$ $F_{eqx} = \begin{bmatrix} 0 & 0 \\ 0 & 0 \\ F_{eqxx3} & 0 \\ 0 & 0 \\ 0 & 0 \\ 0 & F_{eqxx3} \end{bmatrix}$

$N_{eqx} = \begin{bmatrix} -Y_{eqx1} + \frac{4}{h}D_{eqxd1} \\ -Y_{eqx2} + \frac{4}{h}D_{eqxd2} \\ 0 \\ \frac{1}{2}Y_{eqx1} - \frac{5}{2h}D_{eqxd1} \\ \frac{1}{2}Y_{eqx2} - \frac{5}{2h}D_{eqxd2} \\ 0 \end{bmatrix}$ $M_{eq} = \begin{bmatrix} I_{size(i(t))} \\ 0 \\ 0 \\ \frac{1}{2}I_{size(i(t))} \\ 0 \\ 0 \end{bmatrix}$ $K_{eq} = \begin{bmatrix} 0 \\ 0 \\ C_{eqc3} \\ \frac{3}{2}C_{eqc1} \\ \frac{3}{2}C_{eqc2} \\ C_{eqc3} \end{bmatrix}$

Appendix A2: Induction Generator Modeling in SAQCF Standard

The induction generator model is written in the SAQCF format. As mentioned in Chapter 4, SAQCF device model is derived by applying the quadratic integration method to the quadratized device model. Thus, obtaining the quadratized device model is the first step. The quadratized device model is derived from the physically-based machine circuit. The physically-based circuits, the quadratized device model and the SAQCF device model of the induction generator is discussed below.

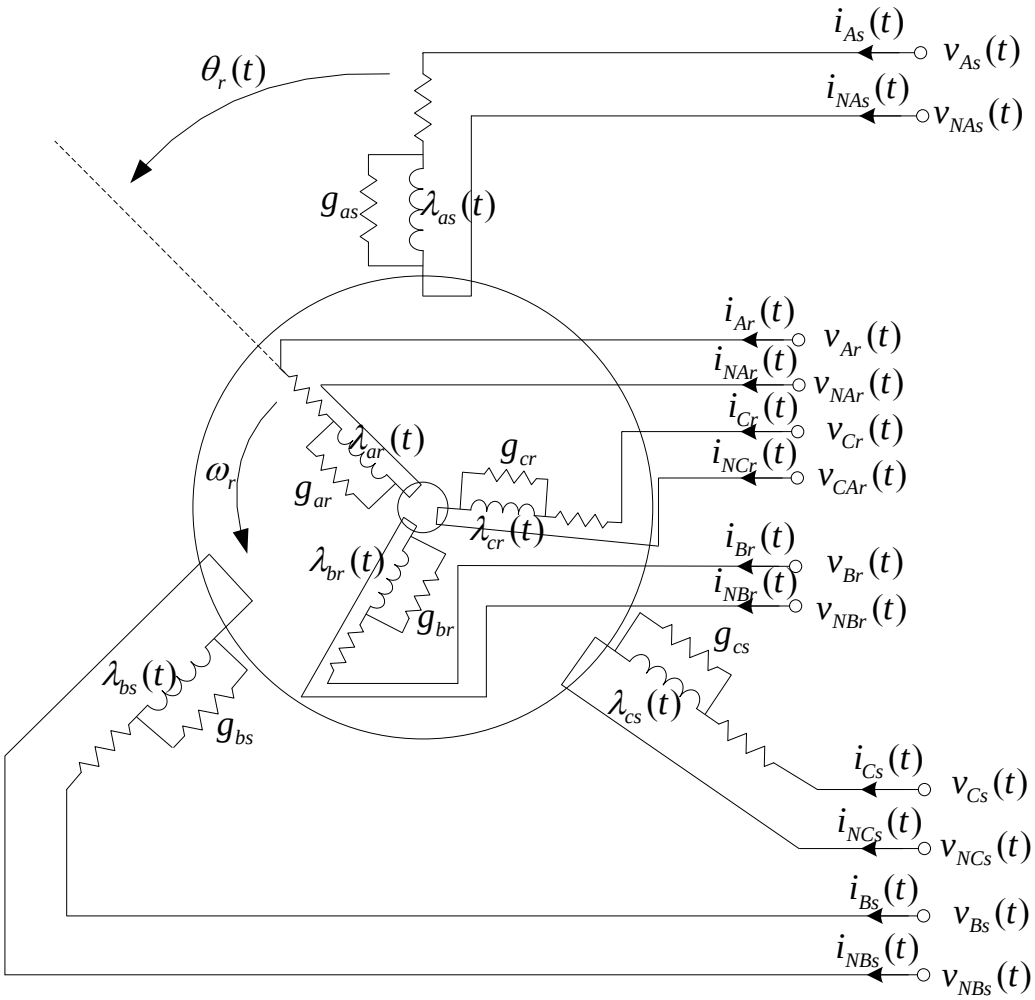

Figure A.2. Physically-Based Circuit of the Induction Generator

Quadratized Model:

$$i_{ABC,s}(t) = i_{abc,s}(t) + g_{abc,s} \cdot e_{abc,s}(t)$$

$$i_{NABC,s}(t) = -i_{abc,s}(t) - g_{abc,s} \cdot e_{abc,s}(t)$$

$$i_{ABC,r}(t) = i_{abc,r}(t) + g_{abc,r} \cdot e_{abc,r}(t)$$

$$i_{NABC,r}(t) = -i_{abc,r}(t) - g_{abc,r} \cdot e_{abc,r}(t)$$

$$T_m(t) = T_{acc}(t) + T_e(t) + T_f(t)$$

$$0 = \frac{d\lambda_{abc,s}(t)}{dt} - e_{abc,s}(t)$$

$$0 = v_{ABC,s}(t) - v_{NABC,s}(t) - e_{abc,s}(t) - R_s \cdot (i_{abc,s}(t) + g_{abc,s} \cdot e_{abc,s}(t))$$

$$0 = v_{ABC,r}(t) - v_{NABC,r}(t) - e_{abc,r}(t) - R_r \cdot (i_{abc,r}(t) + g_{abc,r} \cdot e_{abc,r}(t))$$

$$0 = \theta_r(t) - \frac{p}{2}\theta_m(t)$$

$$0 = \omega_r(t) - \frac{p}{2}\omega_m(t)$$

$$0 = \omega_s - \omega_r(t) - \omega_s \cdot slip(t)$$

$$0 = \frac{d\lambda_{abc,r}(t)}{dt} - e_{abc,r}(t)$$

$$0 = \frac{d\omega_m(t)}{dt} - \frac{1}{J}T_{acc}(t)$$

$$0 = \frac{dc(t)}{dt} - y_1(t)$$

$$0 = \frac{ds(t)}{dt} - y_2(t)$$

$$0 = \frac{d\theta_m(t)}{dt} - \omega_m(t)$$

$$0 = \frac{d\theta_m(t)}{dt} - \omega_m(t)$$

$$0 = T_f(t) - a - b\omega_m(t) - c\omega_m^2(t)$$

$$0 = P_{em}(t) - e_{abc,s}(t)^T i_{abc,s}(t)$$

$$0 = P_{em}(t) - T_e(t) \cdot \omega_m(t)$$

$$0 = y_1(t) + s(t) \cdot \omega(t)$$

$$0 = 1.0 - c^2(t) - s^2(t)$$

$$0 = c_2(t) - c^2(t) + s^2(t)$$

$$0 = s_2(t) - 2c(t)s(t)$$

$$0 = -\begin{bmatrix} \lambda_{abc,s}(t) \\ \lambda_{abc,r}(t) \end{bmatrix} + (A + B \cdot c(t) + C \cdot s(t) + D \cdot c_2(t) + E \cdot s_2(t)) \cdot \begin{bmatrix} -i_{abc,s}(t) \\ i_{abc,r}(t) \end{bmatrix}$$

where:

$$A = \begin{bmatrix} L_s & -M_s & -M_s & 0 & 0 & 0 \\ -M_s & L_s & -M_s & 0 & 0 & 0 \\ -M_s & -M_s & L_s & 0 & 0 & 0 \\ 0 & 0 & 0 & L_{rr} + L_{mr} & -0.5L_{mr} & -0.5L_{mr} \\ 0 & 0 & 0 & -0.5L_{mr} & L_{rr} + L_{mr} & -0.5L_{mr} \\ 0 & 0 & 0 & -0.5L_{mr} & -0.5L_{mr} & L_{rr} + L_{mr} \end{bmatrix}$$

$$B = \begin{bmatrix} 0 & 0 & 0 & L_{sr} & -0.5L_{sr} & -0.5L_{sr} \\ 0 & 0 & 0 & -0.5L_{sr} & L_{sr} & -0.5L_{sr} \\ 0 & 0 & 0 & -0.5L_{sr} & -0.5L_{sr} & L_{sr} \\ L_{sr} & -0.5L_{sr} & -0.5L_{sr} & 0 & 0 & 0 \\ -0.5L_{sr} & L_{sr} & -0.5L_{sr} & 0 & 0 & 0 \\ -0.5L_{sr} & -0.5L_{sr} & L_{sr} & 0 & 0 & 0 \end{bmatrix}$$

$$C=\begin{bmatrix} 0 & 0 & 0 & 0 & -\frac{\sqrt{3}}{2}L_{sr} & \frac{\sqrt{3}}{2}L_{sr} \\ 0 & 0 & 0 & \frac{\sqrt{3}}{2}L_{sr} & 0 & -\frac{\sqrt{3}}{2}L_{sr} \\ 0 & 0 & 0 & -\frac{\sqrt{3}}{2}L_{sr} & \frac{\sqrt{3}}{2}L_{sr} & 0 \\ 0 & -\frac{\sqrt{3}}{2}L_{sr} & \frac{\sqrt{3}}{2}L_{sr} & 0 & 0 & 0 \\ \frac{\sqrt{3}}{2}L_{sr} & 0 & -\frac{\sqrt{3}}{2}L_{sr} & 0 & 0 & 0 \\ -\frac{\sqrt{3}}{2}L_{sr} & \frac{\sqrt{3}}{2}L_{sr} & 0 & 0 & 0 & 0 \end{bmatrix}$$

$$D=\begin{bmatrix} L_{m1} & -\frac{1}{2}L_{t1} & -\frac{1}{2}L_{t1} & 0 & 0 & 0 \\ -\frac{1}{2}L_{t1} & -\frac{1}{2}L_{m1} & L_{t1} & 0 & 0 & 0 \\ -\frac{1}{2}L_{t1} & L_{t1} & -\frac{1}{2}L_{m1} & 0 & 0 & 0 \\ 0 & 0 & 0 & 0 & 0 & 0 \\ 0 & 0 & 0 & 0 & 0 & 0 \\ 0 & 0 & 0 & 0 & 0 & 0 \end{bmatrix}$$

$$E=\begin{bmatrix} 0 & \frac{\sqrt{3}}{2}L_{t1} & -\frac{\sqrt{3}}{2}L_{t1} & 0 & 0 & 0 \\ -\frac{\sqrt{3}}{2}L_{t1} & -\frac{\sqrt{3}}{2}L_{m1} & 0 & 0 & 0 & 0 \\ -\frac{\sqrt{3}}{2}L_{t1}+\frac{1}{2}L_{t2} & \frac{\sqrt{3}}{2}L_{t1}+\frac{1}{2}L_{t2} & \frac{\sqrt{3}}{2}L_{m1}-\frac{1}{2}L_{m2} & 0 & 0 & 0 \\ 0 & 0 & 0 & 0 & 0 & 0 \\ 0 & 0 & 0 & 0 & 0 & 0 \\ 0 & 0 & 0 & 0 & 0 & 0 \end{bmatrix}$$

It is easy to write the above equations into the matrix format as follows:

$$\mathbf{i}(t)=Y_{eqx1}\mathbf{x}(t)+D_{eqxd1}\frac{d\mathbf{x}(t)}{dt}+C_{eqc1}$$

$$0=Y_{eqx2}\mathbf{x}(t)+D_{eqxd2}\frac{d\mathbf{x}(t)}{dt}+C_{eqc2}$$

$$0=Y_{eqx3}\mathbf{x}(t)+\begin{Bmatrix} \vdots \\ \mathbf{x}(t)^T\left\langle F^i_{eqxx3}\right\rangle\mathbf{x}(t) \\ \vdots \end{Bmatrix}+C_{eqc3}$$

where, $\mathbf{i}(t) = [i_{ABCs}(t)\ \ i_{NABCs}(t)\ \ i_{ABCr}(t)\ \ i_{NABCr}(t)\ \ T_m(t)]'$,

$$\mathbf{x}(t) = [v_{ABCs}(t)\ \ v_{NABCs}(t)\ \ v_{ABCr}(t)\ \ v_{NABCr}(t)\ \ \omega_m(t)\ \ e_{abcs}(t)\ \ e_{abcr}(t)\ \ i_{abcs}(t)\ \ i_{abcr}(t)$$
$$T_f(t)\ \ T_e(t)\ \ \theta_r(t)\ \ \theta_m(t)\ \ \omega_r(t)\ \ slip(t)\ \ c\ (t)\ \ s\ (t)\ \ c_2(t)\ \ s_2(t)\ \ y_1(t)\ \ y_2(t)]'$$

Y, D and F are coefficient matrices and C is constant vector.

After applying the quadratic integration method, the **SAQCF model** is:

$$\begin{Bmatrix} i(t) \\ 0 \\ 0 \\ i(t_m) \\ 0 \\ 0 \end{Bmatrix} = Y_{eqx}\mathbf{x} + \begin{Bmatrix} \vdots \\ \mathbf{x}^T \left\langle F_{eqx}^i \right\rangle \mathbf{x} \\ \vdots \end{Bmatrix} + N_{eqx}\mathbf{x}(t-h) + M_{eq}i(t-h) + K_{eq}$$

where: $$Y_{eqx} = \begin{bmatrix} \frac{4}{h}D_{eqxd1} + Y_{eqx1} & -\frac{8}{h}D_{eqxd1} \\ \frac{4}{h}D_{eqxd2} + Y_{eqx2} & -\frac{8}{h}D_{eqxd2} \\ Y_{eqx3} & 0 \\ \frac{1}{2h}D_{eqxd1} & \frac{2}{h}D_{eqxd1} + Y_{eqx1} \\ \frac{1}{2h}D_{eqxd2} & \frac{2}{h}D_{eqxd2} + Y_{eqx2} \\ 0 & Y_{eqx3} \end{bmatrix} \qquad F_{eqx} = \begin{bmatrix} 0 & 0 \\ 0 & 0 \\ F_{eqxx3} & 0 \\ 0 & 0 \\ 0 & 0 \\ 0 & F_{eqxx3} \end{bmatrix}$$

$$N_{eqx} = \begin{bmatrix} -Y_{eqx1} + \frac{4}{h}D_{eqxd1} \\ -Y_{eqx2} + \frac{4}{h}D_{eqxd2} \\ 0 \\ \frac{1}{2}Y_{eqx1} - \frac{5}{2h}D_{eqxd1} \\ \frac{1}{2}Y_{eqx2} - \frac{5}{2h}D_{eqxd2} \\ 0 \end{bmatrix} \qquad M_{eq} = \begin{bmatrix} I_{size(i(t))} \\ 0 \\ 0 \\ \frac{1}{2}I_{size(i(t))} \\ 0 \\ 0 \end{bmatrix} \qquad K_{eq} = \begin{bmatrix} 0 \\ 0 \\ C_{eqc3} \\ \frac{3}{2}C_{eqc1} \\ \frac{3}{2}C_{eqc2} \\ C_{eqc3} \end{bmatrix}$$

REFERENCES

[1] IEEE Power System Relaying Committee, *IEEE Tutorial on the Protection of Synchronous Generators*,2011.

[2] "IEEE Guide for AC Generator Protection - Redline," in *IEEE Std C37.102 -2006 (Revision of IEEE Std C37.102-1995) - Redline*, Feb. 2007.

[3] "IEEE Guide for AC Motor Protection," in *IEEE Std C37.96-2012*, Feb. 2013.

[4] "MOTORWISE Technology White Paper", http://www.technowisegroup.com /PDF/MOTORWISE/MotorWise%20Technology%20White%20Paper%20Ver%2 0008.pdf

[5] P. Pillai, B.G. Bailey, J. Bowen, G. Dalke, B.G. Douglas, etc. "Grounding and Ground Fault Protection of Multiple Generator Installations on Medium-Voltage Industrial and Commercial Power Systems - Part 3: Protection Methods Working Group Report," in *IEEE Trans. on Industry Applications*, vol.40, no.1, pp.24-28, Jan.-Feb. 2004.

[6] S.M.A. Cruz and A.J.M. Cardoso, "Stator Winding Fault Diagnosis in Three-phase Synchronous and Asynchronous Motors, by the Extended Park's Vector Approach," in *IEEE Trans. on Industry Applications*, vol. 37, no. 5, pp.1227-1233, Sep/Oct 2001.

[7] IEEE Guide for Generator Ground Protection," *IEEE Std C37.101-2006* (Revision of IEEE Std C37.101-1993/Incorporates IEEE Std C37.101-2006/Cor1:2007) , pp.1-70, Nov. 2007.

[8] W.K. Sonnemann, "A High-speed Differential Relay for Generator Protection," in *Electrical Engineering*, vol.59, no.12, pp.1250-1252, Dec. 1940.

[9] N.T. Stringer and G. Dalke, "Ground-Differential Protection," in *IEEE Industry Applications Magazine*, vol.6, no.2, pp.53-58, Mar.-Apr. 2000.

[10] H. Leyburn and C.H.W. Lackey, "The Protection of Electrical Power Systems: a Critical Review of Present-Day Practice and Recent Progress," in *Proceedings of the IEE - Part II: Power Engineering*, vol.99, no.67, pp.47-59, Feb. 1952.

[11] G.S. Hope, P.K. Dash and O.P. Malik, "Digital Differential Protection of a Generating Unit Scheme and Real-Time Test Results," in *IEEE Trans. on Power Apparatus and Systems*, vol.96, no.2, pp.502-512, Mar. 1977.

[12] Q. Tian, X. Lin and P. Liu, "A Novel Self-Adaptive Compensated Differential Protection Design Suitable for the Generator With Considerable Winding

Distributed Capacitance," in *IEEE Trans. on Power Delivery*, vol. 22, no. 2, pp. 836-842, April 2007.

[13] S.B. Lee, K. Younsi and G.B. Kliman, "An Online Technique for Monitoring the Insulation Condition of AC Machine Stator Windings," in *IEEE Trans. on Energy Conversion*, vol.20, no.4, pp.737-745, Dec. 2005.

[14] D.S. Baker, "Generator Backup Overcurrent Protection," in *IEEE Trans. on Industry Applications*, vol.IA-18, no.6, pp.632-640, Nov. 1982.

[15] C.H. Griffin and J.W. Pope, "Generator Ground Fault Protection Using Overcurrent, Overvoltage, and Undervoltage Relays," in *IEEE Trans. on Power Apparatus and Systems*, vol.PAS-101, no.12, pp.4490-4501, Dec. 1982.

[16] J.S. Dudor and L.K. Padden, "Protective Relay Application for Generators and Transformer," in *IEEE Industry Applications Magazine*, vol.3, no.4, pp.22-35, Jul.-Aug. 1997.

[17] V. Cook and J. Rushton, "Some Aspects of Generator Backup Protection in Relation to Synchronous-machine Performance During H.V.-System Faults," in *Electrical Engineers*, vol.119, no.7, pp.865-870, July 1972.

[18] E.C. Piesciorovsky and N.N. Schulz, "Fuse Relay Adaptive Overcurrent Protection Scheme for Microgrid with Distributed Generators," in *IET Generation, Transmission & Distribution*, vol.11, no.2, pp.540-549, Jan. 2017.

[19] M.J. Duran, J.L. Duran, F. Perez and J. Fernandez, "Induction-motor Sensorless Vector Control with Online Parameter Estimation and Overcurrent Protection," in *IEEE Trans. on Industrial Electronics*, vol.53, no.1, pp.154-161, Feb. 2006.

[20] G.D. Rockefeller et al., "A Survey of Generator Back-up Protection Practices: IEEE Committee Report," in *IEEE Trans. on Power Delivery*, vol.5, no.2, pp.575-584, Apr 1990.

[21] R.F. Lawrence and R.W. Ferguson, "Generator Negative-Sequence Currents for Line-to-Line Faults [includes discussion]," in *Trans. of the American Institute of Electrical Engineers. Part III: Power Apparatus and Systems*, vol.72, no.2, Jan. 1953.

[22] D.J. Graham, P.G. Brown and R.L. Winchester, "Generator Protection with a New Static Negative Sequence Relay," in *IEEE Trans. on Power Apparatus and Systems*, vol.94, no.4, pp.1208-1213, Jul. 1975.

[23] W.C. Morris and L.E. Goff, "A Negative-Phase-Sequence-Overcurrent Relay for Generator Protection," in *Trans. of the American Institute of Electrical Engineers. Part III: Power Apparatus and Systems*, vol.72, no.2, Jan. 1953.

[24] P.K. Dash, O.P. Malik and G.S. Hope, "Fast Generator Protection Against Internal Asymmetrical Faults," in *IEEE Trans. on Power Apparatus and Systems*, vol.96, no.5, pp.1498-1506, Sept. 1977.

[25] O. Usta and M. Bayrak, "A New Power-Based Digital Algorithm for Generator Protection," in *IEEE Power Engineering Review*, vol.20, no.2, pp.49-52, Feb. 2000.

[26] O. Usta, M. Bayrak and M.A. Redfern, "A New Digital Relay for Generator Protection Against Asymmetrical Faults," in *IEEE Trans. on Power Delivery*, vol.17, no.1, pp.54-59, Jan. 2002.

[27] E.I. Pollard, "Effects of Negative-Sequence Currents on Turbine-Generator Rotors [includes discussion]," in *Trans. of the American Institute of Electrical Engineers. Part III: Power Apparatus and Systems*, vol. 72, no. 2, Jan. 1953.

[28] W.A. Thomas, "Negative-sequence Reactance of Synchronous Machines," in *Electrical Engineering*, vol.55, no.12, pp.1378-1385, Dec. 1936.

[29] F. Briz, M.W. Degner, J.M. Guerrero and P. Garcia, "Stator Windings Fault Diagnostics of Induction Machines Operated From Inverters and Soft-Starters Using High-Frequency Negative-Sequence Currents," in *IEEE Trans. on Industry Applications*, vol.45, no.5, pp.1637-1646, Sept. 2009.

[30] J.E. Barkle and W.E. Glassburn, "Generator Protection From Unbalanced Currents," in *Electrical Engineering*, vol.72, no.11, pp.1012-1012, Nov. 1953.

[31] J.W. Pope, "A Comparison of 100% Stator Ground Fault Protection Schemes for Generator Stator Windings," in *IEEE Trans. on Power Apparatus and Systems*, vol.PAS-103, no.4, pp.832-840, Apr. 1984.

[32] R.L. Schlake, G.W. Buckley and G. McPherson, "Performance of Third Harmonic Ground Fault Protection Schemes for Generator Stator Windings," in *IEEE Trans. on Power Apparatus and Systems*, vol.PAS-100, no.7, pp.3195-3202, July 1981.

[33] M. Zielichowski and R. Mydlikowski, "Optimization of Operating Conditions of Third Harmonic Ground-fault Protection System of Generator-transformer Unit with Two-states Transverse Parameters," in *IEEE Trans. on Power Delivery*, vol.19, no.2, pp.565-569, April 2004.

[34] M. Zielichowski and R. Mydlikowski, "Influence of Difference System Parameters on Operating Conditions of Third Harmonic Ground-fault Protection System of Unit-connected Generator," in *IEEE Trans. on Power Delivery*, vol.19, no.2, pp.560-564, April 2004.

[35] X.G. Yin, O.P. Malik, G.S. Hope and D.S. Chen, "Adaptive Ground Fault Protection Schemes for Turbogenerator Based on Third Harmonic Voltages," in *IEEE Trans. on Power Delivery*, vol.5, no.2, pp.595-603, Apr 1990.

[36] N. Safari-Shad and R. Franklin, "Adaptive 100% Stator Ground Fault Protection Based on Third-Harmonic Differential Voltage Scheme," in *IEEE Trans. on Power Delivery*, vol.31, no.4, pp.1429-1436, Aug. 2016.

[37] F.R. Blánquez, C.A. Platero, E. Rebollo and F. Blázquez, "Novel Rotor Ground-Fault Detection Algorithm for Synchronous Machines With Static Excitation Based on Third-Harmonic Voltage-Phasor Comparison," in *IEEE Trans. on Industrial Electronics*, vol.63, no.4, pp.2548-2558, April 2016.

[38] S. Turner, "Applying 100% Stator Ground Fault Protection by Low Frequency Injection for Generators," in *IEEE 2009 Power & Energy Society General Meeting*, pp.1-6, 26-30 Jul. 2009.

[39] D.V. Haebler and C.H. Meijer, "The PWR Protection System - Present and Future," in *IEEE Trans. on Nuclear Science*, vol.22, no.1, pp.784-797, Feb. 1975.

[40] P.H. Huang, M.S.El Moursi and S.A. Hasen, "Novel Fault Ride-Through Scheme and Control Strategy for Doubly Fed Induction Generator-Based Wind Turbine," in *IEEE Trans. on Energy Conversion*, vol.30, no.2, pp.635-645, June 2015.

[41] Y. Wang, X. Yin and Z. Zhang, "The Fault-Current-Based Protection Scheme and Location Algorithm for Stator Ground Fault of a Large Generator," in *IEEE Trans. on Energy Conversion*, vol.28, no.4, pp.871-879, Dec. 2013.

[42] Y. Wang, X. Yin, Z. Zhang and Z. Li, "A Novel Stator Earth Fault Protection for Large Generator Based on Fault Current," *Power Engineering Conference (UPEC)*, 2013 48th International Universities', Dublin, 2013.

[43] T. Bengtsson, Z. Gajić, H. Johansson, J. Menezes, S. Roxenborg and M. Sehlstedt, "Innovative Injection-based 100% Stator Earth-fault Protection," in *11th IET International Conference on Developments in Power Systems Protection (DPSP 2012)*, Birmingham, UK, 2012.

[44] X. Liu, "The Research and Exploiture of Subharmonic Injection Scheme for Generator Stator Ground Protection," in *CICED 2010 Proceedings*, Nanjing, 2010.

[45] X. Zeng, X. Yin, G. Lin, S. Su and D. Chen, "Improvement of Subharmonic Injection Schemes for Huge Hydro-generator Stator Ground Gault Protection," in 2012 *Proceedings. International Conference on Power System Technology*, vol.2, pp.707-710, 2012.

[46] S. Turner, "Applying 100% Stator Ground Fault Protection by Low Frequency Injection for Generators," in *2009 IEEE Power & Energy Society General Meeting*, Calgary, AB, 2009.

[47] G.J. Lloyd, H.T. Yip and G. Mfillar, "Operation, Design and Testing of Generator 100% Stator Earth Fault Protection Using Low Frequency Injection," in *2008 IET*

9th International Conference on Developments in Power System Protection (DPSP 2008), Glasgow, 2008.

[48] "IEEE Standard Procedures for Obtaining Synchronous Machine Parameters by Standstill Frequency Response Testing (Supplement to ANSI/IEEE Std 115-1983, IEEE Guide: Test Procedures for Synchronous Machines)," *IEEE Std 115A-1987*, 1987.

[49] "IEEE Guide for Test Procedures for Synchronous Machines Part I-Acceptance and Performance Testing Part II-Test Procedures and Parameter Determination for Dynamic Analysis - Redline," *IEEE Std 115-2009*, May 2010.

[50] H.B. Karayaka, A. Keyhani, G.T. Heydt, B.L. Agrawal and D.A. Selin, "Synchronous generator model identification and parameter estimation from operating data," in *IEEE Trans. on Energy Conversion*, vol. 18, no. 1, pp. 121-126, Mar. 2003.

[51] E. Ghahremani, M. Karrari and O.P. Malik, "Synchronous generator third-order model parameter estimation using online experimental data," in *IET Generation, Transmission & Distribution*, vol. 2, no. 5, pp. 708-719, Sept. 2008.

[52] J.H. Chow, M.T. Glinkowski, R.J. Murphy, T.W. Cease and N.Kosaka, "Generator and exciter parameter estimation of Fort Patrick Henry Hydro Unit 1," in *IEEE Trans. on Energy Conversion*, vol. 14, no. 4, pp. 923-929, Dec. 1999.

[53] B. Mogharbel, L. Fan and Z. Miao, "Least squares estimation-based synchronous generator parameter estimation using PMU data," in *2015 IEEE Power & Energy Society General Meeting*, Denver, CO, 2015.

[54] G. K. Stefopoulos, G. J. Cokkinides and A.P. Meliopoulos, "Quadratic integration method for transient simulation and harmonic analysis," in *2008 13th International Conference on Harmonics and Quality of Power*, Wollongong, NSW, 2008, pp. 1-6.

[55] E. Farantatos, G.K. Stefopoulos, G.J. Cokkinides and A.P.S. Meliopoulos, "PMU-Based Dynamic State Estimation for Electric Power Systems," in *2009 IEEE Power & Energy Society General Meeting*, pp.1-8, Jul. 2009.

[56] A.P.S. Meliopoulos, G.J. Cokkinides, Z. Tan, S. Choi, Y. Lee and P. Myrda, "Setting-Less Protection: Feasibility Study," in *2013 46th Hawaii International Conference on System Sciences*, pp.2345-2353, Jan. 2013.

[57] A. P. S. Meliopoulos, G. J. Cokkinides, P. Myrda, Y. Liu, R. Fan, L. Sun, R. Huang and Z. Tan, "Dynamic State Estimation Based Protection: Status and Promise," in *IEEE Trans. on Power Delivery*, 23 Sept 2016.

[58] L. Sun, A. P. S. Meliopoulos, Y. Liu, and B. Xie, “Dynamic State Estimation Based Synchronous Generator Model Calibration Using PMU Data,” to appear in *IEEE Power and Energy Society General Meeting (PES)*, 2017.

[59] E. Farantatos, R. Huang, G. J. Cokkinides and A. P. Meliopoulos, "A Predictive Generator Out-of-Step Protection and Transient Stability Monitoring Scheme Enabled by a Distributed Dynamic State Estimator," in *IEEE Trans. on Power Delivery*, vol. 31, no. 4, pp. 1826-1835, Aug. 2016.